UNIVERSIDADE FEDERAL DO PARANÁ - UFPR

NATALIA PEREIRA MENEZES

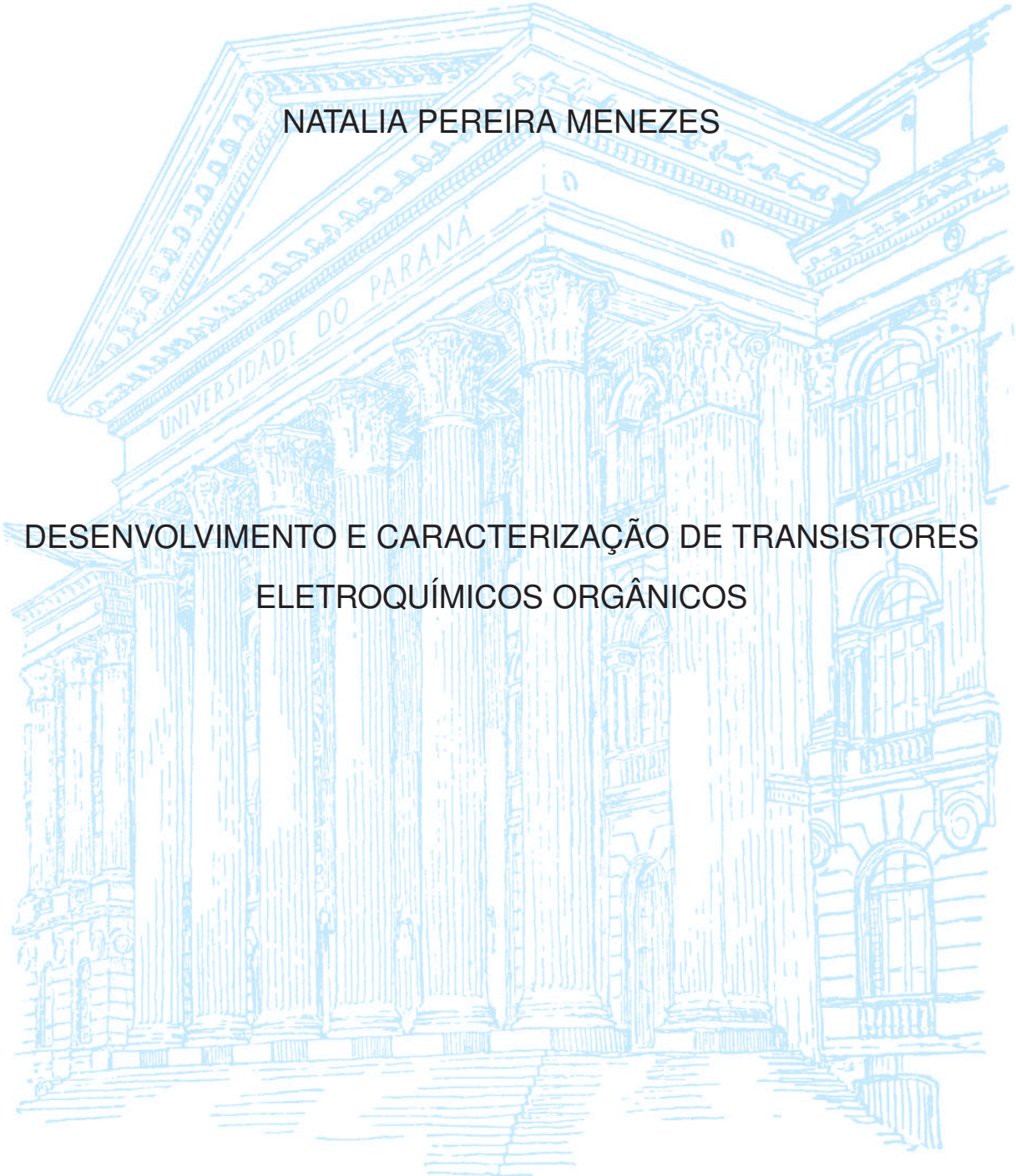

DESENVOLVIMENTO E CARACTERIZAÇÃO DE TRANSISTORES ELETROQUÍMICOS ORGÂNICOS

CURITIBA

2023

NATALIA PEREIRA MENEZES

DESENVOLVIMENTO E CARACTERIZAÇÃO DE TRANSISTORES ELETROQUÍMICOS ORGÂNICOS

Projeto apresentado ao Programa de Pós Graduação em Ciência e Engenharia dos Materiais(PIPE), Setor de Tecnologia, Universidade Federal do Paraná, como parte dos requisitos para obter o título de doutorado em Engenharia e Ciência dos Materiais.

Orientador: Prof. Dr. César Augusto Dartora (PIPE/UFPR)

Coorientador: Prof. Dr. André Augusto Mariano (PPGEE/UFPR)

CURITIBA

2023

DADOS INTERNACIONAIS DE CATALOGAÇÃO NA PUBLICAÇÃO (CIP)
UNIVERSIDADE FEDERAL DO PARANÁ
SISTEMA DE BIBLIOTECAS – BIBLIOTECA DE CIÊNCIA E TECNOLOGIA

Menezes, Natalia Pereira
Desenvolvimento e caracterização de transistores eletroquímicos orgânicos / Natalia Pereira Menezes. – Curitiba, 2023.
1 recurso on-line : PDF.

Tese (Doutorado) - Universidade Federal do Paraná, Setor de Tecnologia, Programa de Pós-Graduação em Ciência e Engenharia de Materiais.

Orientador: César Augusto Dartora
Coorientador: André Augusto Mariano

1. Transistores Eletroquímicos Orgânicos. 2. Eletroquímica orgânica. 3. Transcondutância. I. Universidade Federal do Paraná. II. Programa de Pós-Graduação em Ciência e Engenharia de Materiais. III. Dartora, César Augusto. IV. Mariano, André Augusto. V. Título.

Bibliotecário: Elias Barbosa da Silva CRB-9/1894

MINISTÉRIO DA EDUCAÇÃO
SETOR DE TECNOLOGIA
UNIVERSIDADE FEDERAL DO PARANÁ
PRÓ-REITORIA DE PESQUISA E PÓS-GRADUAÇÃO
PROGRAMA DE PÓS-GRADUAÇÃO ENGENHARIA E CIÊNCIA DOS MATERIAIS - 40001016033P9

TERMO DE APROVAÇÃO

Os membros da Banca Examinadora designada pelo Colegiado do Programa de Pós-Graduação ENGENHARIA E CIÊNCIA DOS MATERIAIS da Universidade Federal do Paraná foram convocados para realizar a arguição da tese de Doutorado de **NATALIA PEREIRA MENEZES** intitulada: **Desenvolvimento e Caracterização de Transistores Eletroquímicos Orgânicos**, sob orientação do Prof. Dr. CÉSAR AUGUSTO DARTORA, que após terem inquirido a aluna e realizada a avaliação do trabalho, são de parecer pela sua APROVAÇÃO no rito de defesa.

A outorga do título de doutora está sujeita à homologação pelo colegiado, ao atendimento de todas as indicações e correções solicitadas pela banca e ao pleno atendimento das demandas regimentais do Programa de Pós-Graduação.

CURITIBA, 29 de Setembro de 2023.

Assinatura Eletrônica
02/10/2023 11:21:30.0
CÉSAR AUGUSTO DARTORA
Presidente da Banca Examinadora

Assinatura Eletrônica
02/10/2023 10:03:42.0
RICARDO CANUTE KAMIKAWACHI
Avaliador Externo (UNIVERSIDADE TECNOLÓGICA FEDERAL DO PARANÁ)

Assinatura Eletrônica
03/10/2023 17:03:50.0
JOSÉ PEDRO MANSUETO SERBENA
Avaliador Interno (UNIVERSIDADE FEDERAL DO PARANÁ)

Assinatura Eletrônica
02/10/2023 19:30:58.0
JEAN CARLOS CARDOZO DA SILVA
Avaliador Externo (UNIVERSIDADE TECNOLÓGICA FEDERAL DO PARANÁ)

Assinatura Eletrônica
03/10/2023 10:05:15.0
EVALDO RIBEIRO
Avaliador Interno (UNIVERSIDADE FEDERAL DO PARANÁ)

Assinatura Eletrônica
02/10/2023 11:19:21.0
ANDRÉ AUGUSTO MARIANO
Coorientador(a) (UNIVERSIDADE FEDERAL DO PARANÁ - DELT/UFPR)

MINISTÉRIO DA EDUCAÇÃO
SETOR DE TECNOLOGIA
UNIVERSIDADE FEDERAL DO PARANÁ
PRÓ-REITORIA DE PESQUISA E PÓS-GRADUAÇÃO
PROGRAMA DE PÓS-GRADUAÇÃO ENGENHARIA E CIÊNCIA DOS MATERIAIS - 40001016033P9

APPROVAL MINUTE

The Examining Board is designated by the Faculty of the Graduate Program of the Federal University of Paraná in ENGENHARIA E CIÊNCIA DOS MATERIAIS where invited to argue the DISSERTATION of PHILOSOPHY DOCTOR by **NATALIA PEREIRA MENEZES** , entitled: **Desenvolvimento e Caracterização de Transistores Eletroquímicos Orgânicos**, under the supervision of Dr. CÉSAR AUGUSTO DARTORA, which and after assessment of the candidate and the work, the Examining Board decided for the APPROVAL in the present rite.

The granting of the title of philosophy doctor is contingent upon the fulfillment of all the requirements indicated by the Examining Board and terms determined in the regulation of the Graduate Program.

CURITIBA, September 29th, 2023.

Eletronic Signature
02/10/2023 11:21:30.0
CÉSAR AUGUSTO DARTORA
President of the Examining Board

Eletronic Signature
02/10/2023 10:03:42.0
RICARDO CANUTE KAMIKAWACHI
External Member (UNIVERSIDADE TECNOLÓGICA FEDERAL DO PARANÁ)

Eletronic Signature
03/10/2023 17:03:50.0
JOSÉ PEDRO MANSUETO SERBENA
Internal Member(UNIVERSIDADE FEDERAL DO PARANÁ)

Eletronic Signature
02/10/2023 19:30:58.0
JEAN CARLOS CARDOZO DA SILVA
External Member (UNIVERSIDADE TECNOLÓGICA FEDERAL DO PARANÁ)

Eletronic Signature
03/10/2023 10:05:15.0
EVALDO RIBEIRO
Internal Member(UNIVERSIDADE FEDERAL DO PARANÁ)

ACKNOLEDGEMENTS

This doctorate title represents more than just academic growth, it also taught me a great deal personally. I will be forever grateful for this time and the people I encountered.

In the personal sphere, I thank my mom and my grandma for their support in all the academic and professional decisions I took. Without them, I wouldn't be able to come to Curitiba to pursue this degree.

I also want to thank all my colleagues at IMS, who were a great support system at an extremely difficult time for all of us.

In the academic sphere, I thank my advisors (all six of them), the co-authors of the " Improved stability of organic electrochemical transistor performance with a low swelling mixed conducting polymer: a comparative study with PEDOT:PSS" paper and laboratories in which this project was developed.

I thank Prof. Cesar Dartora for accepting my submission, accompanying this journey, and especially for being understanding and trusting me.

I thank Prof. André Augusto Mariano for accepting our invitation to be my co-advisor and also for accompanying this journey.

I thank Lionel Hirsch for agreeing to receive me at IMS.

I thank Guillaume Wantz, Mamatimin Abbas, and Damien Thuau for all the important lessons I learned, as well as the support while I was in France and after I returned to Brazil.

I thank Tommaso Nicolini, Micah Barker, Natalie Stingelin, and Olivier Dautel for the collaboration and for allowing me to test the P3HHT films on my devices.

In addition, I would like to acknowledge the laboratories where the experiments were conducted, which are:

- Laboratory for the integration from Material to System (IMS);
- Laboratoire de Chimie des Polymeres Organiques (University of Bordeaux);
- Laboratório de Magnetismo, Medidas e Instrumentação (LAMMI - UFPR).

I also would like to acknowledge the PRINT comission.

This study was financed in part by the Coordenação de Aperfeiçoamento de Pessoal de Nível Superior–Brasil (CAPES) – Finance Code 001.

RESUMO

A convergência das tecnologias de Eletrônica Orgânica e Biossensores representa um mercado em expansão com significativo potencial como uma força transformadora em futuras tecnologias. A fusão desses campos promete atender à crescente demanda por testes diagnósticos rápidos, descomplicados e economicamente viáveis no ponto de atendimento e em situações de emergência. Dentre as diversas tecnologias prontas para contribuir para o monitoramento da saúde, os Transistores Orgânicos Eletroquímicos (OECTs) emergem como particularmente promissores. Os OECTs possuem a capacidade de interagir com ambientes biológicos diversos e intrincados, traduzindo informações biológicas em intensidades mensuráveis. Este projeto de pesquisa propõe uma metodologia experimental fundamentada na microfabricação para avançar no desenvolvimento dos OECTs e explorar seu comportamento e propriedades de material para possíveis aplicações de detecção. Os dispositivos fabricados foram projetados para operar em dois modos distintos: acumulação e depleção. Camadas ativas, especificamente PEDOT:PSS e P3HHT, foram empregadas para elucidar sua influência no desempenho do dispositivo. A análise dos resultados em estado estacionário revelou percepções notáveis. Os OECTs de PEDOT:PSS exibiram sensibilidade direta à composição do eletrólito e à espessura do canal. Por outro lado, a natureza de baixo inchaço do P3HHT, um polímero selecionado para os transistores de modo de acumulação, os tornou suscetíveis a ânions maiores do eletrólito, mas não apresentaram resposta discernível a variações na concentração de íons. Uma distinção crucial entre os OECTs de PEDOT:PSS e P3HHT foi destacada por meio de testes de estabilidade de imersão e estresse elétrico. As propriedades intrínsecas de baixo inchaço do P3HHT emergiram como um fator crucial na estabilidade e reversibilidade estabelecidas para dispositivos de modo de acumulação. Mesmo após um longo período de imersão de 40 dias e 50 ciclos eletroquímicos, o P3HHT demonstrou uma notável resiliência. Em resumo, o objetivo principal deste projeto foi delinear uma metodologia experimental para microfabricar OECTs e explorar seu potencial em aplicações de detecção biológica. O sucesso desta empreitada é destacado pelas conclusões conclusivas de testes de estabilidade e ajuste, afirmando a viabilidade dos OECTs como uma plataforma versátil para detecção biológica em aplicações de saúde e diagnóstico.

Palavras-Chave: Transistores Orgânicos Eletroquímicos; PEDOT:PSS; P3HHT; Transcondutância; Estabilidade;

ABSTRACT

The convergence of Organic Electronics and Biosensor technologies represents a burgeoning market with significant potential as a transformative force in future technologies. The amalgamation of these fields holds promise in addressing the escalating demand for rapid, uncomplicated, and cost-effective Point-of-Care diagnostic and emergency testing. Among the various technologies poised to contribute to healthcare monitoring, Organic Electrochemical Transistors (OECTs) emerge as particularly promising. OECTs possess the capability to interface with diverse and intricate biological environments, translating biological information into measurable intensities. This research project proposes an experimental methodology grounded in microfabrication to advance the development of OECTs and explore their behavior and material properties for potential sensing applications. The fabricated devices were designed to operate in two distinct modes: accumulation and depletion. Active layers, specifically PEDOT:PSS and P3HHT, were employed to elucidate their influence on device performance.The analysis of steady-state results revealed notable insights. PEDOT:PSS OECTs exhibited direct sensitivity to the composition of the electrolyte and channel thickness. Conversely, the low-swelling nature of P3HHT, a polymer selected for the accumulation mode transistors, rendered them susceptible to larger anions from the electrolyte but exhibited no discernible response to variations in ion concentration.A critical distinction between PEDOT:PSS and P3HHT OECTs was underscored through immersion and electrical stress stability tests. The intrinsic low-swelling properties of P3HHT emerged as a pivotal factor in establishing stability and reversibility for accumulation mode devices. Even after a prolonged 40-day immersion period and 50 electrochemical cycles, P3HHT demonstrated remarkable resilience.In summation, the primary objective of this project was to delineate an experimental methodology for microfabricating OECTs and to explore their potential in biosensing applications. The success of this endeavor is underscored by the conclusive findings from stability assays and tuning tests, affirming the viability of OECTs as a versatile platform for biosensing in healthcare and diagnostic applications.

Keywords: Organic Electrochemical Transistors; PEDOT:PSS; P3HHT; Transconductance; Stability;

CONTENTS

LIST OF FIGURES

LIST OF TABLES

LIST OF ABBREVIATIONS

A - Amperes

AC - Alternate Current

Ag/**AgCl** - Silver/Silver Chloride

aq. - Aqueous

Au - Gold

CP - Conductive Polymer

CTAB - Hexadecyl Trimethyl Ammonium Bromide

EG - Ethylene Glycol

FETs - Field-Effect Transistors

f_{ion} - Ion Frequency

gm - transconductance

gm_{max} - Maximum Transconductance

GOPS - (3-glycidyloxypropyl)trimethoxysilane

h^+ - Holes

I_{DS} - Drain Current

I_{GS} - Gate Current

KCl - Potassium Chloride

L - Liter

M^+ - Cations

m - 10^{-3}/ meters

n - 10^{-9}

NaCl - Sodium Chloride

OE - Organic Electronics

OECT - Organic Electrochemical Transistors

OFET - Organic Field-Effect Transistors

OLED - Organic Light Emmiting Diode

OPV - Organic Photovoltaics

P3HT - poly(3-hexylthiphene-2,5-diyl)

P3HHT - poly[3-(6-hydroxy)hexyl thiophene]

PaC - Parylene-C

PBS - Phosphate Buffered Saline

PEDOT:PSS - Poly(3,4-ethylenedioxythiophene) doped with poly(styrene sulfonate)

PET - polyethylene terephthalate

p(g2T-TT) - glycolated thiophene-thienothiophene

PoC - Point-of-Care

S - Siemens

Ti - Titanium

μ - 10^{-6}

μ**C*** - Mobility $\times$ Volumetric Capacitance

V - Volt

$\boldsymbol{V}_{DS}$ - Drain Voltage

$\boldsymbol{V}_{GS}$ - Gate Voltage

$\boldsymbol{V}_{GSeff}$ - Effective Gate Voltage

$\boldsymbol{V}_{rms}$ - Root-Mean-Square Voltage

1 INTRODUCTION

Organic devices, such as Organic Light-Emitting Diodes (OLEDs), Organic Photovoltaics (OPV), and Organic Field-Effect Transistors (OFETs), are known for their ease and low cost of processing, potential large-area printing, compatibility with a variety of substrates, and often, biocompatibility. Although there is still space for technological advances, the field of Organic Electronics (OE) is further being introduced into different sectors of daily life and it is a growing market (SHAW, SEIDLER, 2001; MA et al., 2010; JEN, 2010; MALLIARAS, MCCULLOCH, 2022).

OE is also gaining space in biological applications, mainly as biosensors, due to its flexibility and tunability characteristics, which can fulfill the requirements for performing in complex biological media, as well as providing good signal transduction, high surface-to-volume ratio, high conductivity, chemical stability, and good mechanical properties (PAPPA et al., 2018).

In this context, the integration of Organic Electronics and biology, namely Organic Bioelectronics is a growing field of study that explores the possibilities of using organic electronics materials in biology and medicine. The development of Organic Bioelectronics is motivated by the current and future needs in diagnostic and therapeutic areas of biomedicine (MALLIARAS AND MCCULLOCH, 2022), and refers to devices that integrate living systems and organic electronic materials. Such devices possess the ability to detect different pathologies and, regulate the physiology and processes of cells, tissues, and organs (OHAYON, DRUET, INAL, 2023).

Therefore, there is a growing demand for sensitive assays that provide fast, simple, and inexpensive PoC diagnostic and emergency tests, in addition to the detection of low concentrations of analytes, low amplitude brain activity, and pathogens, as well as the improvement of the compatibility with biological milieux (STRAKOSAS, BONGO, and OWENS, 2015; KERGOAT et al., 2012).

Thus, Point-of-Care (PoC) is a term used to reflect technologies that allow patients to take *in vitro* tests without going to a medical facility, or samples to be sent to laboratories. This is possible because the analysis is carried out locally where the test is taken and the results are received in a matter of minutes, which means the PoC equipment provides clinical analysis in a fast and decentralized manner (COBRA, COSTA, 2015). However, most systems used in clinical analysis are not applied to the PoC sector, especially because there are limitations regarding the device's portability, cost, analysis time, or qualified labor to operate such systems. Accordingly, sensors that employ flexible/organic electronics present the potential to revolutionize conventional diagnostic methods and their instruments through portability, wearability, and real-time monitoring (VASUDEV et al., 2013; WANG; LIU; ZHANG, 2017).

In these circumstamces, biosensors are characterized by turning biological signals into optical, chemical, electrical, or other signals that can be measured and quantified in real time. These devices can be used in configurations that do not require extensive resources or trained professionals.This type of sensor consists of three main operations, namely sampling, chemical testing, and detection and recording of a quantifiable signal, making the biosensing research area an interdisciplinary field, in which physics is integrated into biology, chemistry, materials science, engineering, mathematics, and information technology (SHAVANOVA et al., 2016; CORRIE et al., 2015).

Recent works with biosensors have been reported in industrial and environmental analysis, such as monitoring the chemical and microbiological quality of water, rapid detection of various toxins, heavy metal ions, and evaluation of the concentration of different pesticides and their residues in the environment, food, water, and soil. Furthermore, biosensors are currently used in chemical diagnostics to determine blood characteristics (pH, pCO_2, pO_2), to monitor glucose, lactate, urea, creatinine, cholesterol, and triglycerides, and perform genetic or infectious disease testing for mutational analysis, skin allergy testing, and cancer diagnostics. There are also biosensors being used in contact lenses and direct contact with biofluids through the skin or microneedles (SHAVANOVA et al., 2016; GLENNON et al., 2016).

Hence, wearables pose an important role in medicine, as they enable continuous monitoring of health and vital signs, meaning that devices attached to the skin are drawing attention to the possibility of supervision of electrolytes, metabolites, pH, and other biochemical markers found in bodily fluids, which may indicate dehydration, fatigue, and early symptoms of certain diseases (VASUDEV et al., 2013; GAO et al., 2019; YAO et al., 2018).

There is a range of sensors embedded in smartwatches, bandanas, clothing, and plasters, as well as in small handheld devices that through mobile applications can record and provide users with feedback on different physical performance variables, such as cardiorespiratory function, movement patterns, sweat analysis, tissue oxygenation, sleep, emotional state, and changes in cognitive functions following concussion (PEAKE; KERR; SULLIVAN,2018).

Therefore, the interest in monitoring biochemical parameters from wearable sensors is a research line that has been conquering territory, partly due to the interest of different economic sectors in applications based on new types of technology, which means that wearable biosensors can fulfill an important role in the future of non-invasive real-time health monitoring (GAO et al., 2016b; GLENNON et al., 2016).

1.1 JUSTIFICATION AND OBJECTIVES

The integration of Organic Electronics and biology, namely Organic Bioelectronics is a growing field of study and is motivated by the current and future needs in diagnostic and therapeutic areas of biomedicine. Among these needs are the growing demand for sensitive assays that provide fast, simple, and inexpensive PoC diagnostic and emergency tests, and the detection of low concentrations of analytes, low amplitude brain activity, and pathogens, as well as the improvement of the compatibility with biological milieux (STRAKOSAS, BONGO, and OWENS, 2015; KERGOAT et al., 2012).

Currently, the elected approaches for diagnostic with electrical sensors include electrochemical biosensors, passive metal electrodes, and/or large-scale integrated systems. These approaches involve redox reactions, changes in local potential or impedance, which represent a challenge since the use of these resources require further amplification of the biological signals so they could be detectable. This situation raises a need for more active, sensitive, and biocompatible devices and, the Organic Electrochemical Transistors (OECTs) are a promising technology that could potentially surpass these limitations and fulfill the raising demands (STRAKOSAS, BONGO, and OWENS, 2015).

OECTs perform ionic-to-electronic signal conversion, in which the ionic flux in the electrolyte (equivalent to the dielectric layer found in OFETs) is converted into a readable electronic signal (OHAYON, DRUET, INAL, 2023). In the context of biosensing, OECTs are a valuable tool due to their efficient transduction, large amplification, high sensitivity, biostability, versatility and low detection limits (MARKS et al., 2022).

Examples of metabilites targeted during OECT idelisation are glucose, tyrosine, cortisol, lactate, ethanol, uric acid, urea, dopamine, noradrenaline, adrenaline, ascorbic acid and sialic acid (YAO et al., 2023).

Also, the ability of these devices to work in complex environments, such as blood, milk, tears, sweat, or saliva allows multi-analyte assays and the detection of metabolites that could be essential to the early diagnosis of human diseases. Besides, properties such as high transconductance, low operating voltage, ease of processing, design flexibility, stability in electrolytes, cytocompatibility, and biofunctional modification make OECTs a prosperous match for bioelectronics fabrication, in addition to representing a path to study mixed electronic/ionic conduction (MALLIARAS, MCCULLOCH, 2022; YAO et al., 2023).

One important advantage of using conducting polymers is their tunable properties, which are receptive to chemical modifications, biofunctionalization, and fabrication on a variety of substrates by using different processing techniques. Also, their compatibility with photolithography techniques allows microfabrication (STRAKOSAS, BONGO, and OWENS, 2015). Then, the simple structure of OECTs put together with the characteristics of conducting polymers, allows the adoption of both common photolithography fabrication processes and printing technologies, which are

compatible with a variety of substrates, such as plastic, paper, glass, or textile fibers (POLYRAVAS et al., 2020).

Even though there has been great progress in the study and development of OECTs, these devices are a considerably less mature technology than Organic Field Effect Transistors (OFETs) and there is still room for technological growth, especially due to challenges regarding (i) innovations in the active layer, with improved conductivity, stability, patterning, and restorability; (ii) fabrication of devices that enable integration to complex sensory systems, and (iii) optimization of the response time. By overcoming these obstacles, the application of OECTs in practical biological systems would be accelerated, mainly in the wearable and brain-interfacing domains (STRAKOSAS, BONGO, and OWENS, 2015; BAI et al., 2019; MARKS et al., 2022).

In addition, there are some regimens in which OECTs work that need further research to be understood, one of them being the influence of trapped ions into the active layer, and despite the guidelines to design OECTs with less influence from parasitic resistances, more detailed rules could be laid out if additional studies reported the cause of such resistances, which are unknown (FRIEDLEIN et al., 2018; RIVNAY, 2018).

As stated previously, organic bioelectronics is an interdisciplinary field of study, in which it is possible to interface electronics and biology so that biomedical technologies can evolve and, the OECTs are a big part of this evolution, being applied to various biological domains due to the properties previously listed (RIVNAY et al., 2018; BAI et al., 2019; HUTTER et al., 2013).

In this context, it is possible to conclude that despite the advances of the last two decades in both OECT technology and in organic bioelectronics in general, there are still some unknown variables, which are essential to fully understand the workings of such organic transistors and to escalate their use as biosensors to promote Point-of-Care testing and the monitoring of healthcare in remote areas.

Furthermore, wearable devices that detect health and physical activity parameters are considered one of the most effective and viable methods for daily consumer health monitoring, as healthcare services require patients to travel to diagnostic centers and hospitals, and not provide continuous, real-time analysis. In this context, wearable devices have begun to revolutionize biomedicine through digital, remote, and continuous health and wellness monitoring, providing opportunities to improve health care in a variety of sectors, such as within hospitals, clinics, at home and in geographically remote areas, including rural and resource-poor settings (WANG; LIU; ZHANG, 2017; NAKATA et al., 2017; DUNN; RUNGE; SNYDER, 2018).

An important fact about OECTs and organic bioelectronics is that these fields are still are early stages of technological maturity and there is a good amount of fundamental work to be done, which includes a better understanding of the working mechanisms and communication between the organic materials and biology, mixed conduction efficiency, and finding new applications

(MALLIARAS, MCCULLOCH, 2022).

1.1.1 Objectives

To overcome the obstacles regarding OECT design and performance and to target bioelectronics applications, this project proposes, as its main goal, to develop Organic Electrochemical Transistors, study their behavior, properties, and to explore different materials as active layer, to investigate their potential as biosensors.

To fulfill the overall purpose of the research, the following specific objectives were determined:

- Adjust materials choice and fabrication process according to availability and feasibility;
- Create characterization setup dedicated to testing OECTs;
- Validate the experimental methodology;
- Explore the influence of device design on the performance of the OECTs, such as geometry, electrolyte, materials choice and gate electrode;
- Study the impact of different polymers as active layer by exploring diverse and new materials with mixed conductivity;
- Investigate the stability of the fabricated devices under environmental conditions and electrical stress.

1.2 STRUCTURE OF THE PROJECT

In this chapter, the concepts of Organic Electronics, Point-of-Care, and Biosensors were presented along with the problem this research will approach, its justification, scientific contributions, and objectives. Chapter 2 analyzes the State-of-the-Art in the OECT area. Furthermore, Chapter 3 discusses the materials choice and experimental methodology adopted to fabricate and characterize the reported OECTs. In addition, Chapters 4 and 5 exhibit the results acquired from the investigation on the steady-state and stability of accumulation and depletion mode OECTs, as well as additional active layers that were explored and did not present a response. Finally, Chapter 6 presents the conclusions drawn from the demonstrated methodology, overall results, and future perspectives for the project.

2 LITERATURE OVERVIEW AND STATE-OF-THE-ART ORGANIC ELECTROCHEMICAL TRANSISTORS

OECTs were first demonstrated by White, Kittlesen, Wrighton. (1984) in a microelectrode array, where the conductivity of a poly(pyrrole) film was modulated by an electrolyte through the application of a potential to the gate. This was the first time the gate electrode was separated from the conducting channel with an electrolyte, and paved the route for the OECTs reported nowadays (WHITE, KITTLESEN, WRIGHTON 1984; BERNARDS and MALLIARAS, 2007; BAI et al., 2019).

2.1 INTRODUCTION TO ORGANIC ELECTROCHEMICAL TRANSISTORS

OECTs are a special category of organic transistors that present mixed conductivity abilities (both ions and electrons contribute to their operation). The basic structure of an OECT, seen in Figure 2.1, recalls a common transistor with source and drain connected by an active layer (usually a hydrated, ion-permeable conducting polymer capable of changing its conductivity) and a gate electrode. What differentiates these devices from OFETs, for example, is the electrolyte in contact with the channel, in which the gate electrode is immersed (BERNARDS, MALLIARAS, 2007; STRAKOSAS, BONGO, OWENS, 2015; RIVNAY et al., 2018; SESSOLO et al., 2013).

Figure 2.1: Basic strutucture of an OECT, in which Source and Drain electrodes are found on the base of the device in contact with the conductive channel. Interfacing the channel, an electrolyte plays the role of the dielectric found in OFETs, and the Gate electrode is immersed in such solution.

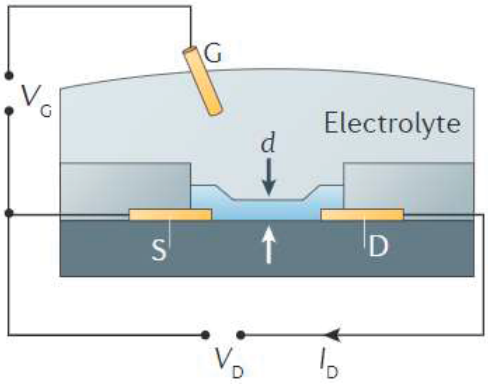

SOURCE: Rivnay et al. (2018).

The architecture of OECTs plays an important role in device performance and the most common configurations are bottom contact, top contact, coplanar, and vertical. As seen in Figure 2.2.a, the bottom contact architecture is characterized by the deposition of the channel on the

substrate with D and S electrodes on top of it. On the other hand, Figure 2.2.b depicts a top contact configuration, in which the channel is deposited on top of the D and S electrodes. The coplanar architecture consists of positioning the channel and G electrode on the same substrate, Figure 2.2.c, as the vertical configuration stacks D and S on top of each other with an insulating layer in between them, Figure 2.2.d (OHAYON, DRUET, INAL, 2023).

Figure 2.2: Common OECT architecture. (a) Bottom contact; (b) Top contact; (c) Coplanar; (d) Vertical.

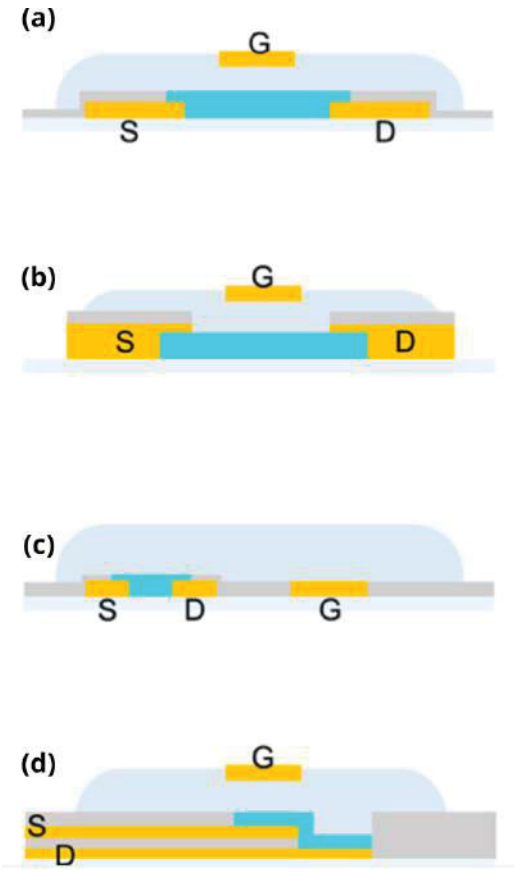

SOURCE: Ohayon, Druet, Inal (2023).

Regarding fabrication, the most commonly adopted techniques are photolithography, photoresist patterning, metal deposition, dry etching, some type of coating, and peel-off of the insulating layer. There are other methods that could be adapted, such as inkjet printing, spray printing, and roll-to-roll fabrication (OHAYON, DRUET, INAL, 2023).

Also, OECTs can be processed in low temperatures, and this characteristic allied to the use of an electrolyte instead of the dielectric layer allows the adoption of diverse substrates, including flexible and stretchable materials, such as plastic, paper, and cotton fibers (PAUDEL et al., 2021).

As in common Field-Effect Transistors (FETs), in OECTs, the potential applied between Drain and Source (V_{DS}) establishes a current (I_{DS}) in the channel, which is modulated by an applied voltage to the gate electrode (V_{GS}) due to a doping/de-doping process upon the conducting/conjugated polymer. The I_{DS} current is proportional to the mobile carriers found in the channel, holes for p-type semiconductors and electrons for n-type materials (RIVNAY et al., 2018,

OHAYON, DRUET, INAL, 2023).

In tha case of OECTs, the electrolyte plays the main role in doping and de-doping the conductive channel since it is responsible for injecting ions into the organic film upon an applied V_{GS}, enabling changes in its doping state, and, therefore, its conductivity. One of the advantages of the OECTs is that the doping/de-doping of the channel happens in its integrity, through the whole volume of the film, and therefore, it allows large changes in I_{DS} with small values of V_{GS}, which results in one of the most important characteristics of these devices, high transconductance (*gm*) going up to the order of mS (SAVVA, WUSTONI, INAL, 2019).

To guarantee high performances from OECTs, each ion pushed from the electrolyte into the channel must fully penetrate the polymer before accessing the site it will replace the designated electronic charge (SAVVA, WUSTONI, INAL, 2019). Independent of the working principle of the device, one of the most important characteristics of OECTs is the volumetric interaction between the ions found in the electrolyte and the conducting channel since this relationship directly influences the transduction capacity of the transistors, e.g. their transconductance (SAVVA et al., 2019).

The transconductance, Eq. 2.1, indicates efficient ion-to-electronic signal conversion and describes the ability of the OECT to amplify a small signal, usually at voltages below 1 V, and considering water electrolysis, it enables the use of aqueous electrolytes, an essential parameter for developing technologies aiming at physiological solutions (ZEGLIO, INGANAS,2018; STRAKOSAS, BONGO, OWENS, 2015; PATERSON et al., 2015; PAPPA et al., 2018).

$$gm = \frac{\partial Id}{\partial Vg} \tag{2.1}$$

Since OECTs can achieve large modulations of the drain current at low gate voltages, it makes them effective switches and powerful amplifiers. Also, the use of electrolytes allows different processing adaptations, including the adoption of diverse substrates, forms and, biofunctionalization. Furthermore, the tunability of organic conducting polymers can bring improvements to the transport of ions and electrons and simplify bio-interfaces (BAI et al., 2019; RIVNAY et al., 2018; ZEGLIO, INGANAS ,2018; FRIEDLEIN et al., 2018).

Another important property of OECTs is the product of the volumetric capacitance (C*) and the carrier mobility (μ), which are material parameters linked to ionic and electronic properties, respectively. The μC* product is, therefore, a figure of merit for mixed ionic/electronic conducting materials (FRIEDLEIN et al., 2018). The volumetric capacitance indicates the extent of ion penetration, transport, and storage capabilities of the channel, while μ represents the transport of electronic charges across the channel. Both parameters depend on the potential applied to the gate and are influenced as well by the size, charge, and polarity of ions in the channel (OHAYON,

DRUET, INAL, 2023).

Another figure of merit to evaluate the modulation of I_{DS} in OECTs is the ON/OFF ratio, which depends on distinct parameters, such as processing and composition of the conducting channel, device geometry, material of the gate electrode, and nature of the electrolyte (KUMAR et al., 2015; POLYRAVAS et al., 2020). The ON/OFF is determined by the ratio of the maximum I_{DS} when the transistor is ON and the current at OFF state. OECTs with large and stable ON/OFF ratios are eligible for logic circuits and neuromorphic applications once high and static I_{DSON} enables effective signal output. On the other hand, low I_{DSOFF} represents less power and background noise for sensors (OHAYON, DRUET, INAL, 2023).

OECTs with high ON/OFF ratios are preferred for biosensor applications since they improve signal-to-noise ratio, which means that lower limits of detection can be achieved (OHAYON, DRUET, INAL, 2023).

Another commonly used steady-state performance parameter is the threshold voltage (V_{th}), which is generally described as the readiness of the channel to ion penetration. (V_{th}) dictates the noise margin and the circuit power consumption and can be influenced by the nature of the gate electrode, as well as the side-chains of the polymer used in the channel (affects ion penetration) and the type and concentration of ions in the electrolyte (OHAYON, DRUET, INAL, 2023).

There are some models to describe the doping/de-doping phenomenon in OECTs, but the most accepted are the ones that separate the device into an ionic and an electronic circuit. In those models, the ions move vertically from the electrolyte into the channel while the charge carriers are restricted to a horizontal movement between Source and Drain (KAPHLE et al., 2020).

The model for p-type OECTs developed by Bernards and Malliaras (2007) describes the working principle of the OECTs through the two main strands: ionic circuit and electronic circuit. The ionic circuit models the flow of ions in the gate/ electrolyte/channel through a series configuration of a resistor (ions in the electrolyte) and a capacitor (ions stored in the channel) with negligible gate/electrolyte capacitance.

On the other hand, the electronic circuit includes the electronic charges in the source/channel/drain interfaces and is described by Ohm's law, which means that electronic transport is defined by hole density and mobility, it also is represented as a resistor with charges drifting by influence of an applied potential. Therefore, the interaction between electronic and ionic circuits translates the ions being pushed from the electrolyte into the conducting channel, which is an essential principle in the behavior of OECTs (BERNARDS, MALLIARAS, 2007; RIVNAY et al., 2018).

Lastly, OECTs present a growing field of applications and recently, have been applied for both *in vitro* and *in vivo* testing, and their high sensitivity allowed the development of low-cost biosensors for small molecules, analytes, and to monitor the function of electrogenic cells (ZEGLIO, INGANAS,2018; POLYRAVAS et al., 2020).

Some examples of domains where OECTs have been applied in the last two decades are monitoring of brain activity, cardiac rhythm, and eye movement, cell transport measurement, signal recorders, neuromorphic systems (neuronal and peripheral nerve stimulation and neuromodulation), barrier tissue arrangement, disposable electronics, drug delivery, photostimulation of biological tissues, active-matrix physical sensors, digital logic, chemical, and biological sensors, more recently to detect COVID-19 and develop artificial synapses with self-healing dielectric layers (HUTTER et al., 2013; PATERSON et al.,2019; FRIEDLEIN et al., 2018; BAI et al., 2019; GUO et al., 2021; BERGGREN et al., 2022; GAO et al., 2023).

2.2 TUNING THE PERFORMANCE OF OECTS

As explained previously, OECTs are three-terminal organic devices characterized by the presence of an electrolyte in the interface between the channel and the gate electrode. The working principle of these devices is based on the doping and de-doping of the conducting channel through ions, from the electrolyte, that are injected throughout the whole volume of the film. This is one of the most important properties of these devices since it guarantees their figure of merit characteristic, the high transconductance. In this context, this section further explores the influence of the materials choice, device design and elected electrolyte in the performance of the OECTs and discusses the State-of-the-Art by depicting diverse reports on the topic.

2.2.1 Materials Choice

Regarding materials choice, the active layer is one of the most important in the fabrication of OECTs, especially because it can completely change the behavior of the devices according to the type of polymer employed. There are two operation modes in which OECTs can function, depletion mode (ON state @ V_{GS} = 0 V) and accumulation mode (OFF state @ V_{GS} = 0 V), and this property can be selected according to the adopted active layer (BAI et al., 2019; LI and LEI, 2021).

Therefore, depletion mode, Figure 2.3a, means that while there is no V_{GS} applied to the gate, there will be current flowing in the channel (ON state), and when positive voltages are applied to the gate the cations found in the electrolyte are injected into the channel and compensate the anions found in the polymer backbone, therefore, reducing the hole (h^+) current since the electronic charges collected at the drain are not substituted by new ones injected through the source (OFF state). On the other hand, accumulation mode OECTs, which means these devices are normally on OFF state due to a lower number of mobile holes in the channel, as seen in

Figure 2.3b. With $V_{GS} < 0$ V, anions are injected into the channel and then an accumulation of h^+ occurs, leading it to the ON state (RIVNAY et al., 2018).

Figure 2.3: Working principle of: (a) Depletion mode OECTs. While V_{GS} = 0 V, the device is ON and when V_{GS} > 0 V, cations from the electrolyte compensate the negative charges in the conducting polymer resulting in the holes not being replenished, and therefore, the device turns off. (b) Accumulation mode OECTs. If V_{GS} = 0V, the device is OFF, but when $V_{GS} < 0$ V, anions are injected into the channel and holes accumulate to compensate the negative charge, resulting in an ON OECT.

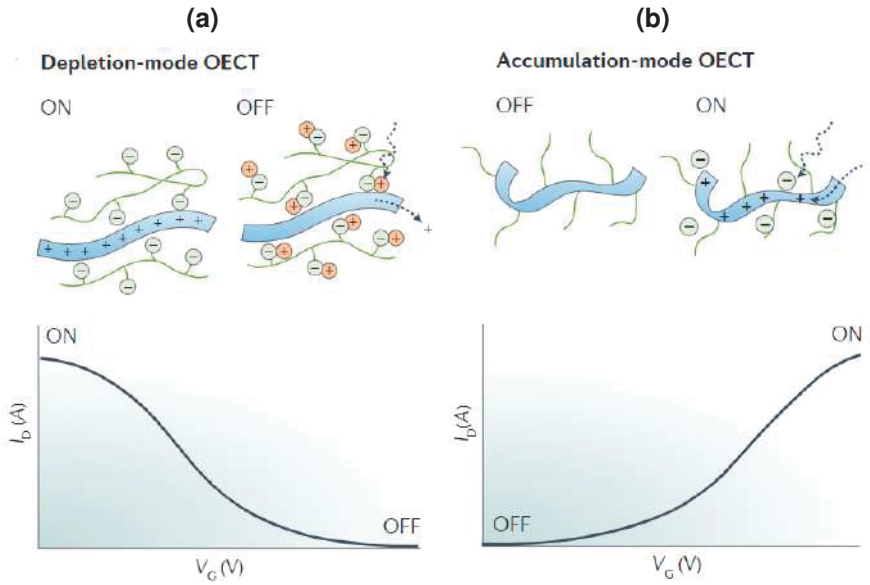

SOURCE: Rivnay et al. (2018).

Accumulation mode OECTs are not as extensively explored as their depletion counterparts, however, they represent an interesting alternative to different uses, especially sensing applications. Since the channel is naturally de-doped (OFF-state) at VGs = 0V, and is doped (ON-state) at applied potentials at the gate, these devices have the advantage of low power consumption.

Accumulation mode devices have been demonstrated with various active layers, e. g. poly(3-hexylthiphene-2,5-diyl) (P3HT) (FLAGG et al., 2018), and an approach to facilitate ion mobility and water uptake is the addition of side chains with hydrophilic groups, as an example of oligoethylene glycol, to the polymer backbone as reported for PTHs (INAL et al. 2014), p(gNDI-gT2) (GIOVANNITTI et al., 2016), P3MEEMT (FLAGG et al., 2019), [p(g2T-TT)] (CENDRA et al., 2019) and gBDT-g2T (NIELSEN et al., 2016). This is mainly to address the challenges faced with the adoption of intrinsic mixed conductors due to their propensity to hydrophobicity and performance requirements such as stability in aqueous environments and reversibility. Yet, these additions to the polymer backbone that can affect the electronic charge transport lead to higher susceptibility to environmental conditions, and influence the structural, mechanical, and electronic properties of the material (NICOLINI et al., 2021; LI and LEI, 2021).

Design strategies that enhance ion conductivity include adding hydrophilic side chains, such as Ethylene Glycol (EG) chains, and optimizing the film morphology. However, the electrolytes

can also introduce traps and disorder in the film, which can hinder charge carrier transport and reduce ion mobility. Therefore, achieving high ion conductivity while maintaining high charge carrier mobility is still a challenge in OECT design (LI and LEI, 2021).

Poly(3,4-ethylenedioxythiophene) doped with poly(styrene sulfonate), i.e. PEDOT:PSS, seen in Figure 2.4, is a p-type conducting polymer (CP) widely adopted as the active layer in OECTs in which the PSS negative charges compensate for the holes found in the PEDOT backbone. Also, OECTs based on PEDOT:PSS usually take advantage of the polymer's high electronic and ionic mobilities ($\sim$1-2 cm^2 V^{-1} s^{-1} and 1×10^{-3} cm^2 V^{-1}s^{-1}, respectively), high transconductance, ease of processing, and commercial availability (KEENE et al., 2020).

PEDOT:PSS presents both electronic conductivity, reaching 1000 S/cm, and ionic conductivity and this represents one of the main reasons why this CP is so explored with OECTs, in addition to its stability in a large pH range, which makes it appropriate for applications in enzymatic sensing in neutral environments, for example (STRAKOSAS, BONGO, and OWENS, 2015; BAI et al., 2019; KIM et al., 2018; YANG et al., 2018).

Figure 2.4: Molecular structure of PEDOT:PSS.

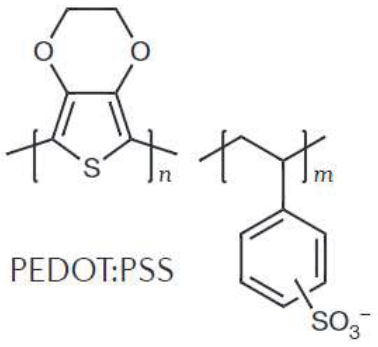

SOURCE: Rivnay et al. (2018).

PEDOT:PSS OECTs work in depletion mode, which means that a hole current is established at the channel upon an applied drain voltage. In this case, when a positive gate voltage is applied, cations (M^+) from the electrolyte are pushed into the PEDOT:PSS to de-dope it by compensating the PSS^- charges and, therefore, the holes being drained are not replenished and I_{DS} decreases (ATHANASIOU et al., 2019; TARABELLA et al., 2010; KAPHLE et al., 2020; BAI et al., 2019).

As this material operates in depletion mode, the intrinsic doping results in high operating currents ($\sim$mA), which requires high V_{GS} to keep the OECT in the OFF state (Vth $\sim$ 0,8 V) (KEENE et al., 2020).

The doping/de-doping process is a reversible phenomenon, which means that in PEDOT:PSS OECTs when V_{GS} = 0 V the cations injected in the channel are removed from it and the PSS^- forms new ionic bonds with the PEDOT, oxidizing it back to its conductive state and recovering V_{GS} (BERNARDS et al., 2008).

A fact about PEDOT:PSS films is that they swell to double their initial thickness/volume when in aqueous environments (consequence of the PSS^- phase) and the cation transport happens in this swollen phase that is almost physically separated from the PEDOT backbone.

Savva, Wustoni and Inal (2019) explored the relationship between ion-to-electronic coupling and the thickness of PEDOT:PSS channels, and considered that for thicker films just a small quantity of cations compensate the PSS^- chains and the uptake of these ions results in more water molecules that are absorbed. The study shows that this process is not entirely reversible so the PEDOT:PSS film does not return to its original mass after the polarization bias is removed. For thinner films, on the other hand, the majority of the cations compensate the holes and then leave the material once the bias is reversed. The group reported that PEDOT:PSS swell up to 86% regardless of its original thickness due to the diffusion of water molecules and ions in the film (SAVVA, WUSTONI, INAL, 2019).

In this sense, it is important to consider that PEDOT:PSS is soluble in water and since OECT applications incite contact with aqueous environments, it is necessary to adapt the solution so it can be deposited without interfering in the performance of the devices. Adding 3-glycidoxypropyltrimethoxy (GOPS) crosslinker provides better adhesion to substrates and prevents delamination of the film when in contact with aqueous solutions. While the GOPS makes the PEDOT:PSS more resistant to delamination, it still presents swelling and a drop in the conductivity of the polymer, in the order of 300 S/cm (STRAKOSAS, BONGO, and OWENS, 2015). To improve the conductivity of the films after adding the GOPS component, it is possible to adopt Ethylene Glycol (EG) (RIVNAY et al., 2018).

Also, it is possible to add Dodecylbenzenesulfonic Acid (DBSA) to the PEDOT:PSS solution to improve the adhesion of the film to the substrate (KHODAGHOLY et al., 2013).

2.2.2 Device Geometry

The device performance is also influenced by the thickness of the channel, especially due to its impact on ion-exchange happening throughout the volume of the channel and in the charge transport, meaning that the transconductance is proportional to the channel thickness so to achieve high transconductance values, one can increase the channel thickness (KUMAR et al., 2015; POLYRAVAS et al., 2020).

Friedlein et al. (2018) discussed the influence of the geometry of the channel on the performance of OECTs and concluded that the transconductance in these devices is directly proportional to the $W \times d/L$ ratio (W stands for the width of the channel, d the thickness, and L the length) resulting from the electrochemical doping/de-doping throughout the volume of the conducting channel. Thus, this property allows the design of high-transconductance OECTs without

interfering in the footprint of the devices (FRIEDLEIN et al., 2018).

Khodagholy et al. (2013) demonstrated a flexible PEDOT:PSS OECT, in Figure 2.5a, with a well definied channel and high values of transconductance in the order of 2.7 mS @ V_{GS} = 0.275 V. The transfer and transconductance curves found in Figure 2.5b show three main characteristics of PEDOT:PSS OECTs, which are the drain current in the range of mA, the depletion mode behavior and the bell-shaped transconductance curve that clearly indicates the gm_{max} value (KHODAGHOLY et al., 2013).

Figure 2.5: (a) Microscopic view of the OECT channel with a patterned PEDOT:PSS well. It is possible to see the overlap of the channel upon the Source and Drain electrodes; (b) Transfer and Transconductance curves for PEDOT:PSS OECTs. It is important to highlight the bell-shaped *gm* curve, which is a typical characteristic of these devices.

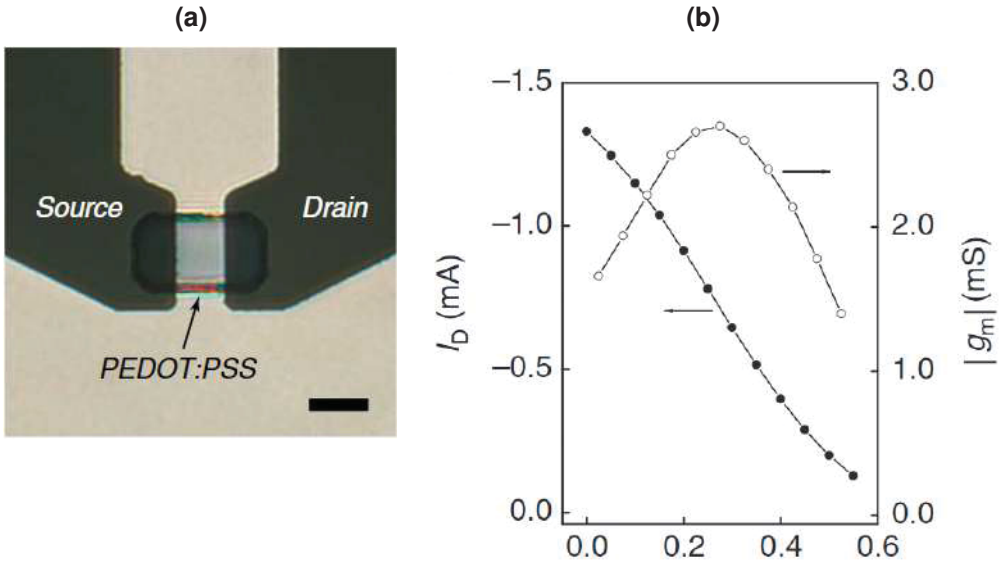

SOURCE: Khodagholy et al. (2013).

The authors confirmed that as the frequency increases, the transconductance as well as the injected ion charge, both shown in Figure 2.6a, decrease. The group also proved that thinner PEDOT:PSS films promote faster time responses since fewer ions are necessary to de-dope the material, however, as affirmed by Polyravas et al. (2020), thinner films also result in lower values of transconductance (KHODAGHOLY et al., 2013).

Rivnay et al. (2013) reported PEDOT:PSS OECTs with maximum transconductance @ V_{GS} = 0 V by exploring the transfer characteristics of the devices. To achieve the final gm_{max} = 2 mS, the influence of channel geometry on the OECT performance was investigated through the variation of design parameters such as W/L and the thickness of the CP. By keeping constant thickness and increasing W/L, larger values of *gm* were achieved, while increasing the thickness of the channel provides higher *gm* and higher V_{GS} *(*gm_{max}*)*. Besides, as seen in Figure 2.6b and Figure 2.6d, the paper describes an increase in I_{DSon} when the W/L ratio is increased and so the V_{GS} *(*gm_{max}*)*. With this, the authors concluded that modifying the channel geometry is an effective method to

tune the V_{GS} in which gm_{max} is obtained. Figure 2.6c shows the trends in device performance for the fabricated OECTs and allows the combination of design parameters that can be used to achieve gm_{max} @ V_{GS} = 0 V (RIVNAY et al., 2013).

In both Khodagholy et al. (2013) and Rivnay et al. (2013) works the basic structure of the OECTs consist of a double Parylene-C (PaC) layer, in which the first is usually employed as a protective layer and the second represents a sacrificial layer used to pattern the conductive channel. Most of the reports, some are listed in Table 2.1, in the literature, adopt the PaC sacrificial layer to define the CP well, but there are works, such as Zhang et al. (2016) and Wang et al. (2018), that use a three-step photolithography process to achieve the same effect as the PaC mechanical lift-off technique (KHODAGHOLY et al., 2013; RIVNAY et al., 2013; BERNARDS, MALLIARAS, 2007; ZHANG et al., 2016; WANG et al., 2018).

Figure 2.6: (a) Frequency depence of the transconductance in OECTs. The left axis depicts (square shaped points) *gm* decreasing as the frequency increases; (b) Transfer curve for a PEDOT:PSS OECT with 140 nm channel thickness. Each curve represents a different channel geometry: W (μm)/ L (μm) = 100/10, 50/25, 25/50, 10/100 from green to blue (top to bottom); (c) V_{GS} necessary to achieve gm_{max} in function of channel geometry and thickness. The colors depict the gm values; (d) Transconductance curve for a PEDOT:PSS OECT with 140 nm channel thickness. Each curve represents a different channel geometry: W (μm)/ L (μm) = 100/10, 50/25, 25/50, 10/100 from green to blue (top to bottom).

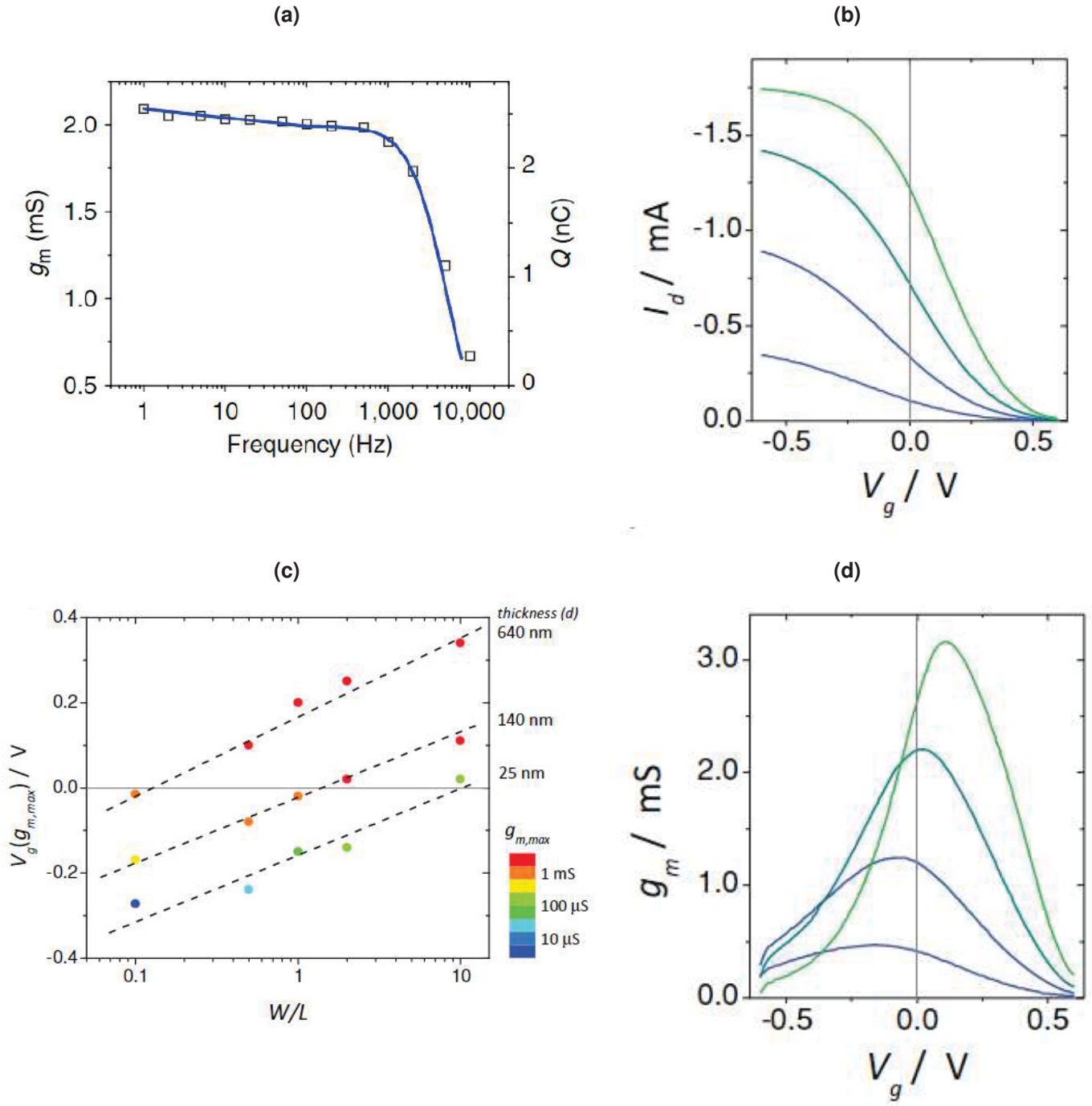

SOURCE: Khodagholy et al. (2013) and Rivnay et al. (2013).

In addition, Kumar et al. (2015) investigated the effect of the thickness of the channel (500, 180, 110, and 50 nm) and the composition of the electrolyte (0.01 M NaCl and 0.001 M CTAB) upon the performance of PEDOT:PSS OECTs. As seen in Table 2.1, commonly used electrolytes are Sodium Chloride (NaCl (aq.)), Potassium Chloride (KCl (aq.)) and Phosphate Buffered Saline (PBS) (STRAKOSAS, BONGO, OWENS, 2015). The group reported increases in the conductivity

of the CP as the thickness of the film increased, from $\sim$300 S$\times$cm^{-1} ($\sim$50 nm) to $\sim$450 S$\times$ cm^{-1} ($\sim$110 nm), which corresponds to a transition from percolation to bulk-like transport. On the other hand, thicker films were proven to have lower electronic resistance than thinner films. Furthermore, the volumetric capacitance (C*) is higher for thinner films and translates to a more effective doping/de-doping process (KUMAR et al., 2015).

Also, Polyravas et al. (2020) investigated the influence of the channel thickness on the noise characteristics of PEDOT:PSS OECTs, and reported the following conclusions: (i) although the transconductance increases with the channel thickness, the cut-off frequency decreases (998 Hz @ $\sim$140 nm to 138 Hz @ $\sim$1330 nm); (ii) the relative noise of the device decreases with increasing channel thickness; (iii) The root-mean-square voltage (V_{rms}), which quantifies the minimum voltage that can be detected by the transistor, decreases as the gm increases (hence increasing of the thickness) (POLYRAVAS et al, 2020).

Table 2.1: List of reports on the OECT topic. Where PT stands for Photolithography and PDMS is Poly(dimethylsiloxane).

Literature	Device	Substrate	Metallic Layers	Protect. Layer	Channel Composition	Channel Patterning	Electrolyte	Gate
Khodagholy et al. (2013)	Flexible OECT	PaC	Titanium (Ti) + Gold (Au)	PaC	PEDOT:PSS + EG + DBSA	PaC Lift-off	0.1 M NaCl	Ag/AgCl wire
Rivnay et al. (2013)	Arrays of Transistors	Glass	Chromium (Cr) + Au	PaC	PEDOT:PSS + EG + GOPS + DBSA	PaC Lift-off	0.1 M NaCl	Ag/AgCl pellet
Spyropoulos, Gelinas and Khodagholy (2019)	Flexible and Biocompatible OECT	Quartz	Ti + Au	PaC	PEDOT:PSS + D-sorbitol + GOPS + DBSA	PaC Lift-off	PBS	Ag/AgCl
Cicoira et al. (2010)	H_2O_2 Sensor (OECT)	Glass	Pt	PaC	PEDOT:PSS + EG + DBSA	PaC Lift-off	0.1 M NaCl	Ag/AgCl wire
Leleux et al.(2014)	Electrophysiological App. (OECT)	Glass	Ti + Au	PaC	PEDOT:PSS + EG + DBSA + GOPS	PaC Lift-off	0.1 M NaCl	Ag/AgCl wire
Gkoupidenis et al. (2015)	Neuromorphic App. (OECT)	Glass	Cr + Au	PaC	PEDOT:PSS + EG + DBSA + GOPS	PaC Lift-off	0.1 M KCl	PEDOT:PSS
Khodagholy et al. (2011)	OECT arrays	Glass	Ti + Au	PaC	PEDOT:PSS + EG + DBSA + GOPS	PaC Lift-off	PBS	Pt wire
Sessolo et al. (2014)	Ion Sensitive OECTs	Glass	Cr + Au	PaC	PEDOT:PSS + EG + DBSA + GOPS	PaC Lift-off	0.1 M KCl	Ag/AgCl

(To be continued)

Table 2.2: List of reports on the OECT topic. Where PT stands for Photolithography and PDMS is Poly(dimethylsiloxane).

(Continuation)

Literature	Device	Substrate	Metallic Layers	Protect. Layer	Channel Composition	Channel Patterning	Electrolyte	Gate
Inal et al. (2014)	Accumulation Mode OECT	Glass	Au	PaC	PTHS + DI Water + GOPS + EG	PaC Lift-off	0.1 M NaCl	Ag/AgCl pellet
Venkatraman et al. (2018)	OECT for biosignal amplification	Glass	Cr + Au	PaC	p(g2T-TT) +$CHCl_3$ and PEDOT:PSS + EG + GOPS + DBSA	PaC Lift-off	0.1 M NaCl	Ag/AgCl pellet
Rivnay et al. (2015)	OECT	-	Au	PaC	PEDOT:PSS + EG + DBSA + GOPS	PaC Lift-off	0.1 M NaCl	Ag/AgCl pellet
Donahue et al. (2018)	Vertical OECT	Glass	Cr + Au	PaC	PEDOT:PSS + EG + DBSA + GOPS	PaC Lift-off	0.1 M NaCl	Ag/AgCl pellet
Wustoni et al. (2019)	OECT for Metal Cations Detection	Glass	Cr + Au	PaC	PEDOT:PSS + EG + DBSA + GOPS	PaC Lift-off	10 mM NaCl and 10 mM KCl	Functinalized Polymers
Rashid, Ciechowski and Rivnay (2020)	Laser Cut OECTs	Glass and PaC	Cr + Au	PaC	PEDOT:PSS + EG + DBSA + GOPS	Teflon AF 2400 + Laser Cutter	0.1 M NaCl	Ag/AgCl pellet
Savva et al. (2019)	OECTs	Glass	Cr + Au	PaC	p(g2T-TT)	PaC Lift-off	$\neq$ Conc. of NaCl	Ag/AgCl pellet

SOURCE: The author

Figure 2.7 shows a typical characteristic of PEDOT:PSS OECTs, which is the bell-shaped transconductance curves. In this case, Polyravas et al. (2020) proved the theory stated by Kumar et al. (2015) that the gm in OECTs is proportional to the channel thickness. As seen in Figure 2.7, as the thickness increases, the values of *gm* also increase, resulting in *gm* = 22.8 mS (@ $\sim$ 1330 nm), which is 10.5 times and 3.8 times higher than the transconductance at $\sim$ 140 nm and $\sim$315 nm, respectively (POLYRAVAS et al., 2020).

Figure 2.7: Transconductance in function of gate voltage in OECTs with different channel thickness.

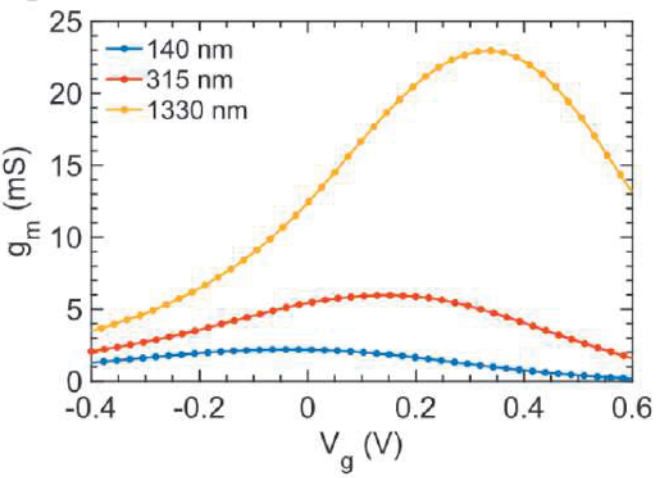

SOURCE: Polyravas et al. (2020).

2.2.3 Influence of the Electrolyte

As ionic sensors, OECTs rely on the role of the electrolyte to affect device performance, especially because the ion concentration affects the drain current. Strakosas, Bongo, and Owens (2015) reported that with an increase in the concentration of a KCl electrolyte, there is a shift in the transfer curve of a PEDOT:PSS OECT to lower values of V_{GS}. This behavior is explained from the ionic circuit point-of-view, in which the increase in ion concentration leads to a higher ionic charge at the interface with the PEDOT:PSS that shifts the effective gate voltage ($V_{GS,eff}$) to higher values and de-dopes the channel (STRAKOSAS, BONGO, OWENS, 2015).

Savva et al. (2019) discussed the effect of water on the behavior of p(g2T-TT) OECTs, especially when exposed to different concentrations of NaCl (aq.) solutions. As the concentration of the electrolyte decreases, the hydration of the dopant anion (Cl^-) increases, which allows the study of the channel hydration on OECT operation. On the other hand, the water uptake also brings disadvantages, such as speed limitations regarding switching of the devices and affects the reversibility of the doping process (SAVVA et al., 2019).

The p(g2T-TT) films were characterized in four concentrations of NaCl (aq.) solutions (10 mM, 100 mM, 1 M and 6 M). The authors determined that as the concentration increased the hydration

shell around the anions and the quantity of water molecules in the electrolyte decrease (SAVVA et al., 2019).

Ion solvation refers to the mechanisms in which ions are surrounded and stabilized by solvent molecules, forming a solvation shell. The size of the ion can influence its solvation, meaning that larger ions present higher solvation shells, while smaller ions have smaller solvation shells. In this context, the size of the ion also plays a crucial role in its mobility, in which smaller ions exhibit higher mobilities since they can move more freely (ANGARITA-GOMEZ AND BALBUENA, 2022).

The influence of the electrolyte concentration in OECT performance is seen in Figure 2.8, where (a) depicts the I_{DS} response while (b) exhibits the *gm* behavior. The drain current intensities are more negative for more concentrated electrolytes and there is a shift in V_{th}, which indicates that a larger potential is required to induce ion injection in the channel (SAVVA et al., 2019).

Figure 2.8: (a) I_{DS} and (b) *gm* in function of electrolyte concentration.

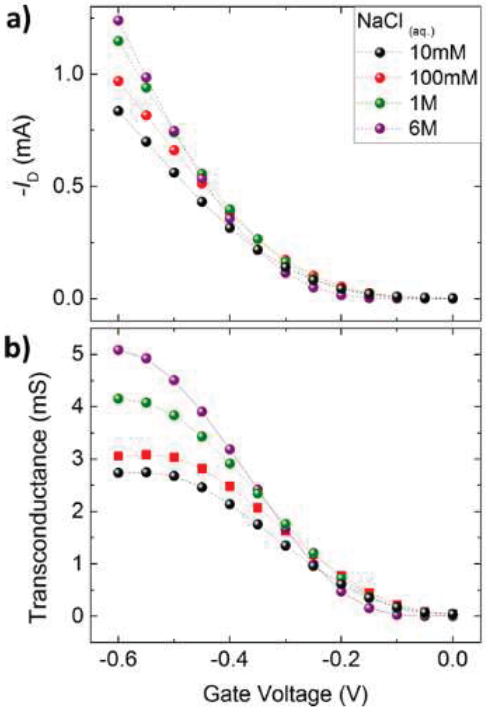

SOURCE: Savva et al. (2019).

In addition, Flagg et al. (2018) and Cendra et al. (2018) reported the influence of the electrolyte composition in P3HT and p(g2T-TT) OECTs, and detailed how performance parameters depend on the anions found in the electrolyte.

As seen in Figure 2.9a, I_{DS} increases in the order KF $>$ KCl $>$ KBr $>$ $KClO_4$ $>$ KPF_6 $>$ KTFSI, while V_{th} decreases in the following order KTFSI $>$ KPF_6 $>$ $KClO_4$ $>$ KBr $>$ KCl $>$ KF, which indicates that the use of larger molecular, Figure 2.9c, anions leads to lower V_{th} values and higher I_{DS} magnitudes and, also the doping level reaches higher levels (FLAGG et al. 2018; FLAGG et al. 2019).

Furthermore, Flagg et al. (2018) concluded that smaller/slightly polarizable anions present

solvation shells with $\sim$ 10 water molecules, whereas larger/ highly polarizible anions exhibits fewer water molecules, which results in faster doping rates (FLAGG et al., 2018).

Figure 2.9: (a) Anion dependent P3HT OECT; (b) Anion depedent p(g2T-TT) OECT.

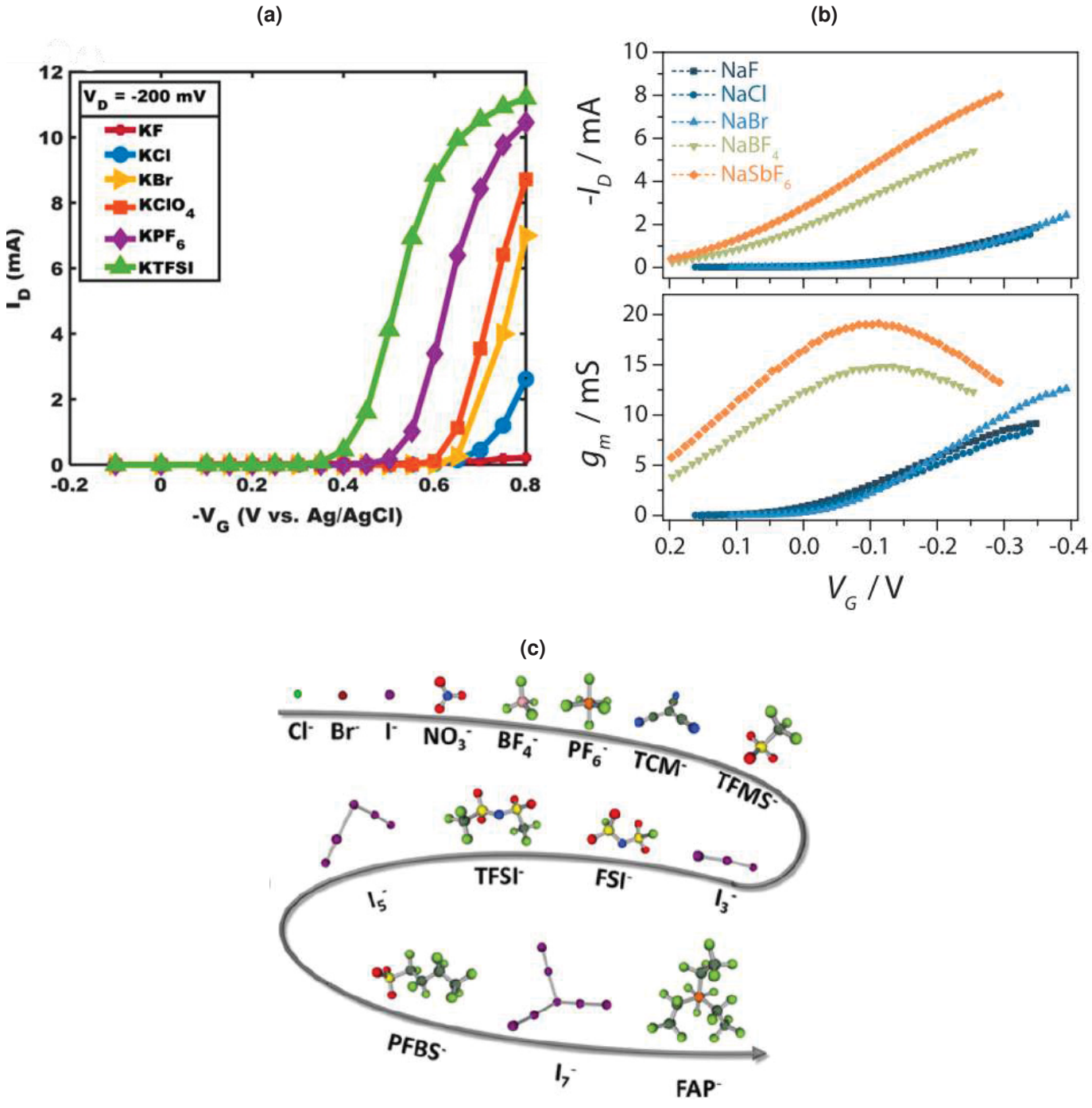

SOURCE: Flagg et al. (2018), Cendra et al.(2018), and Abe, Tsuzuki and Ozawa (2018).

Ultimately, Cendra et al. (2018) tested p(g2T-TT) devices in different aqueous electrolytes in the same concentration (NaF, NaCl, NaBr, $NaBF_4$, and $NaSbF_6$). It is possible to verify in Figure 2.9b that the performance parameters tend to present higher values when larger anions, Figure 2.9c, are adopted in the electrolyte.

One of the disadvantages of OECTs is their low switching speed derived from the low mobility of ions in the electrolyte and the speed of the redox reactions. The time response can be ruled

both by the ionic circuit or by the electronic circuit, but is most commonly influenced by the ionic circuit. The ion injection into the channel can be represented by a capacitance found between the gate electrode and the active layer, therefore, the model for the transient behavior of OECTs implies that the time response, to a change in V_{GS}, is based on an R*C time constant (HUTTER et al. 2013; RIVNAY et al., 2018; FRIEDLEIN et al., 2018; KAPHLE et al., 2020).

Hutter et al. (2015) reported that faster response times can be obtained in printed biosensors by decreasing the length of the source-drain line (HUTTER et al. 2013).

As for the composition of the electrolyte, Kumar et al. (2015) have proved that the ON/OFF ratios are higher for devices tested with Hexadecyl Trimethyl Ammonium Bromide (CTAB) and for those with NaCl, as an example of $\sim$50 for CTAB in contrast to $\sim$1.0 for NaCl, both for 474$\pm$90 nm thick films. However, the CTAB presents a slower doping/de-doping process due to lower ion conductivity ($\sim$0.1 mS/cm for CTAB and $\sim$2.0 mS/cm for NaCl) (KUMAR et al., 2015).

To support the information that using CTAB as an electrolyte would result in slower time responses, Kumar et al. (2015) estimated time constants, as proposed by Bernards and Malliaras (2007), τ = RC for the doping/de-doping of PEDOT:PSS, τ $\sim$0.8 s in NaCl and $\sim$1.7 s in CTAB, and τ $\sim$2.4 s in NaCl and $\sim$5.0 s in CTAB for 50 nm and 500 nm thickness, respectively. However, these results also showed that the doping/de-doping processes, in the presence of bulky ion, is slower for thicker films (KUMAR et al., 2015; BERNARDS, MALLIARAS, 2007).

The nature of the electrolyte (liquid, gel, or solid) and the ion concentration influence the response time of the transistor due to the electrolyte conductivity, which determines the resistor of the ionic circuit. OECTs with liquid electrolytes present time responses of tens of ms, which is appropriate for most biosensors and electrophysiological recording applications while gel or solid electrolytes present an even slower response, which indicates that devices with such electrolytes need to be employed where rapid responses are not necessary (BAI et al., 2019; RIVNAY et al., 2018).

In addition, it is important to pay attention to the working frequency of OECTs, especially due to ion mobility that renders a slower time response to these devices. At the same time, at low frequencies, the ions have time to drift throughout the volume of the channel, while at frequencies above the ion frequency (f_{ion}), only a part of the channel is upon doping/de-doping since the ions do not travel through the whole channel depth, meaning that at higher frequencies, the ions do not penetrate entirely into the semiconductor and the OECT shows FET behavior (FRIEDLEIN et al., 2018).

Not only does the nature of the electrolyte influence the active layer, but the polymer swelling has a direct relationship with ion transport, since it can enhance ion diffusion. Even though the swelling can hinder the electronic charge percolation, it impulses ion diffusion throughout the whole volume of the polymer and facilitates ion stabilizing nearby electronic charges (WU et al.,

2022). Overall, the electrolyte and the active layer have an important relationship to OECT operation, where the electrolyte controls the response of the active layer, which enables the functioning of OECTs (RASHID et al., 2022).

2.2.4 Influence of the Gate Electrode and Other Parameters

Strakosas, Bongo, and Owens (2015) attested that the size of the gate influences directly the sensitivity of OECTs applied to enzymatic biosensors, the smaller the gate electrode, the higher the sensitivity. This phenomenon can be explained by the voltage drop at the gate/electrolyte and electrolyte/channel interfaces. In the case of a gate electrode that is much bigger than the conducting channel, the drop is negligible. Also, OECTs that present small gates have smaller background noise and show improved sensibility (STRAKOSAS, BONGO, and OWENS, 2015; BAI et al., 2019).

The gate voltage drop across the channel is influenced not only by the geometry of the gate electrode but also by its nature. When polarizable electrodes, such as platinum (Pt) and gold (Au) are adopted as the gate, two capacitors are formed in the ionic circuit, the first is found on the electrical double layer at the gate/electrolyte interface and the second is the volumetric capacitance of the channel. Since both capacitors are in series, the voltage drops on the smaller capacitor, therefore, the capacitance at the gate electrode must be at least ten times larger than the capacitance of the channel, which means that for polarizable electrode materials, the gate must present a large area to operate efficiently (OHAYON, DRUET, INAL, 2023).

On the other hand, non-polarizable gates, such as silver-silver chloride (Ag/AgCl), enable negligible voltage drops at the gate/electrolyte interface. Therefore, the materials choice or size of the gate can span device properties, including the extent of gating and the transient response time (RIVNAY et al., 2018; BERNARDS, MALLIARAS, 2007).

Paterson et al. (2015) studied the influence of contact resistance (Rc) on accumulation mode N-type OECTs and determined that Rc has an impact, but is not dominant over the device. Accordingly, Rc responds to the potential applied to the gate through two regimens, while at low V_{GS} the contact resistance presents influence over the operation of the transistor, at high V_{GS} the ionic doping compensates for Rc (PATERSON et al., 2015).

Friedlein et al. (2018) also studied the effect of parasite resistance on the performance of the OECTs and reported inaccuracy in material parameters such as threshold voltage and carrier mobility in addition to affecting the transconductance and distorting output and transfer curves. One of the strategies to avoid the effects of parasitic resistance on the transconductance, whether being reduction of values or shifting of the peak to more positive V_{GS}, is to design devices with higher channel resistance so the series resistance has a small contribution to the total resistance.

Another option is to conduct gated four-point probe measurements, which are not influenced by line resistance and contact resistance (FRIEDLEIN et al., 2018).

2.3 DEVICE STABILITY

Regarding device stability, there are two main approaches that are commonly adopted to characterize OECTs, them being immersion and electrical stress stability. Kim et al. (2018) tested PEDOT:PSS OECTs in both ways, at first immersing the devices in a 0.1 M NaCl electrolyte for 21 days. Figure 2.10a depicts the transfer curves for crystalline PEDOT:PSS (Crys-P) and PEDOT:PSS with ethylene glycol (EP-P) for the immersion period, while Figure 2.10b exhibits the *gm* behavior for each active layer (KIM et al., 2018).

As the results suggest, the crystalline PEDOT:PSS did not suffer significative variations in its ON drain current, while the EG-P samples presented a drop of approximately 50% in I_{DSon} and its maximum transconductance dropped 49% from day 0 to day 21. The authors concluded that the degradation in the EG-P transistors is caused by the swelling of the film (thickness increased in 220%), which could lead to a decrease in the channel conductivity (KIM et al., 2018).

Figure 2.10: (a) Transfer curves acquired for crystalline PEDOT:PSS and PEDOT:PSS with the addition of ethylene glycol; (b) transconductance response during the immersion period; (c) ON/OFF behavior of the PEDOT:PSS devices during a electrical-stress stability test (V_{GS} switching up to 2000 cycles).

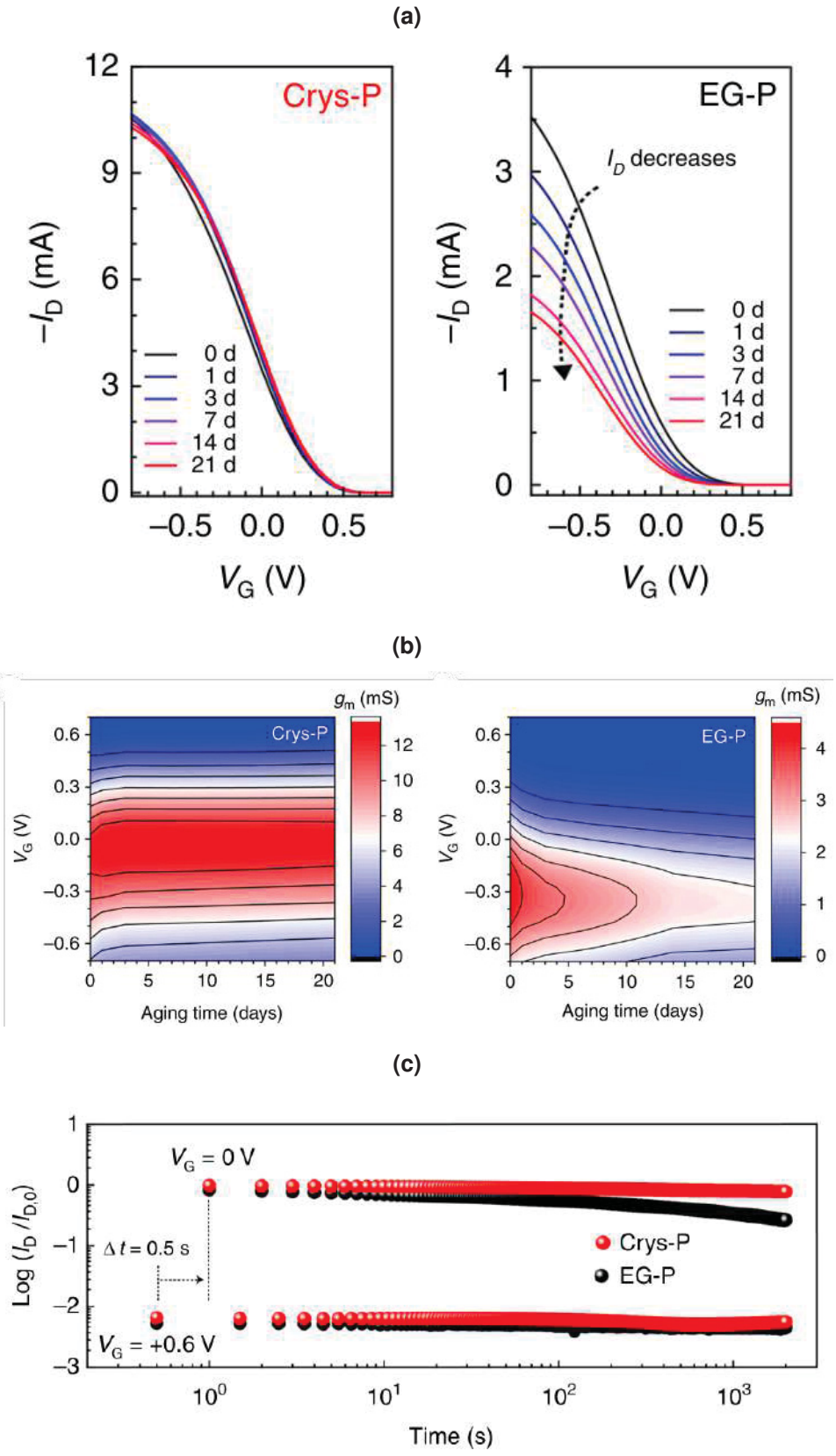

SOURCE: Kim et al. (2018).

Figure 2.10c presents the response of PEDOT:PSS OECTs to the electrical stress stability test, which occured through repeated gate bias switching on and off. The Crys-P device exhibited

stable I_{DSon} and I_{DSoff} values after the 2000 cycles ($\sim$ 25% variation) in comparison with the EG-P transistors that presented a larger drop in the current intensities ($\sim$ 75% variation). This behavior suggestd that the EG-P OECTs are more susceptible to repeated bias switching under water immersion for long periods(KIM et al., 2018).

In this context, Zhang et al. (2016) also studied the effects of immersion in PEDOT:PSS OECTs, however, the report discussed the influence of the adopted substrate on film delamination. The films were deposited in polyethylene terephthalate (PET) (no GOPS added to the solution) and glass (PEDOT:PSS + GOPS) substrates and, were immersed in aqueous milieux for 3 months (ZHANG et al., 2016).

Figure 2.11 presents the results of the immersion stability tests with PEDOT:PSS on glass and PET substrates. Films that do not contain GOPS delaminate after 1 day in water, whereas those containing GOPS delaminate after 3-months. Films on PET do not delaminate even after 3-month in DI water or PBS (ZHANG et al., 2016).

Figure 2.11: PEDOT:PSS films on glass and PET substrates after solvent immersion. (a) PEDOT:PSS on glass after after 1 day in DI water; (b)PEDOT:PSS on glass after after 3-months in DI water;(c) PEDOT:PSS on PET after 3-months in PBS; and (d) DI water.

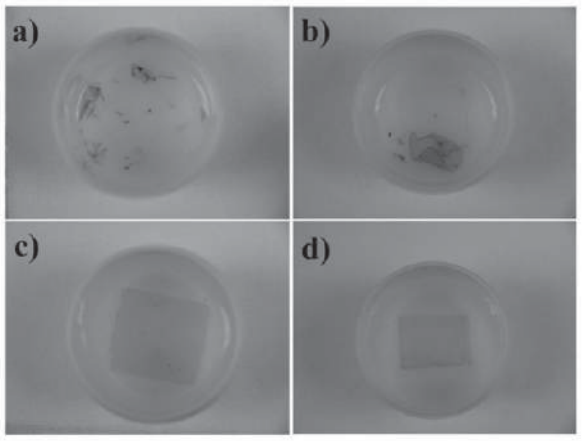

SOURCE: Zhang et al. (2016).

Furthermore, Giovannitti et al. (2016) demonstrated electrical stress stability tests for N-type OECTs characterized in a 0.1 M NaCl aqueous electrolyte during 5 minutes, as verified in Figure 2.12.a, and 2 hours experiments, Figure 2.12.b. As seen, the device maintained its perfomance for both tests and only presented signs of degradation gate potentitals higher than 0.5 V were applied (GIOVANNITTI et al., 2016).

Figure 2.12: Response of N-type OECTs to gate switching for a (a) 5 minute period and (b) a 2 hour time span.

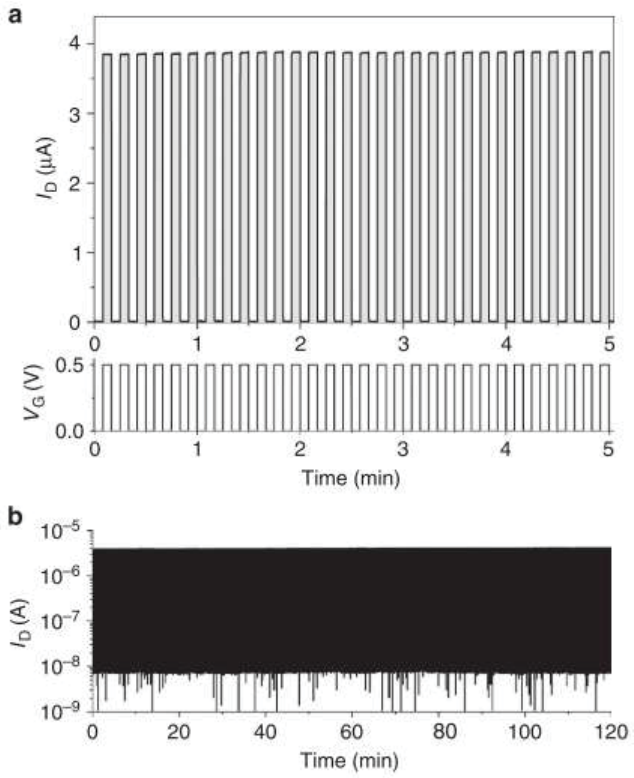

SOURCE: Giovannitti et al. (2016).

Moser et al. (2020) reported the electrical stress stability of OECTs fabricated with p(g3T2), Figure 2.13.a, p(g2T2-g4T2), Figure 2.13.b, p(g1T2-g5T2), Figure 2.13.c, and p(g0T2-g6T2), Figure 2.13.d, over 2 hours of continuous cycling ($\sim$ 700 cycles) (MOSER et al., 2020).

Figure 2.13: Electrical stress stability for (a) p(g3T2), (b) p(g2T2-g4T2), (c) p(g1T2-g5T2), and (d) p(g0T2-g6T2) over 700 swqitching cycles.

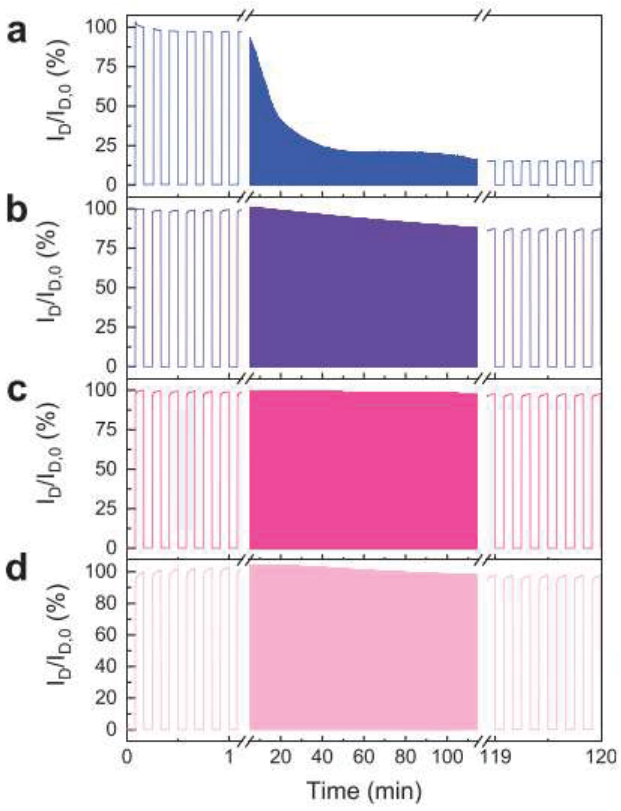

SOURCE: Moser et al. (2020).

The stability of the devices tested varied from a 85% drop in the drain current for p(g3T2) to 13%, 2% and 2% drops for p(g2T2-g4T2), p(g1T2-g5T2), and p(g0T2-g6T2), respectively. The difference among the devices can be an indication of the swelling properties of the films, in which the devices that presented less swelling are more stable. Films that exhibited larger volumetric expansion also lead to more morphological changes in the material that are detrimental to OECT performance (MOSER et al., 2020).

Under these circumstances, there are two important factors to consider during materials choice for OECTs are the swelling and recovery characteristics of the polymer applied to the active layer. In organic bioelectronics, flexible/polar side chains are employed to add solubility or processability and to assist ion diffusion, being hydrophilic components, such as glycolated side chains the most common additions. This modification has been successful in P-type, N-Type and ambipolar OECTs, but often leads to sensitivity to environmental conditions, especially to humidity.

In this context, Nicolini et al. (2021) studied a mixed conductor that presented hydroxylated alkyl side chains poly[3-(6-hydroxy)hexyl thiophene] (P3HHT), which presented potential for application in OECTs since it exhibited low-swelling abilities (NICOLINI et al., 2021).

At first, $\sim$92 nm P3HHT films were exposed a 0.1 mol/L KCl electrolyte to analyze their swelling behavior and compare them to other polymers. The P3HHT samples exhibited a small variation (2.4%) in thickness, as depicted in Figure 2.14a, while polymers, such as p(g2T-TT) and PE-

DOT:PSS presented changes in the order of 15% and 85% under the same conditions. These results suggest that the P3HHT posseses lower bulk hydrophilicity than PEDOT:PSS, for example (NICOLINI et al., 2021).

Nicolini et al. (2021) also concluded that P3HHT takes up less electrolyte and, in assays with applied potential to the film, the polymer presented an increase of less than 10% in its thickness and it fully restored to its initial state after the potential was removed (NICOLINI et al., 2021).

Figure 2.14: (a) Variation in the thickness of the P3HHT film; (b) μC* characteristics for P3HHT OECTs.

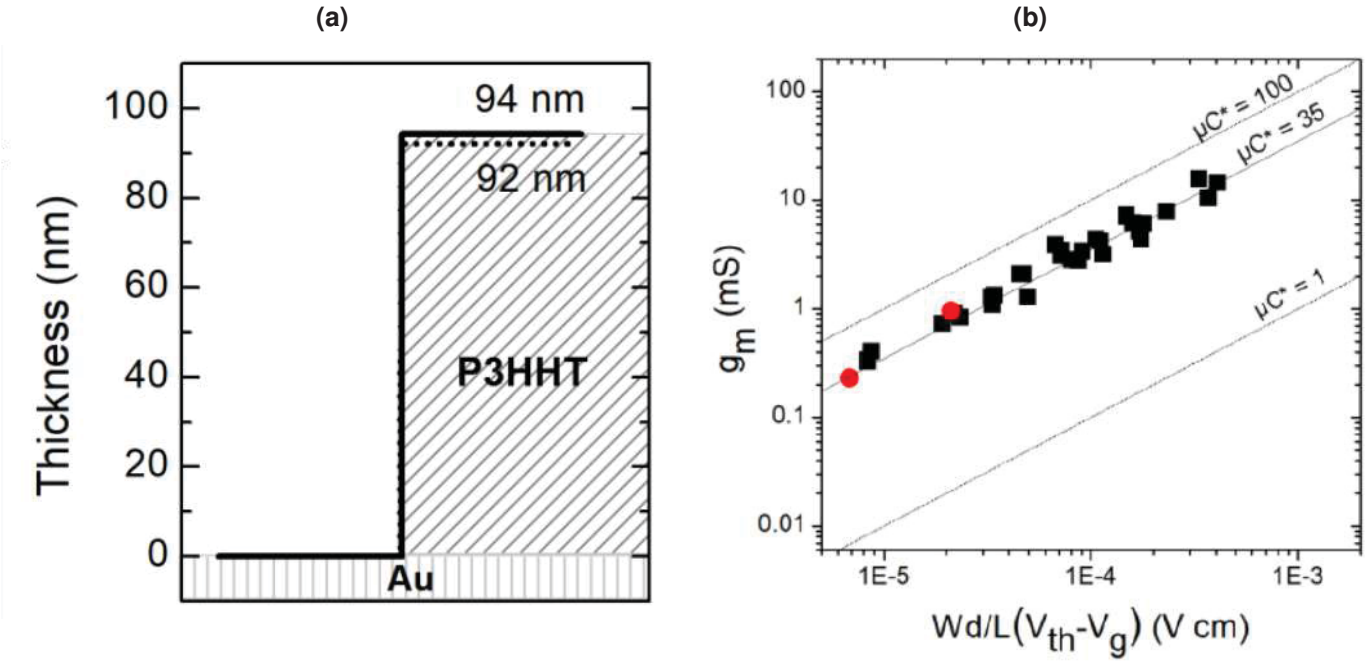

SOURCE: Nicolini et al. (2021).

Regarding application in OECTs, P3HHT presented low gate currents (I_{GS} = $\sim$ 1 nA) and a high ON/OFF ratio of 10^4. The fabricated devices also showed μC* characteristics, Figure 2.14b, of 35 F$\times$cm$^{-1}\times$V$^{-1}\times$s^{-1}, which is not significantly smaller than the intensity measured for PEDOT:PSS of 47 F$\times$cm$^{-1}\times$V$^{-1}\times$s^{-1} (NICOLINI et al., 2021).

2.4 CHAPTER CONCLUSIONS

This chapter presented examples of State-of-the-Art OECTs that have been recently reported. In addition, the working principle and figures of merit of these devices were explored, as well as the main factors that usually influence performance parameters, such as transconductance, drain current, cut-off frequency and ON/OFF ratio.

As much as the OECTs and the experimental methodology exhibit satisfatory results, there are properties that can be tuned by optimizing the active layer, geometry of the channel, electrolyte composition/concentration or, by making changes to the gate and trais of the devices.

In bioelectronic applications, good performances do not depend exclusively on the material used in the channel, it can be also determined by a variety of factors, including channel thickness, channel geometry, adopted electrolyte, long-term immersion stability, and stability to electrical stress.

3 EXPERIMENTAL METHODOLOGY FOR OECT FABRICATION AND CHARACTERIZATION

As seen in previous sections, the basic structure of an OECT consists of substrate, source and drain electrodes, conductive channel, protective layer, electrolyte, and gate electrode since, at first, the objective was to create a viable fabrication process for the proposed OECTs, from which essential fabrication parameters and techniques could be extracted and then, used in further steps on the project, the chosen structure for the proposed OECTs is depicted in 3.1.

Therefore, this chapter is dedicated to discussing the materials choice and development of the fabrication process used to create functioning OECTs.

Figure 3.1: Proposed strutucte for the OECTs.

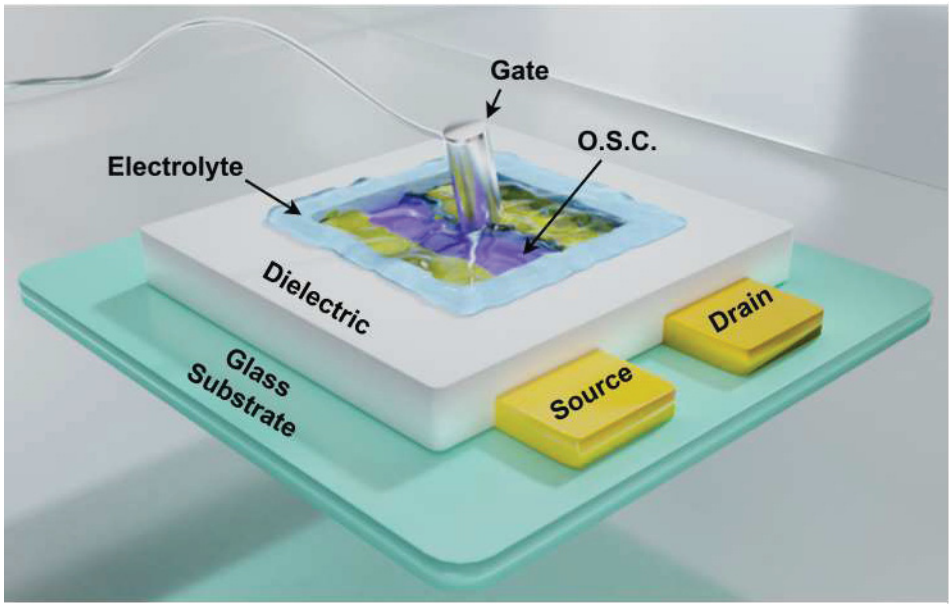

SOURCE: The author.

3.1 MATERIALS CHOICE

In view that the objective was to adopt a structure based on operational State-of-the-Art OECTs, and then adapt their processing to the materials and equipment available, the proposed transistors present a 4-inch borosilicate glass substrate, over which the adhesion (titanium) and metallic (gold) layers are deposited to pattern the trails, source and drain electrodes and, measurement pads. Once patterned, the device should present a protective layer (SU-8 2002), which was adapted from the normal PaC-2 protective and sacrificial layers commonly reported in the literature, to define the area where the conductive channel is positioned and isolate the rest of

the metallic contacts from the electrolyte. At last,the top components of the OECT are the aqueous electrolyte and an Ag/AgCl gate electrode. In this context, the following items list the elected materials and justify their choice.

- Borosilicate Glass: material commonly used as substrate for OECTs that are not flexible. It is important to consider the ion release from the glass into the system, especially because OECTs are sensible to them, in this case, borosilicate glass was chosen, but the ideal is to utilize non-alkaline glass, which is an expensive material. Borosilicate glass also has a higher chemical stability when in contact with water, chemicals or pharmaceuticals than ordinary window glasses (KOCH, RINKE, 2020).
- Titanium: commonly used adhesion layer for gold. Chosen mainly because of availability.
- Gold: good conductor and resistant to corrosion. Chosen due to availability. Also commonly applied to OECTs.
- Active Layer: as for the active layer, a group of polymers, doped and de-doped, was applied to the channel of the fabricated OECTs, among them are Magic Quebec, RGH-14, PEDOT:PSS in various forms, and P3HHT.
- SU-8 2002: SU-8 is a negative photoresist that after crosslink is resistant to most solvents, which means that, in this case, this resin could do two jobs, pattern the wells and openings and, isolate certain parts of the device.
- Ag/AgCl pellet: these electrodes are non-polarizible, which means there is no voltage drop in the interface between electrolyte and gate.

3.2 PHOTOLITHOGRAPHY

Before discussing the fabrication of the OECTs, it is important to review concepts regarding photolithography processes.

Photolithography is a microfabrication technique in which there is a structuring process of ceramic, metallic, organic, or semiconductor materials through photosensitive films, called photoresists. Usually, for applications in microelectronics, optics, or mechanics, this technique takes place on substrates such as silicon, quartz, or glass, mostly in form of wafers (KOCH AND RINKE, 2020).

Photolithography processes can include steps of deposition of the photoresist that be done by means of Spin Coating, Spray Coating, or Dip Coating, which is followed by a soft bake to dry the coated film, and subsequently, the main process of microstructuring takes place by the exposure

step. The exposure enables a chemical process that allows the resist to became more, in case of positive photoresists, or less, for negative photoresists, soluble to developer solutions (KOCH AND RINKE, 2020).

Another step in photolithographic processes is the post-exposure bake that can be complementary to the exposure or perform the crosslinking of some photoresists (KOCH, RINKE, 2020).

After exposure, the photoresist already presents a faded image of the desired patterning, but in order to completely fabricate the structure, it is necessary to dissolve the exposed (positive resists) or the unexposed (negative resists) areas of the film in a developer solution in a process called development (KOCH, RINKE, 2020).

It is important to highlight that photolithography is a technique that depends heavily on the elected photoresist, its thickness, and its purpose, therefore, the steps commented previously could vary along with the applied parameters (KOCH, RINKE, 2020).

3.3 FABRICATION PROCESS

The adopted fabrication process for the OECTs consists of four main phases, them being Conditioning, Photolithography 1, Photolithography 2, and Conducting Channel, which are depicted in Figure 3.2 and Figure 3.3 as an overview of the elected processing.

Figure 3.2: Flowchart of Phases 1 and 2 of the adopted fabrication process to obtain OECTs.

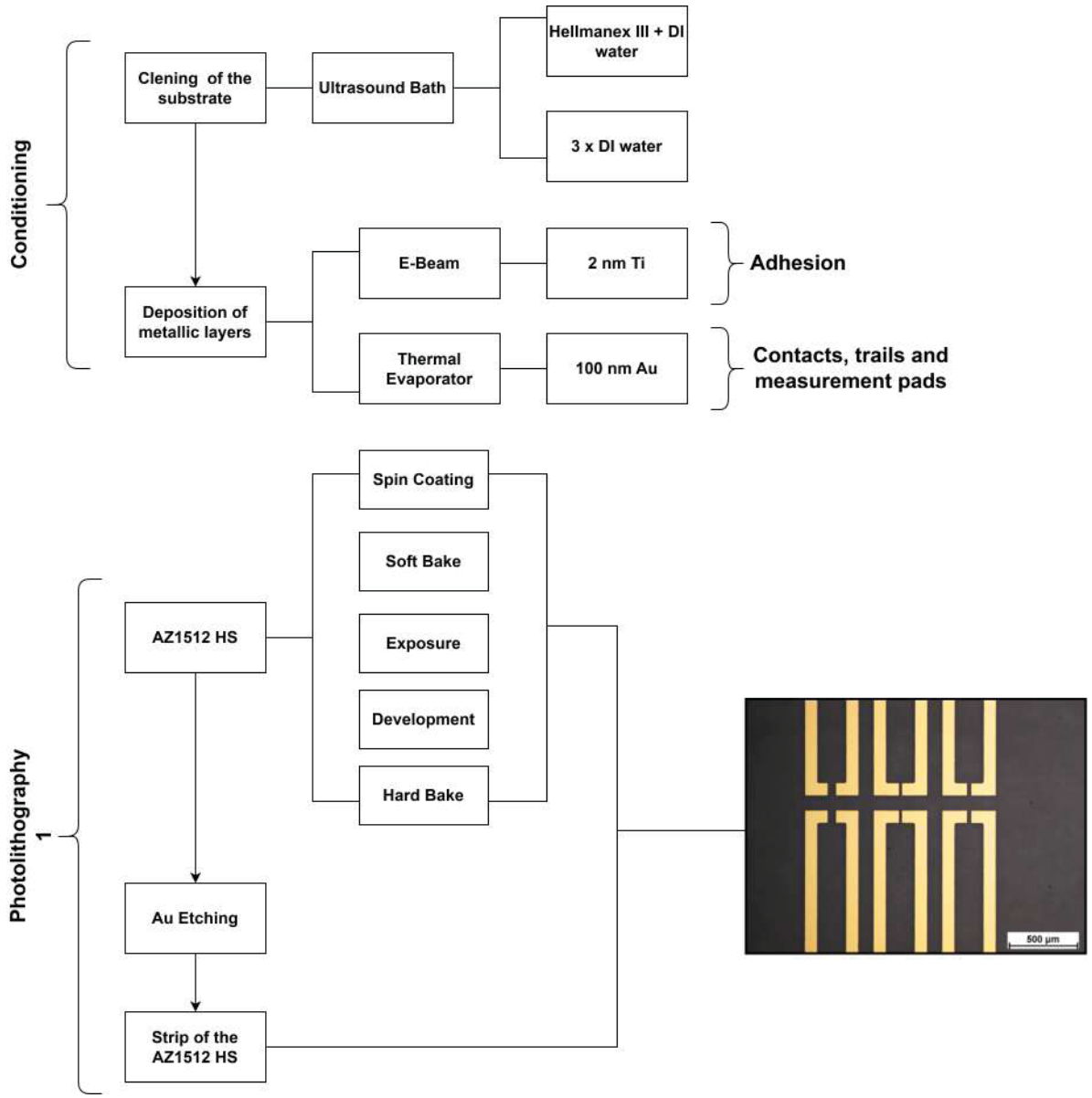

SOURCE: The author.

Figure 3.3: Flowchart of Phases 3 and 4 of the adopted fabrication process to obtain OECTs.

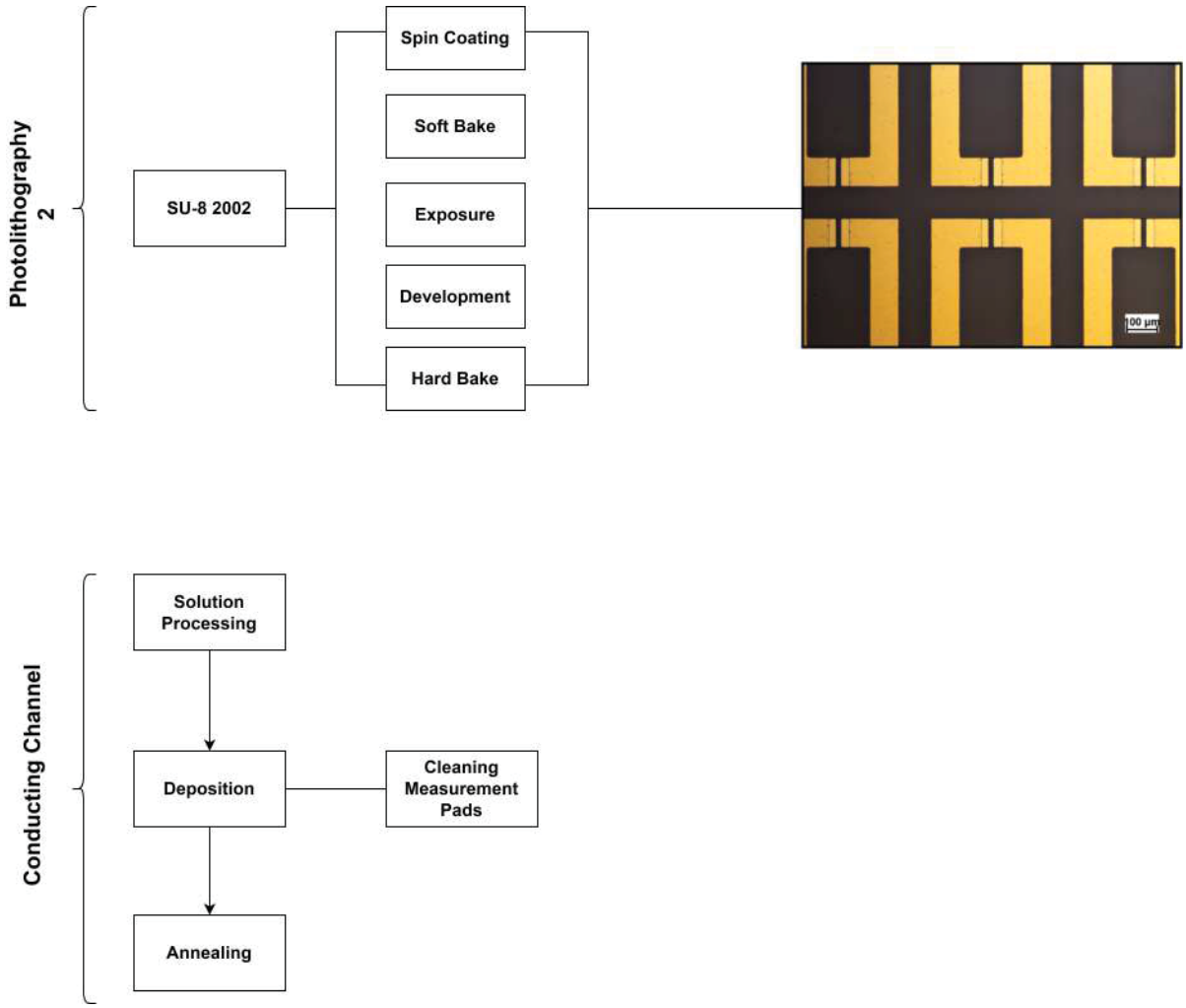

SOURCE: The author.

It is important to highlight that for each phase of photolithography a mask is necessary to enable the patterning through the UV exposure step. These masks were designed according to the desired structure of the devices, so for Photolithography 1, as illustrated in Figure 3.4a, the mask depicts the trails, contacts, and measurement pads for six OECTs in a 15 mm x 15 mm chip (called SET), and therefore, for a four-inch glass wafer substrate, it is possible to fabricate sixteen sets of six OECTs each. On the other hand, in Photolithography 2, the wells to accommodate the conducting channels are patterned, as seen in Figure 3.4b, and are positioned on top of the channel openings and a portion of the Source and Drain electrodes.

Figure 3.4: Masks used for (a) Photolithography 1 (b) Photolithography 2 in a set with different channel lengths (L = 50μm, 10μm and 20μm) and W = 100 μm. In the first mask it is possible to visualize the patterning of six OECTs, in which their channels gather at the center of the chip with a 100 μm horizontal spacing between the upper and lower sides.

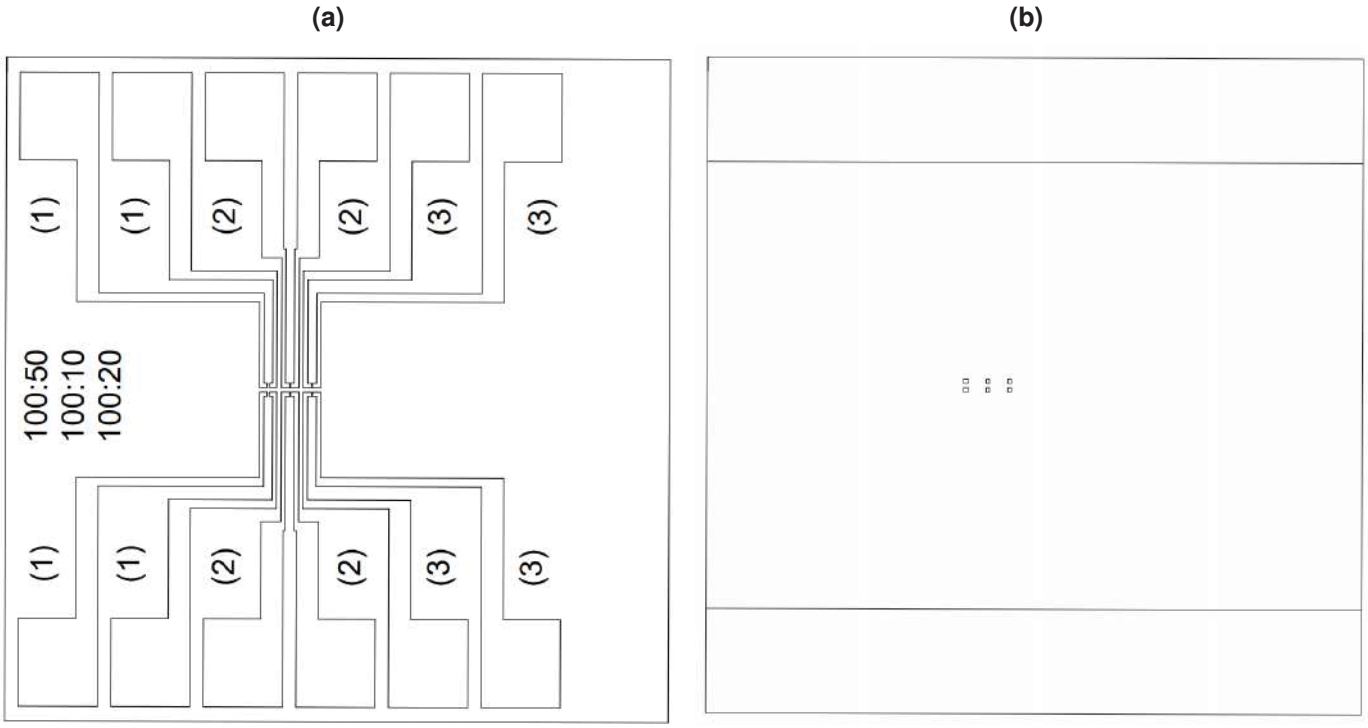

SOURCE: The Author.

The conditioning phase includes the cleaning of the substrates and deposition of the metallic layers, both titanium and gold, upon the whole surface of the glass wafers. By the end of the first step, the samples present a mirror-like appearance. As for the Photolithography 1 phase, the trails, measurement pads, and Source and Drain contacts are patterned by using an AZ1512 HS photoresist, a positive photoresist which becomes soluble when exposed to UV light, followed by the etching of the Au that is not protected by the resin. The result of this phase, after the stripping of the AZ1512 HS, is shown in the flowchart in Figure 3.2, in which it is possible to visualize six channel openings with different lengths (50 μm, 10 μm, and 20 μm), which are named Mixed Channel Sets. In addition to the Mixed Channel Sets, there are Fixed Channel Sets with 10 μm openings, each group represents eight out of the sixteen sets patterned in the glass wafer.

The decision to adopt a 2 nm Ti layer was backed up by etching and conductivity tests. Firstly, the adhesion layer had 5 nm, however, during Photolithography 1 the titanium was not etched, even after an hour of immersion in the etchant. Therefore, a concern regarding its effect on the final devices was raised, especially when it represented short circuit risks. For that reason, a conductivity test was conducted to determine if the Ti layer was thin enough not to be conductive, and through a 4-probe setup, the final resistance of the film resulted in 1.36 kΩ, which does not represent a fully insulating layer. In this context, the thickness of the film decreased to 2 nm to guarantee adhesion without conductivity.

The Photolithography 2 phase describes the patterning of the channel wells and the protective layer with openings for the measurement pads, and in this case, the used photoresist is a SU-8 2002 layer, which is a negative photoresist, meaning that the areas that are exposed to the UV light are not soluble in the developer. Since SU-8 is a resistant epoxy resin after crosslink, it is an ideal protective layer to provide contact exclusively between the electrolyte and the channel. The patterned wells are seen in the flowchart, Figure 3.3, by the end of the third step, and the final view of the wafer is depicted in Figure 3.5a.

Figure 3.5: (a) Borosilicate glass wafer after the microfabrication of the OECTs.; (b) Diced chip with six OECTs .

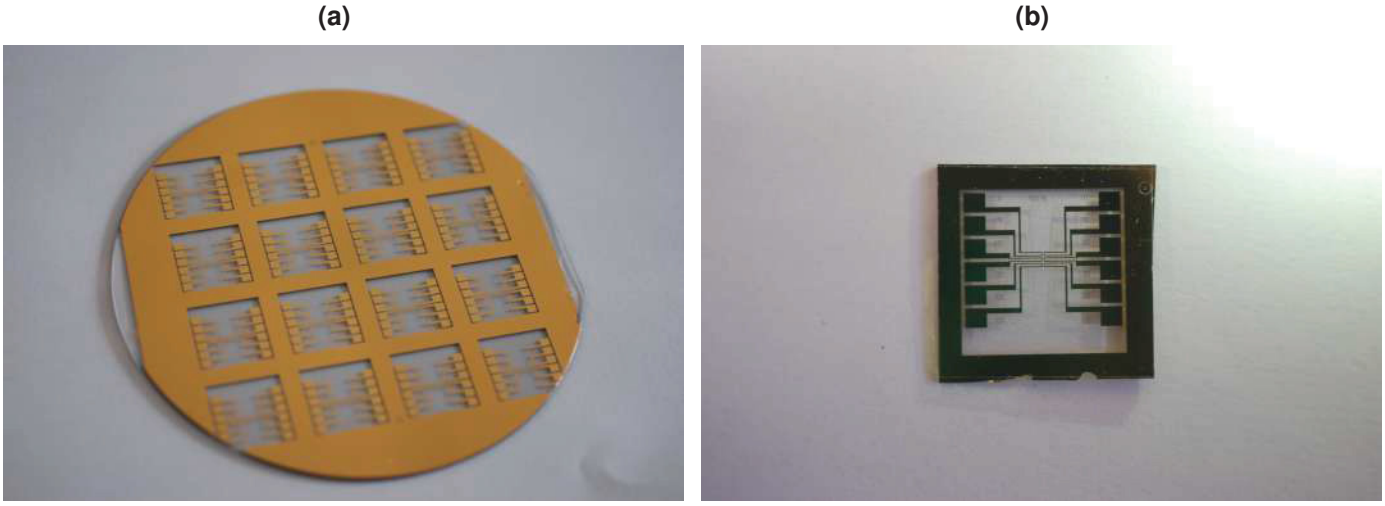

SOURCE: The author.

To get to the point where the channels were fully opened and patterned, tests were conducted to determine the time in which the SU-8 was immersed in the developer, as well as its composition. The wafers with SU-8 were immersed in periods of 2, 3, 5, and 6 minutes and then rinsed with DI water, however, as seen in Figure 3.6, the channels were not well opened. Therefore, the SU-8 was diluted in cyclopentanone (50/50 ratio) to allow thinner films.

In that context, the diluted SU-8 was not developed correctly even after two development sessions and the hard bake. There were traces of SU-8 inside the channels, but none on top of the gold contacts, which was the opposite of the targeted result.

The solution to the challenges regarding the development of the SU-8 films was to change the rinsing method. Once the DI water was replaced by isopropanol, the channels were fully opened and patterned, as shown in Figure 3.3.

After the fabrication in the cleanroom, the wafers are diced into chips and then proceed to the active layer depositision. Figure 3.5b exhibits a chip with six OECTs with channel dimensions of W = 100 μm and L = 10 μm.

Figure 3.6: Channel after photolithography 2. This result led to exploring the possibilities to remove the SU-8 from the well.

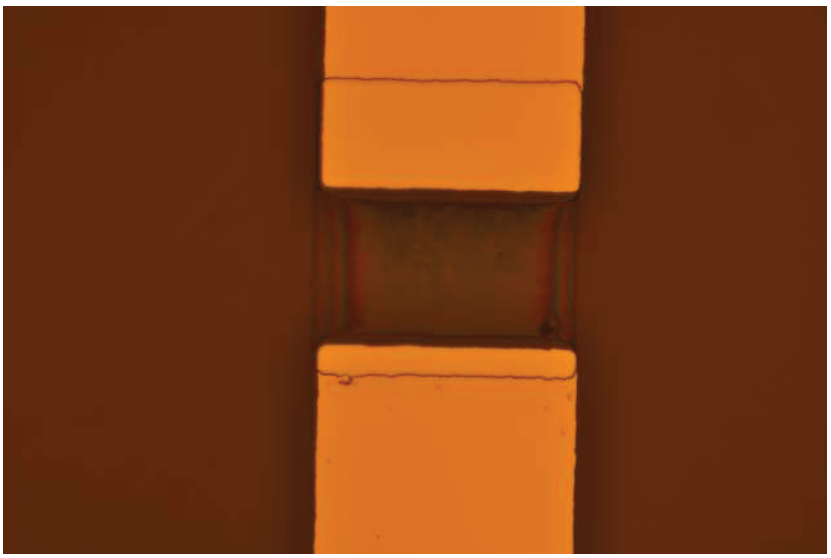

SOURCE: The author.

3.3.1 Active Layer

As previously stated, the operation of the OECTs can vary accordingly to the material deposited as the active layer. In the case of conducting polymers, it is possible to obtain depletion mode transistors, while semiconducting polymers enable the fabrication of accumulation mode devices.

In this context, as one of the established objectives for this project is to study the impact of applying different polymers in the channel, OECTs in both depletion and accumulation modes were fabricated.

The conducting polymer of choice was the PEDOT:PSS, as it is one of the most studied active layers for OECTs and also due to availability and ease of processing. On the other hand, poly[3-(6-hydroxy)hexylthiophene] (P3HHT) was adopted in the accumulation mode transistors since it is a low-swelling mixed conductor obtained through a partnership with the Institut Charles Gerhardt Montpellier and the School of Materials Science & Engineering and School of Chemical &Biomolecular Engineering at Georgia Institute of Technology.

The phase that addresses the preparation and deposition of the active layer is classified as Conducting Channel and the processes are described in the diagrams depicted in Figure 3.3.

PEDOT:PSS OECTs

The solution processing for the depletion mode OECTs consisted of 4 mL PEDOT:PSS, 200 μL of Ethylene Glycol (EG), 10 μL of 4-Dodecylbenzenesulfonic acid (DBSA) and 40 μL of (3-glycidyloxypropyl)trimethoxysilane (GOPS). As seen in diverse works in the literature, the

EG is responsible for enhancing the conductivity of the PEDOT:PSS, the DBSA as a surfactant improves film formation, and the GOPS, which is a crosslinker accountable for the film's resistance to aqueous environments (RIVNAY et al., 2013; DONAHUE et al., 2018; WUSTONI et al., 2019; LELEUX et al., 2014).

The PEDOT:PSS solution (100 μL) is deposited through spin coating and since there is not a step to pattern the polymer it is necessary to clean the measurement pads with water right after deposition. In this case, no patterning step means that there is PEDOT:PSS covering parts of the SU-8 2002 surface and no well definied channel well. To complete the fabrication process, there is a crosslinking step in which the chips are submitted to annealing at 140°C for 1 hour.

P3HHT OECTs

The P3HHT solution (15 mg/mL NMP heated to 60℃ over stirring) is deposited over the channel via doctor blade technique at ambient conditions and dried overnight, resulting in a film of approximately 110 nm as described in the study made by Nicolini et al. (2021).

It is important to highlight that the fabricated OECTs were handed to the team at the Laboratoire de Chimie des Polyméres Organiques for the P3HHT deposition and then returned to the author for characterization.

Other Active Layers

In order to explore the response of the fabricated OECTs to different active layers, besides the ones established previously, other variations of PEDOT:PSS and a couple of other polymers were applied to the transistor channels. Them being:

- PEDOT:PSS without Ethylene Glycol (EG): as established in the literature review, the EG component is added to the PEDOT:PSS solution to increase the conductivity, which decreases as the GOPS crosslinker is used. In this case, the idea was to verify how the OECT operation would undergo without the added EG. The procedure is the same applied to the original PEDOT:PSS solution, except that the EG is not used.

- PEDOT:PSS with YO_3 nanoparticles and NbO_5 microparticles: the intent of using the particles was to analyze the usage of these components in organic devices other than photovoltaic devices, in which they presented great addition to the operation. The PEDOT:PSS solution is maintained as proposed originally, and the particles are added after it is stirred for 30 minutes. After the addition of the particles, the solution is stirred again for another 30 minutes. For each 2 mL of PEDOT:PSS, 5.3 mg of NbO_5 or 4.5 mg of YO_3 are added. The deposition and annealing procedures are maintained.

- RGH-14 and Magic Quebec: both polymers are thiophene-related and were provided by colleagues at IMS to be tested as possible active layers on OECTs. RGH-14 was synthesized focusing on OLED applications while Magic Quebec was used for OPVs and is composed of a dual layer, the conjugated polymer Quebec, and a dopant named Magic Blue. In this case, the polymers were provided without information on their entire composition or fabrication process. The deposition method was maintained as proposed for the PEDOT:PSS.

3.3.2 Patterning the Active Layer

As seen in the literature review, most OECTs present a patterned active layer, in which the polymer is confined to the channel well. This feature is reached through a PaC sacrificial layer that is separated from the other films by means of mechanical lift-off. Since using PaC was not an option for fabricating the OECTs, hence the use of SU-8 as the protective layer, an alternative was needed.

Therefore, a new structure was proposed, in which a third step of photolithography would be used to pattern a bigger well in a Poly(methyl methacrylate) (PMMA) layer with O_2 Reactive Ion Etching (RIE). The PMMA would replace the PaC sacrificial layer and be deposited on top of the protective layer (SU-8). The idea was to promote the chemical lift-off of the PMMA with chlorobenzene after the PEDOT:PSS spin coating and, therefore, pattern the conductive channel. Figure 3.7 describes the step to step of the patterned films.

Figure 3.7: Visual description of the patterning structure and deposition processes. (a) Deposition of the metallic layers; (b) Deposition of the AZ1512 HS photoresist; (c) Photolithography 1 - Patterning of the Au; (d) Photolithography 2 - Patterning of the SU-8; (e) Deposition of the PMMA layer; (f) Deposition of an AZ1512 HS layer; (g) O_2 RIE to open the channel well; (h) Deposition of the active layer and chemical lift-off; (i) OECT after patterning of the active layer; (j) final structuire of the OECT.

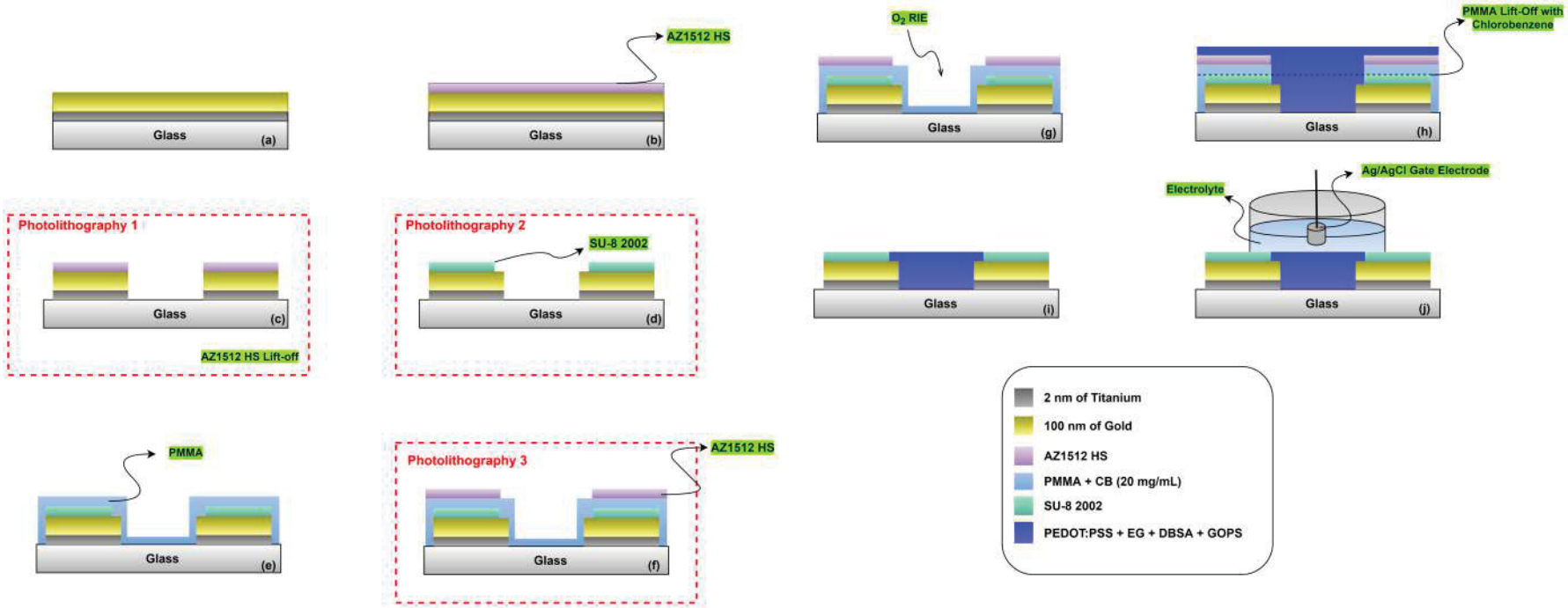

SOURCE: The author.

To test the efficiency of the chemical lift-off, five glass slides were coated with (a) PEDOT:PSS solution (2 @ 1500 rpm and 1 @ 3000 rpm) and (b) PMMA (20 mg/mL in chlorobenzene) + PEDOT:PSS solution (1 @ 1500 rpm and 1 @ 3000 rpm). The adopted deposition parameters for the PMMA are as follows.

- Spin speed: 1000 rpm;
- Spin time: 60 s;
- Volume of PMMA: 100 μL;
- Annealing @ 80 °C for 1 hour in vacuum.

Figure 3.8 shows the appearance of the glass slides before the immersion in chlorobenzene. The slides with PEDOT:PSS did not depict signs of delamination, even after one hour plus an ultrasound bath. On the other hand, the slides with PMMA presented delamination, and when in the ultrasound bath, the whole layer peeled off.

Figure 3.8: Glass slides with PMMA and PEDOT:PSS before immersion in chlorobenzene.

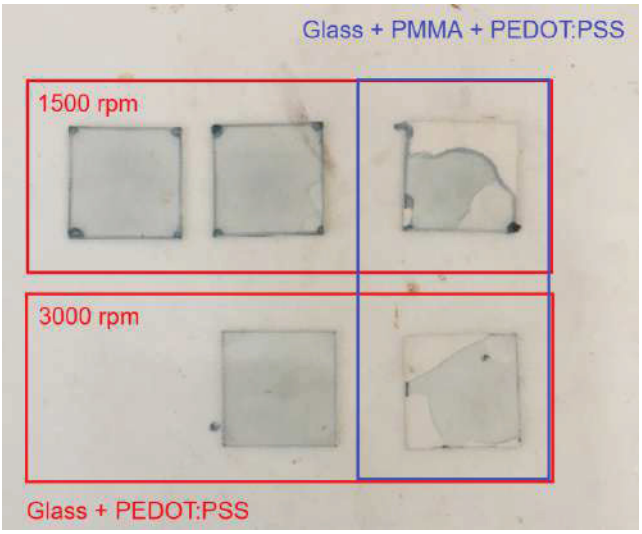

SOURCE: The author.

Due to this result, using the PMMA layer to pattern the channel seemed viable, however, during the deposition of the polymer on the SU-8 film, Figure 3.7.e, the photoresist presented hydrophobic behavior and it was not possible to form a PMMA film on the whole wafer as planned.

As the hydrophobic behavior could be related to the size of the samples, four glass slides were coated with SU-8, PMMA, and then PEDOT:PSS. Figure 3.9.a shows the slides after the deposition of the films and annealing of the PEDOT:PSS. As seen, two annealing temperatures were used to verify the effectiveness of the chemical lift-off.

Though there was uniform film formation of the PMMA on top of the SU-08, as depicted in Figure 3.9.b, there were no signs of lift-off after immersion in chlorobenzene. The samples presented

in Figure 3.9.b were submitted to one-hour immersions, overnight immersions, and immersions on heated chlorobenzene. The achieved lift-off was cracking on the films.

Figure 3.9: (a) Glass slides before immersion in chlorobenzene; (b) Glass slides after diverse immersion methods.

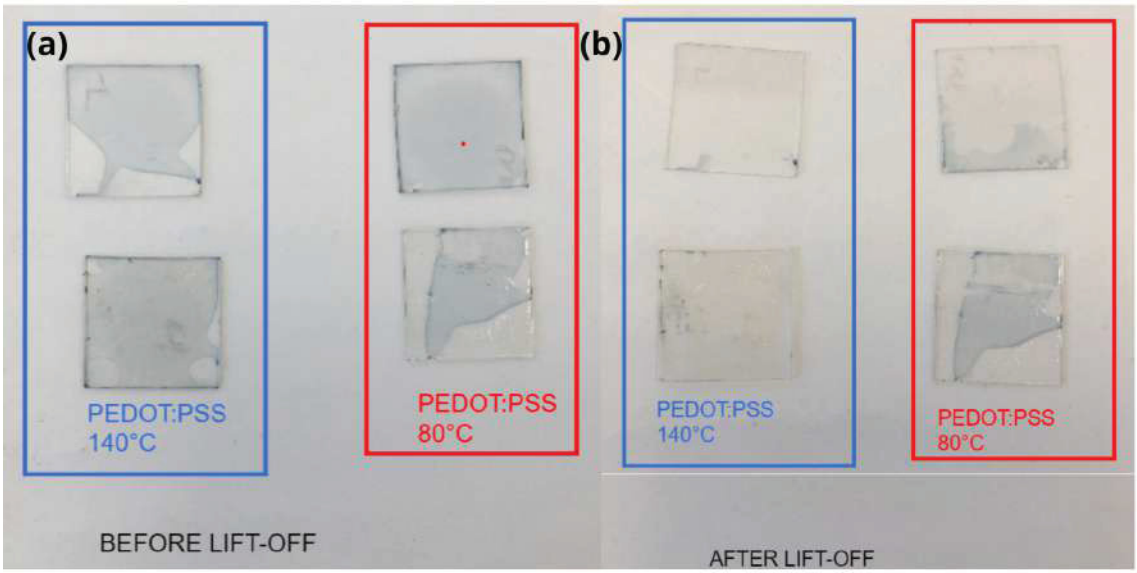

SOURCE: the author.

To improve the susceptibility of the PMMA to the chemical lift-off, the SU-8 films were submitted to UV Ozone beforehand. The samples were in UV Ozone for periods of 1/2, 1, 2, 5, 10, and 15 minutes. Film formation and wettability characteristics did not improve until the 10 and 15-minute marks, which presented good wettability and film formation, but there was no repeatability on the lift-off results that was successful for the 10-minute samples, but not for the 15-minute slides.

Therefore, the study regarding using PMMA as a patterning strategy showed that using the polymer was not viable, since the chemical lift-off was time-consuming and not reliable. Consequently, the fabrication process continued without the patterning of the channel.

3.4 DEVICE CHARACTERIZATION

As for the characterization of the OECTs, a characterization setup, Figure 3.10, was developed in a metal box where the sets are pinched from both sides with measurement clips to establish contact with all Source and Drain electrodes. Since there are six OECTs in each set, there is a mechanical switch installed to the box so that the selection among the transistors could take place.

Of the possible ways to characterize a transistor, the most common one is to acquire Output and Transfer curves, which could provide important information on the devices, such as threshold

Figure 3.10: Characterization setup built to accomodate the fabricated sets of OECTs.

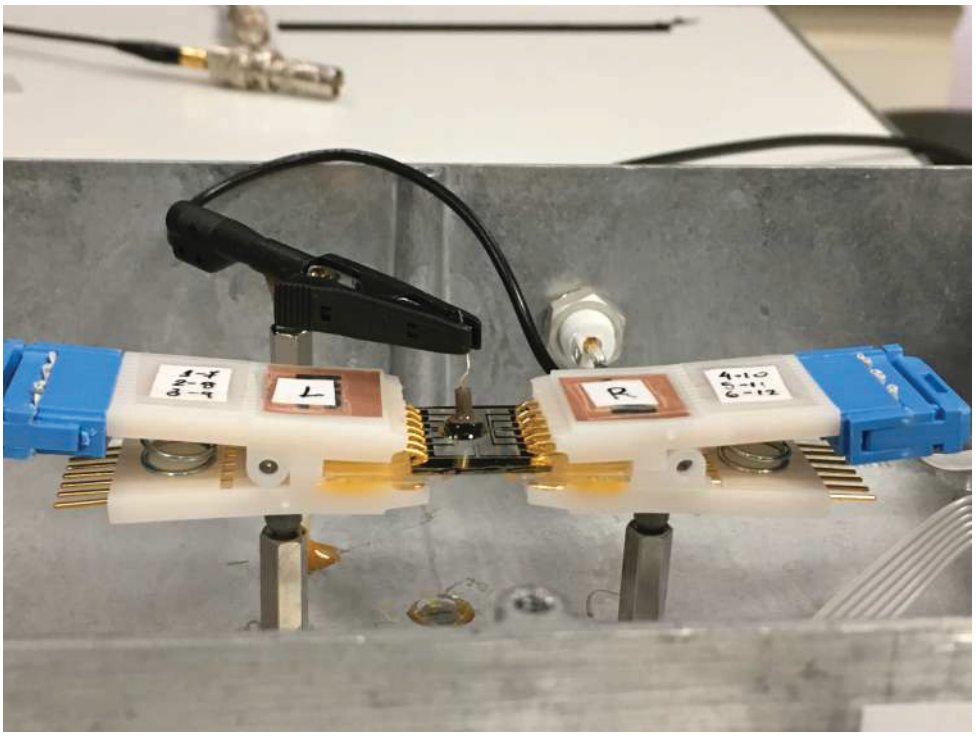

SOURCE: the author.

voltage (V_{th}), ON/OFF ratio, and transconductance (*gm*). For the devices fabricated in the present project, the Output and Transfer curves were obtained by means of a Keithley 4002 Parameter Analyzer, in which Source was connected as a common ground, Drain was determined as SMU 1 and Gate as SMU 2.

The project of the characterization box is found in Figure 3.11, where the connections between the measurement clips and the OECT arrays are established, as well as the BNC connectors used for polarizing the setup and measuring device responses.

The polarization of the transistors varied depending on the targeted characterization. In Table 3.1, it is possible to observe the applied voltages corresponding to each active layer.

Table 3.1: Parameters applied to parameter analyzer in order to acquire the Output and Transfer curves for the fabricated OECTs. The polarization used on PEDOT:PSS devices was also used on the RGH-14 nd Magic Quebec devices

		V_{GS}	V_{DS}
PEDOT:PSS	Transfer Curves	-0.2 V to 0.6 V (0.01 V steps)	-0.6 V
	Output Curves Curves	-0.2 V to 0.6 V (0.05 V steps)	0 to -0.6 V (- 0.01 V steps)
		V_{GS}	V_{DS}
P3HHT	Transfer Curves	-0.6 V to 0.2 V (-0.01 V steps)	-0.6 V
	Output Curves Curves	-0.6 V to 0.2 V (0.05 V steps)	0 to -0.6 V (- 0.01 V steps)

SOURCE: The Author.

Figure 3.11: Project of the setup built to characterize the fabricated OECTs.

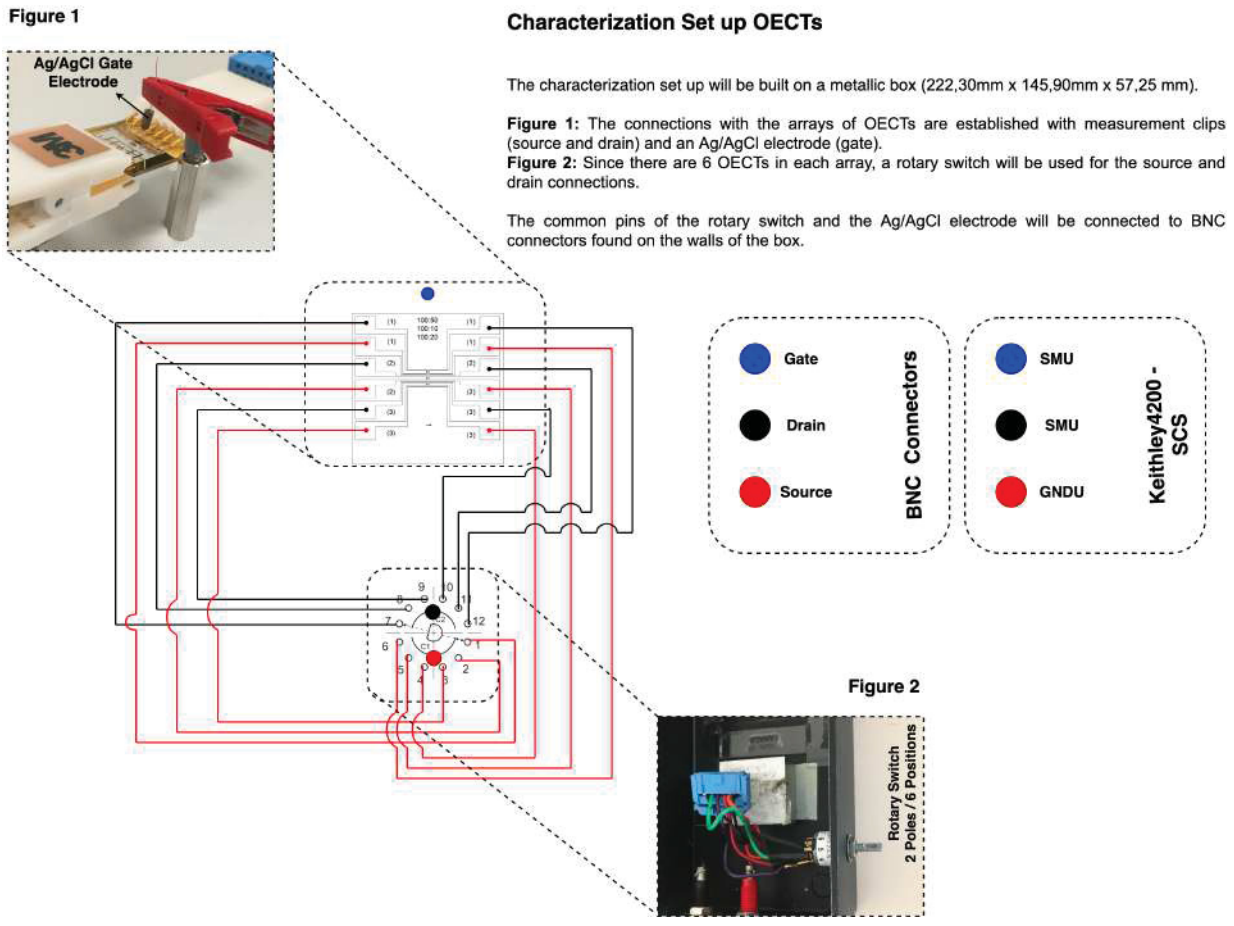

SOURCE: the author.

3.5 CHAPTER CONCLUSION

This chapter discussed the conception of the experimental methodology used to fabricate Organic Electrochemical Transistors and characterize them. The elected struture was exposed and the fabrication steps were unraveled. Three subsections were dedicated to explaining how the final fabrication process was created and why there is no step to pattern the active layer. In addition, the project of the characterization setup was ilustrated through a diagram and the polarizations used to analyze OECT operation were determined.

4 EXPERIMENTAL APPROACHES TO ANALYZE OECT OPERATION

This chapter exhibits and discusses the steady-state characteristics of both the proposed active layers. At first, the results for the PEDOT:PSS OECTs are presented, and the influence of the electrolyte as well as the impact of the channel thickness are debated. Consequently, the properties of the P3HHT OECTs are displayed as transfer curves for different aqueous electrolytes.

In this context, some parameters analyzed for both the depletion and accumulation modes are the transconductance, maximum transconductance, threshold voltage, and ON drain current.

4.1 VALIDATING THE EXPERIMENTAL METHODOLOGY

As stated previously, one of the specific objectives of this project was to analyze common fabrication processes used in State-of-the-Art OECTs, create a methodology and then validate it. Two concentrations of NaCl were employed, 0.1 M and 0.154 M, the first was adopted for comparison merits and the latter was chosen due to commercial availability.

In Figure 4.1a the transfer curve acquired for the OECTs fabricated through the adapted process and tested with 0.1 M NaCl is shown along with a *gm* x V_{GS} curve. It is possible to verify that it presents some typical depletion-mode OECT characteristics, such as the bell-shaped *gm* curve, *gm* values around mS, high Id and de-doping with applied positive voltages. The latter can be confirmed by the Output curve seen in Figure 4.1b.

Figure 4.1: (a) I_{DS} x V_{GS} (Transfer) and *gm* x V_{GS} curves for Set 3 1R OECT tested with a 0.1 M NaCl droplet. These curves were obtained with a constant applied Vd = -0.6 V and a variant V_{GS} = -0.2 V to 0.6 V; (b) I_{DS} x V_{DS} (Output) curve correspondent to the curves presented in (a). The curve was acquired in a drain range of V_{DS} = 0 V to - 0.6 V and V_{GS} = -0.2 V to 0.6 V.

(a)

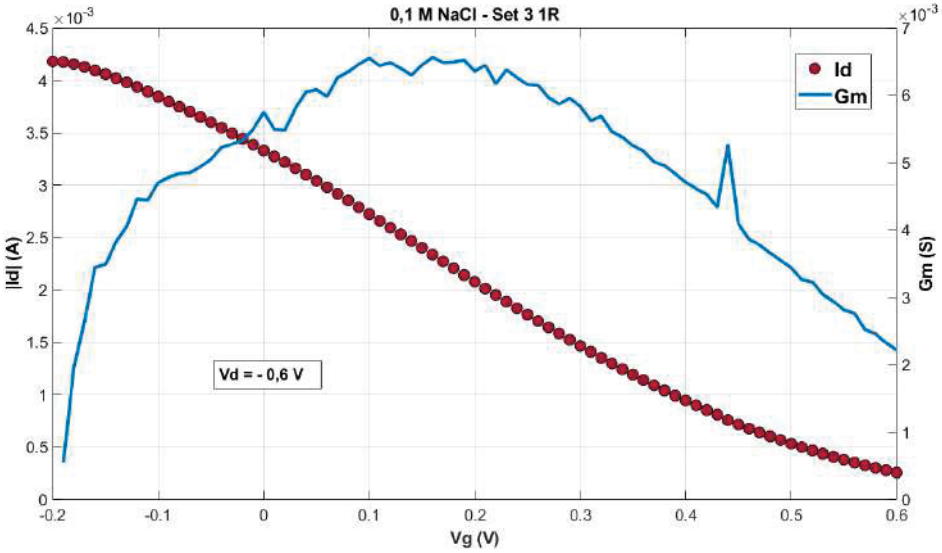

(b)

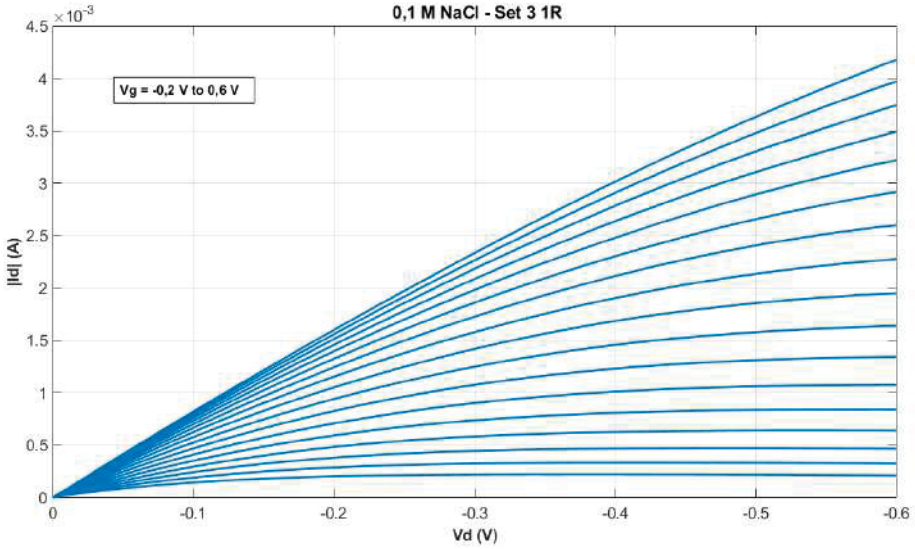

SOURCE: The Author.

In comparison with the State-of-the-Art devices seen in Rivnay's or Mallliaras group, as an example of Khodagholy et al. (2013), shown in Figure 4.2, the devices developed here present similar behavior and comparable or better values for the performance parameters, therefore, proving that the adaptations made to the fabrication process are as effective as the original on the patterning of the devices. Another detail that should be highlighted is the patterning of the PEDOT:PSS well, which, based on the current results, was proven not to be an essential step in the structuring of the devices (KHODAGHOLY et al., 2013).

In this line, Figure 4.3a and Figure 4.3b exhibit the transfer and transconductance curves

related to the responses of devices Set 3 1R, Set 2 3L, Set 2 2R, and Set Mixed 2R when tested with a 0.154 M NaCl electrolyte. It is important to remember that the Set 3 1R in these tests is from a different batch from the Set 3 1R device tested in 0.1 M NaCl. From the transfer curves, it is possible to observe the depletion mode behavior, in which at first the device is ON, and when a positive potential is applied to the gate, the drain current drops and the transistor turns off. Besides, in the transconductance curves, the typical bell shape is visible and confirms an OECT performance.

Figure 4.2: Transfer and *gm* x V_{GS} curves for the PEDOT:PSS OECT proposed by Khodagholy et al. (2013).

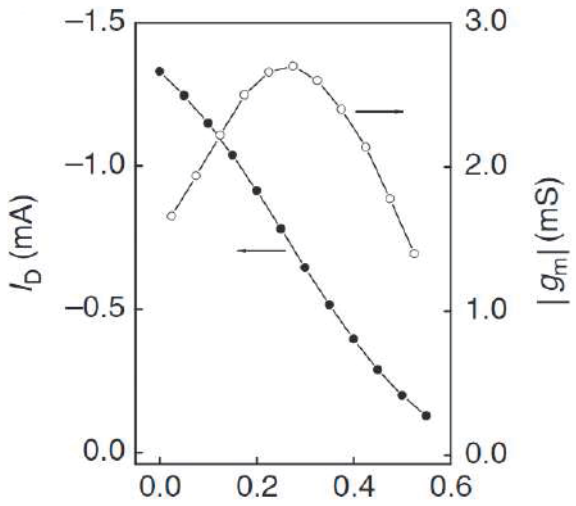

SOURCE: Khodagholy et al. (2013).

Table 4.1 presents the performance parameters extracted from the selected samples, as well as design parameters established during fabrication. As seen in both Figure 4.3a, Figure 4.3b, as well as in Table 4.1, the values of I_{DSON} and gm_{max} can vary from device to device, which happens due to the non-standardized fabrication since the deposition of the PEDOT:PSS is a manual process as well as the annealing and organization of the molecule that are not uniform. Although there are divergences in the values, this is a normal response to the adopted processing and the devices are in fact reproducible with high values of *gm*, in the order of mS, and follows the values of V_{th} reported by Keene et al. (2020) (KEENE et al, 2020).

Figure 4.3: (a) I_{DS} x V_{GS} (Transfer) and (b) *gm* x V_{GS} (Transconductance) for the OECTs tested with a 0.154 M NaCl droplet. These curves were obtained with a constant applied V_{DS} = -0.6 V and a variant V_{GS} = -0.2 V to 0.6 V.

(a)

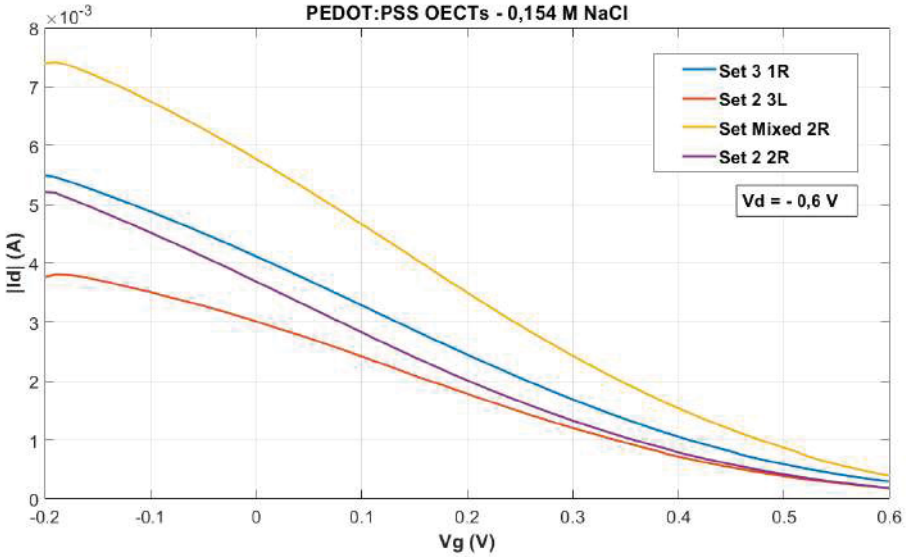

(b)

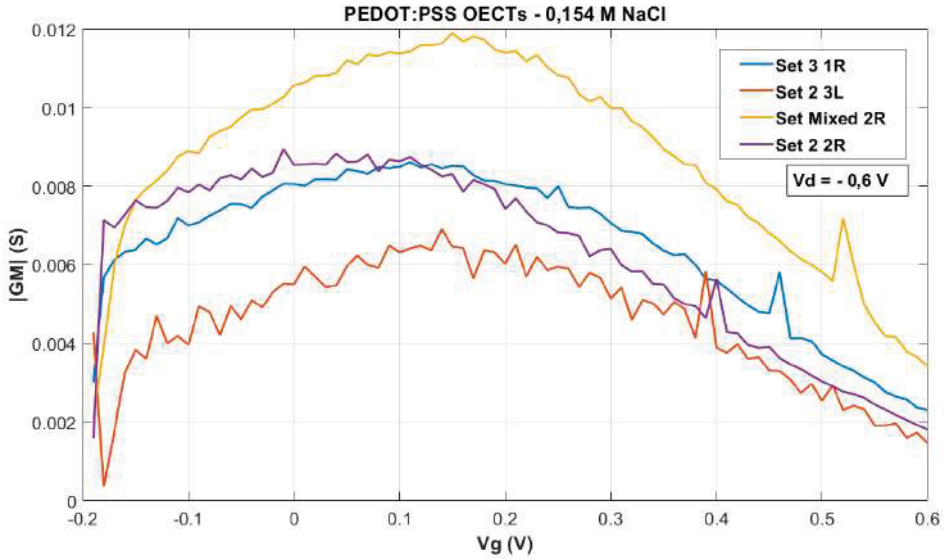

SOURCE: The Author.

Table 4.1: Design parameters and performance parameters of the fabricated OECTs, where Spin Speed defines the speed adopted during spin coating to obtain the channel thickness. For all devices the channel dimensions (W/L) is 100/10 and the thickness is 240 nm.

Sample Name	Electrolyte Concentration	Spin Speed	gm_{max}	I_{DSON}	V_{th}
Set 3 1R (0.1 M)	0.1 M NaCl	1500 rpm	6.7 mS	4.2 mA	0.8 V
Set Mixed 2R	0.154 M NaCl	1500 rpm	11.9 mS	7.4 mA	0.79 V
Set 2 3L	0.154 M NaCl	1500 rpm	6.9 mS	3.8 mA	0.76 V
Set 2 2R	0.154 M NaCl	1500 rpm	8.9 mS	5.2 mA	0.76 V
Set 3 1R (0.154 M)	0.154 M NaCl	1500 rpm	8.6 mS	5.5 mA	0.79 V

SOURCE: The Author.

4.2 PEDOT:PSS OECTs

The PEDOT:PSS transistors were characterized to explore parameters such as I_{DSon}, gm_{max}, and V_{th} in various conditions, which included aqueous electrolytes with different ionic compositions and concentrations of NaCl, and different deposition velocities (800 rpm, 1500 rpm, and 3000 rpm).

Influence of Electrolyte Composition and Concentration

The impact of a range of NaCl concentrations (0.05 M, 0.1 M, 0.154 M, 0.3 M, and 0.5 M) was explored, as depicted in Figure 4.4, where the transfer curves are presented as well as the relationship between the maximum transconductance and the different NaCl concentrations.

As seen, the ON drain current decreases as the concentration of the electrolyte increases, and this trend is also verified for the maximum transconductances. There was a decrease of approximately 75% in I_{DSon} while gm_{max} presented a 68% decrease between 0,005 M and 0,5M.

Figure 4.4: Influence of electrolyte concentration in PEDOT:PSS OECTs.

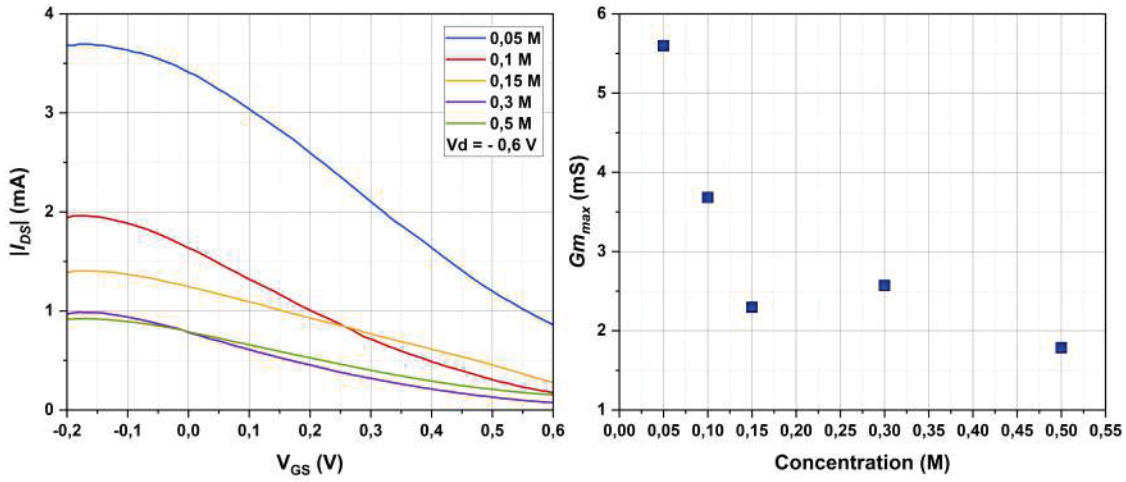

SOURCE: The author.

These results validate the discussion of Savva et al. (2019), where it was demonstrated that as the concentration of the electrolyte decreases, the performance parameters should increase. This happens due to the hydration of the channel since the cation transport takes place in the swollen phase, which is well reported that PEDOT:PSS channels swell up to 86% of their initial mass when exposed to aqueous environments (SAVVA et al., 2019; SAVVA, WUSTONI, INAL, 2016).

As seen in Figure 4.4, an increase in concentration leads to lower performance parameter intensities, which could be a consequence of the decrease in the hydration shell around the ions as well as in the number of ion-free water molecues in the electrolyte.

On the other hand, the effect of the adopted electrolyte was investigated through the analysis of device response at different compositions (0.1 M NaCl, 0.1 M KCl, and 0.1 KPF_6).

As seen in Figure 4.5, the transfer curves acquired indicate divergence in the performance of the OECTs when electrolytes with different compositions are adopted. The device tested with the 0.1 M KPF_6 presented the highest value of I_{DSon} with 6.08 mA, while the NaCl and KCl electrolytes exhibited similar values with 4.18 mA and 4.01 mA.

Figure 4.5: Influence of electrolyte composition in PEDOT:PSS OECTs.

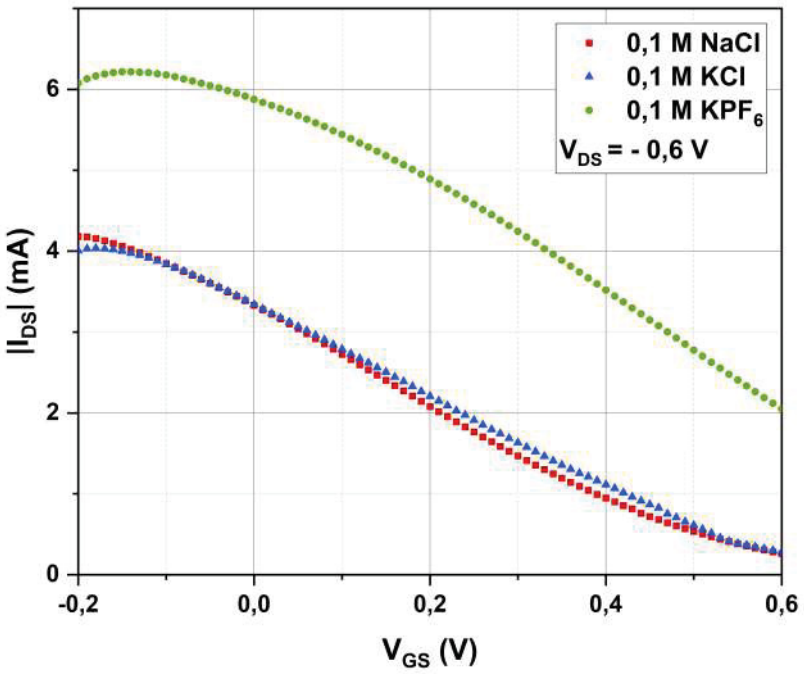

SOURCE: The author.

The different performances could be explained as a consequence of the capacity of the ions pushed into the channel to dope/de-dope the polymer. Usually, larger molecular ions present better abilities than smaller ones due to their hydration shell.

Influence of Channel Thickness

To validate the effects of the channel thickness on the performance of OECTs, three deposition velocities were applied to the PEDOT:PSS channel conditioning phase, i.e. 800 rpm, 1500 rpm, and 3000 rpm, which resulted in channels of 390 nm, 240 nm, and 140 nm, respectively.

Figure 4.6.a depicts the transfer curves acquired for each film when exposed to a 0.154 M NaCl aqueous electrolyte. In addition, Figure 4.6.b shows the bell-shaped transconductance curves typical for PEDOT:PSS OECTs.

As expected, as thicker the layer, the higher the maximum transconductance (POLYRAVAS et al., 2020) and $V_{GSgmmax}$are (PAUDEL et al. 2021). For a 390 nm film, gm_{max} = 15.69 mS @ V_{GS}

Figure 4.6: Transfer and *gm* x V_{GS} curves for the PEDOT:PSS OECTs with different channel thicknesses.

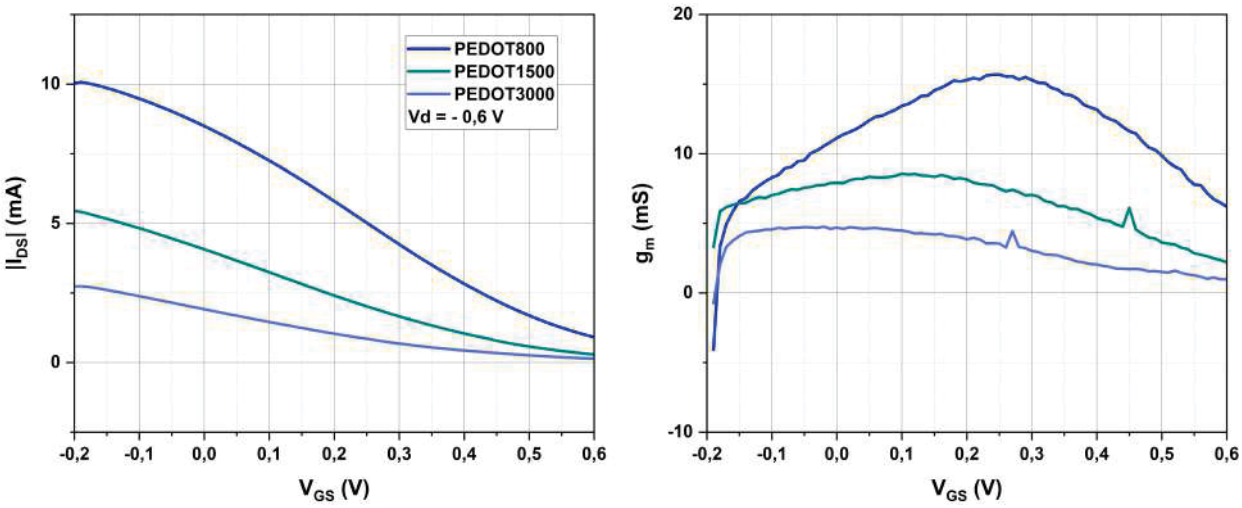

SOURCE: The author.

= 0.25 V while for the 240 nm and 140 nm, gm_{max} is 8.56 mS @ V_{GS} = 0.1 V and 4.77 mS @ V_{GS} = - 0.02 V, respectively.

In addition to the gm_{max} values changing according to the channel thickness, I_{DSon} also showed improvement as the thickness increased. I_{DSon} presented values of 10.03 mA, 5.45 mA, and 2.73 mA for the 390 nm, 240 nm, and 140 nm films, respectively.

Table 4.3 presents the mean, variance and standard deviation values for I_{DSon}, gm_{max} and V_{th} for the groups of spin speed.

Table 4.2: Values of I_{DS} ON, G_m max and V_{th} for PEDOT:PSS 800, PEDOT:PSS 1500 and PEDOT:PSS 3000.

		I_{DSon}	gm_{max}	Vth
PEDOT:PSS 800	Mean Values	9 mA	14.12 mS	81.1 mV
	Variance	3.02 e^{-6}	6.04 e^{-6}	422.88 e^{-6}
	Standard Deviation	0.001	0.002	0.020
		I_{DSon}	gm_{max}	Vth
PEDOT:PSS 1500	Mean Values	3.30 mA	7.41 mS	778 mV
	Variance	8.32 e^{-7}	6.45 e^{-6}	0.006
	Standard Deviation	0.0009	0.002	0.076
		I_{DSon}	gm_{max}	Vth
PEDOT:PSS 3000	Mean Values	3.38 mA	6.08 mS	790 mV
	Variance	3.36 e^{-6}	5.35 e^{-6}	0.003
	Standard Deviation	0.002	0.002	0.060

SOURCE: The Author.

4.3 P3HHT OECTs

Influence of Electrolyte Composition and Concentration

Similar to the PEDOT:PSS OECTs, the performance of the P3HHT transistors was also analyzed when different electrolyte compositions and concentrations are employed.

As exhibited in Figure 4.7a, the transfer curves of OECTs characterized with two different anions(Cl^- and $PF_6{}^-$) are presented. As shown, the value for ON-state drain current in KPF_6 is 8 to 10 times higher than in electrolytes with chlorine anions. This behavior is also seen in Figure 4.7b for the transconductance analysis, in which the 2.66 mS maximum transconductance for KPF_6 is 8 to 10 times higher than the values obtained for NaCl and KCl. In addition, there is a shift to the right in the threshold voltage for $PF_6{}^-$ anions around -0.26 V.

Accordingly, the nature of the anions found in the electrolyte plays an important part in the performance of OECTs, especially in their transfer characteristics and transconductance values as larger molecular anions represent lower threshold voltages and higher drain currents, and also higher doping levels. The shift in V_{th} can be explained by the more facile doping of the polymer with the use of KPF_6 (FLAGG et al., 2019; CENDRA et al., 2018; FLAGG et al., 2018).

Figure 4.7: (a) Transfer curves for the P3HHT OECTs tested with different aqueous electrolytes; (b) Performance parameters for P3HHT exposed to 0.1 M NaCl, 0.1 M KCl and 0.1 M KPF_6

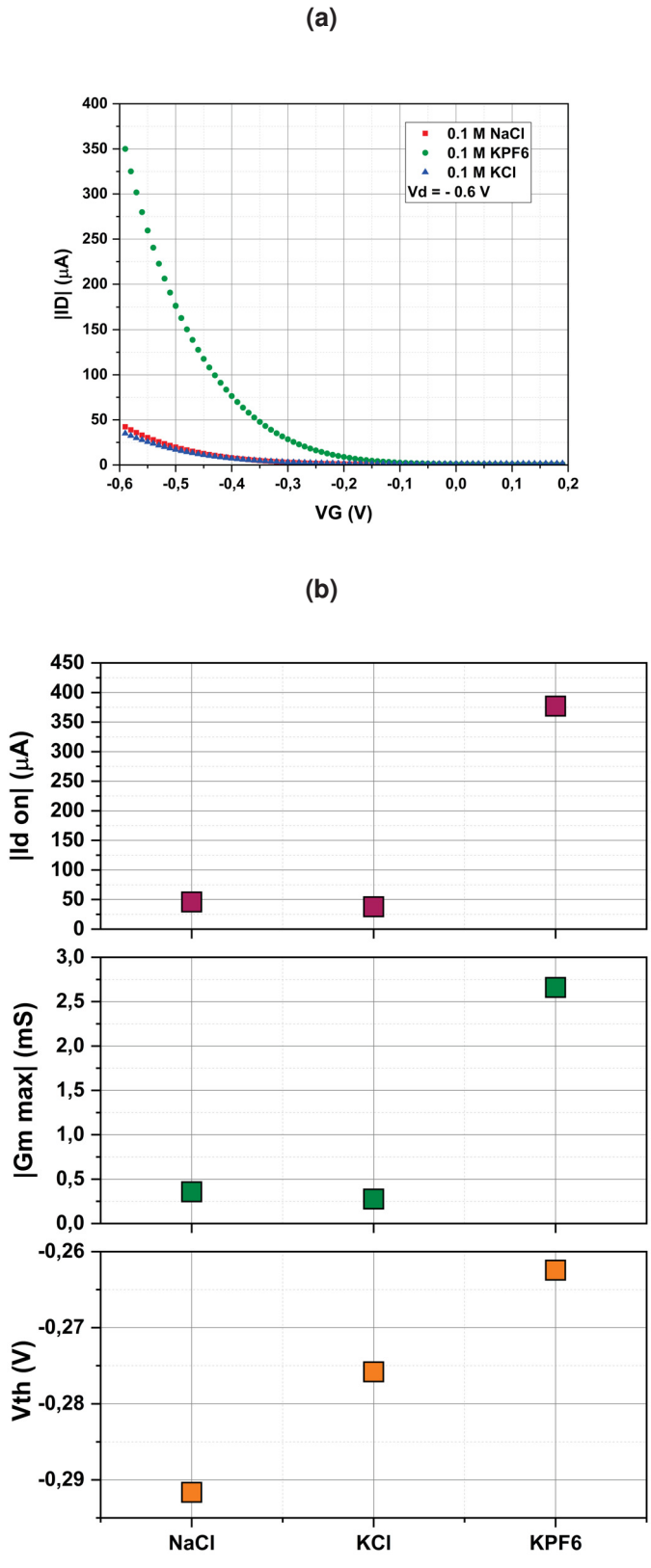

SOURCE: The author.

Regarding the concentration levels of the electrolyte, the transfer curves are presented in Figure 4.8 as well as the maximum transconductance for each concentration. Diverging from the results obtained for the PEDOT:PSS OECTs, there is no clear relationship between the elec-

trolyte concentration and the performance parameter for the P3HHT active layer. This behavior was noted for other P3HHT devices as well, in which I_{DSon} and gm_{max} vary randomly as the concentration increases.

Figure 4.8: Influence of electrolyte concentration in P3HHT OECTs.

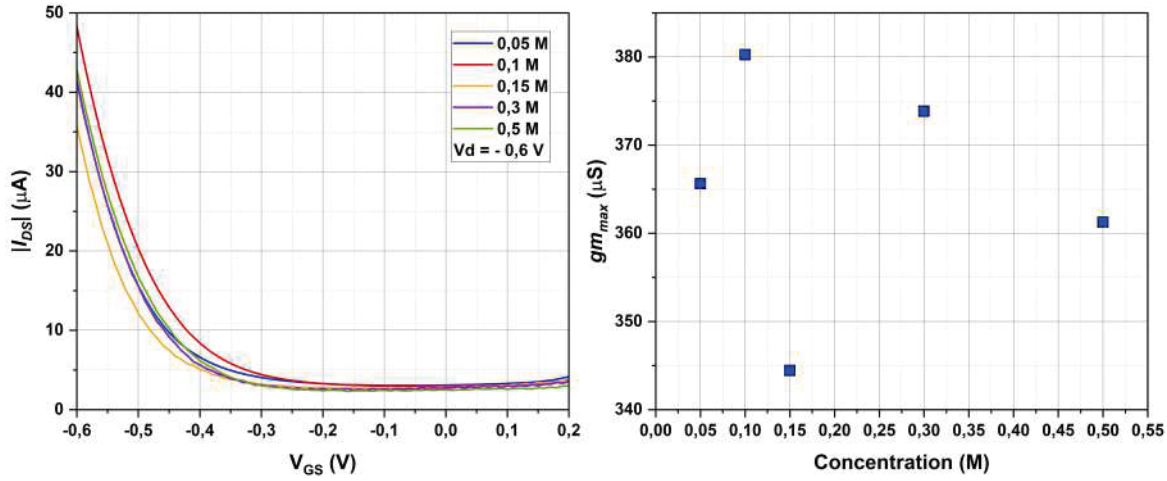

SOURCE: The author.

4.4 MODIFYING THE ACTIVE LAYER

Aside from validating the developed methodology and studying the effects of device design, the OECT operation was analyzed as the materials in the active layer were modified. Mostly, there were variations of PEDOT:PSS, which included a different deposition technique, taking the EG component out of the solution, and adding nanoparticles and microparticles to the PEDOT:PSS solutions. Besides, two thiophene-based polymers were applied to the devices to verify their potential as active layers in OECTs.

4.4.1 PEDOT:PSS - Casting as Deposition Technique

The casting technique consists of depositing a drop of a solution on top of a surface. In the case of the OECTs, the casting deposition created PEDOT:PSS films of 3 μm, which are thicker than those obtained through spin coating. The PEDOT:PSS (EG+GOPS+DBSA) film was submitted to the same annealing process as the proposed fabrication process.

The curves presented in Figures 4.9a, 4.9b, 4.10a and 4.10b describe the inconsistent behavior of the four working samples of the casted PEDOT:PSS. It is possible to verify that most of the typical characteristics of PEDOT:PSS OECTs are not seen, except for the Set 2 3R transistor that still showed less I_{DS} modulation than the original devices. Likewise, the average gm_{max} value for this group is 3.025 mS, which is lower than the thinnest film obtained with spin coating. Table 4.3

lists the values acquired for the PEDOT:PSS Casting samples.

Figure 4.9: I_{DS} x V_{GS} (Transfer) and *gm* x V_{GS} (Transconductance) for the OECTs tested with PEDOT:PSS deposited through drop casting. (a) Set 1 1L; (b)Set 2 2R.

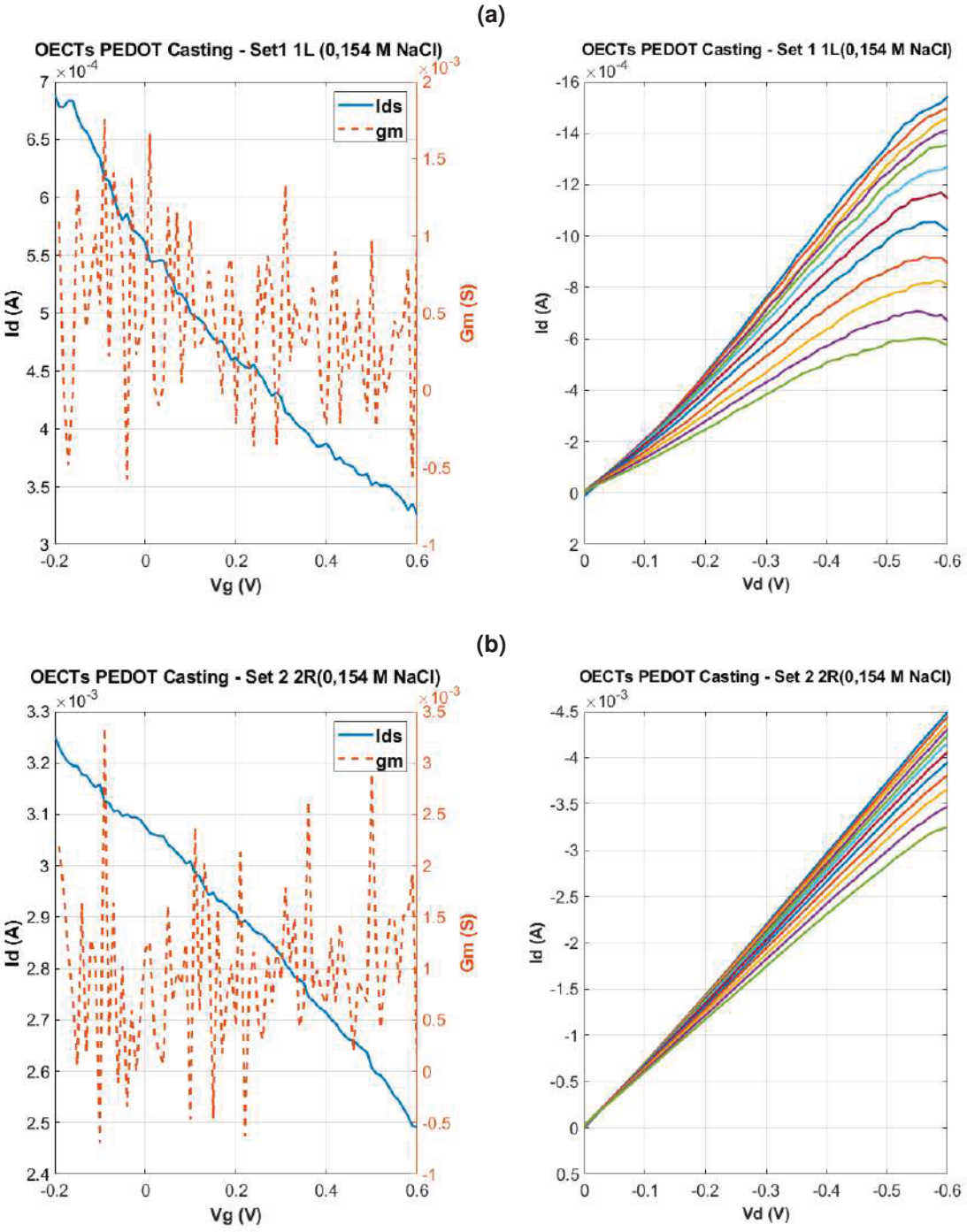

SOURCE: The Author.

Figure 4.10: I_{DS} x V_{GS} (Transfer) and *gm* x V_{GS} (Transconductance) for the OECTs tested with PEDOT:PSS deposited through drop casting. (a) Set 2 3L; (b) Set 2 3R.

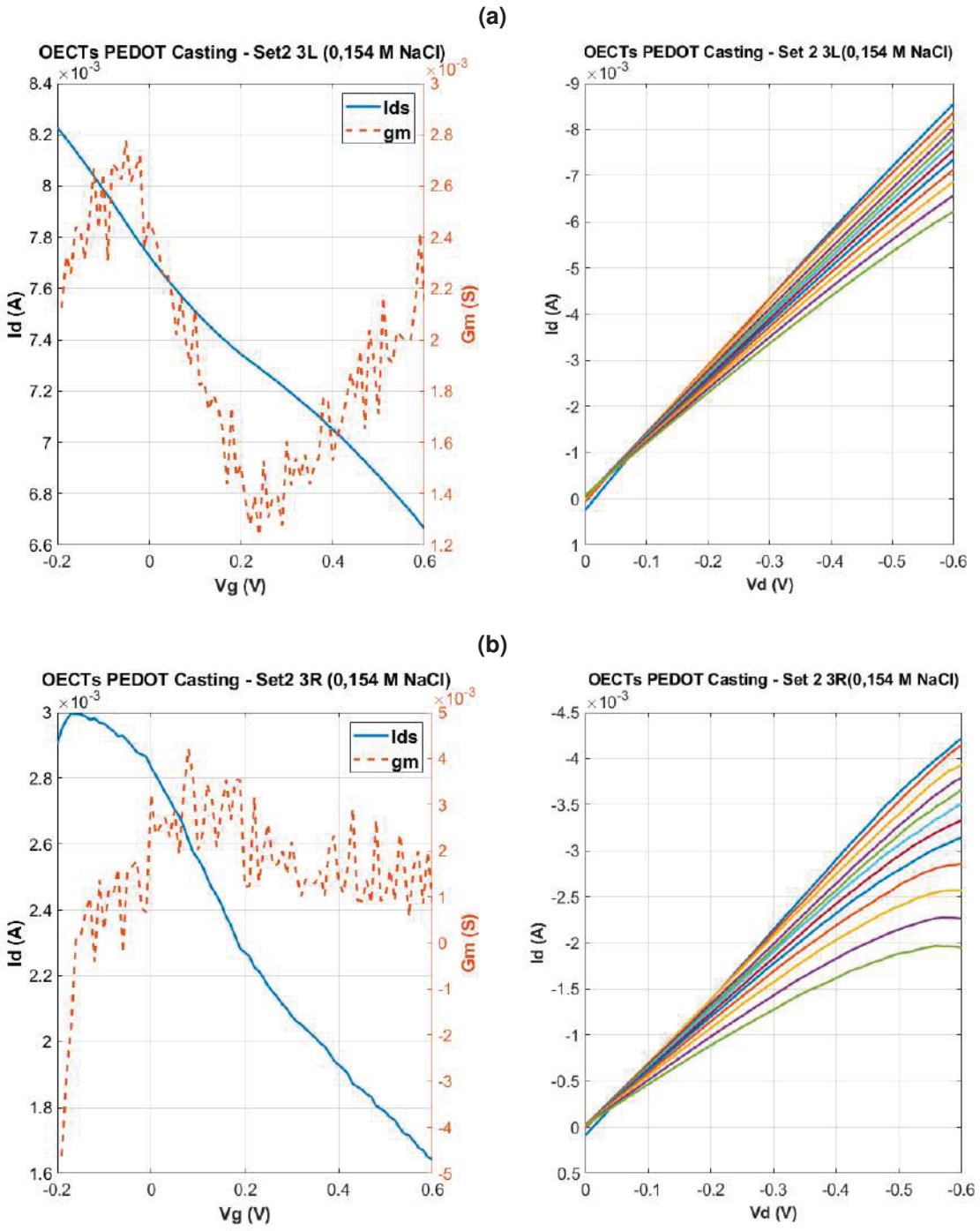

SOURCE: The Author.

Table 4.3: Mean, variance and standard deviation values for I_{DSon} and gm_{max} in PEDOT:PSS casting OECTs.

	I_{DSon}	gm_{max}
Mean	4.8 mA	3 mS
Variance	7.52 e^{-6}	7.52e^{-7}
Standard Deviation	0.002	0.008

SOURCE: The Author.

It is important to remember that each fabricated chip contains six OECTs, meaning that twelve samples were tested, only four (one from Set 1 and three from Set 2) presented a response to the applied potentials, and from those samples, one showed OECT behavior comparable to other working OECTs. For that reason, this test proved that the oroginally applied deposition technique (spin coating) offers more possibilities to obtaining working and reproducible OECTs.

4.4.2 PEDOT:PSS without Ethylene Glycol

The PEDOT:PSS EG OECTs represent a group of transistors that were tested without the ethylene glycol. The idea was to explore the behavior of the devices when there is no component to increase the conductivity after the crosslink with the silane component.

As shown in the curves depicted in Figure 4.11a,for example, these devices present better responses than the ones seen for the PEDOT:PSS Casting samples, with *gm* curves similar to the traditional bell-shaped curves PEDOT:PSS OECTs show. In addition, the modulation of I_{DS} is clear for samples from Set 2 such as 1R, Figure 4.13a, 3R, Figure 4.13b, and 1L, Figure 4.12b, and the curves show a more stable response.

Figure 4.11: I_{DS} x V_{GS} (Transfer) and *gm* x V_{GS} (Transconductance) for the OECTs tested with PEDOT:PSS without the EG component.(a) Set 1 1L; (b) Set 1 2L.

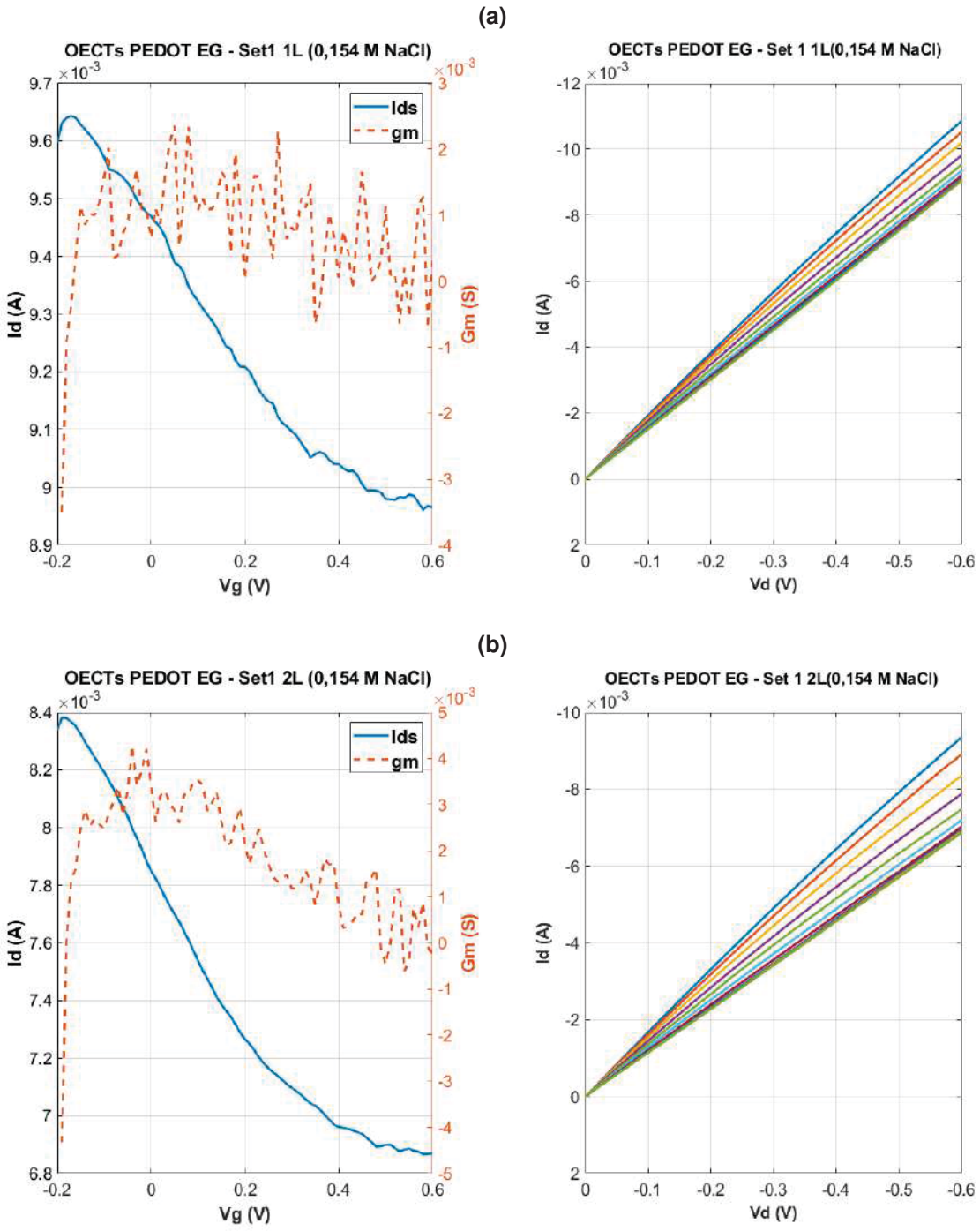

SOURCE: The Author.

Figure 4.12: I_{DS} x V_{GS} (Transfer) and *gm* x V_{GS} (Transconductance) for the OECTs tested with PEDOT:PSS without the EG component. (a) Set2 2L; (b) Set 2 1L.

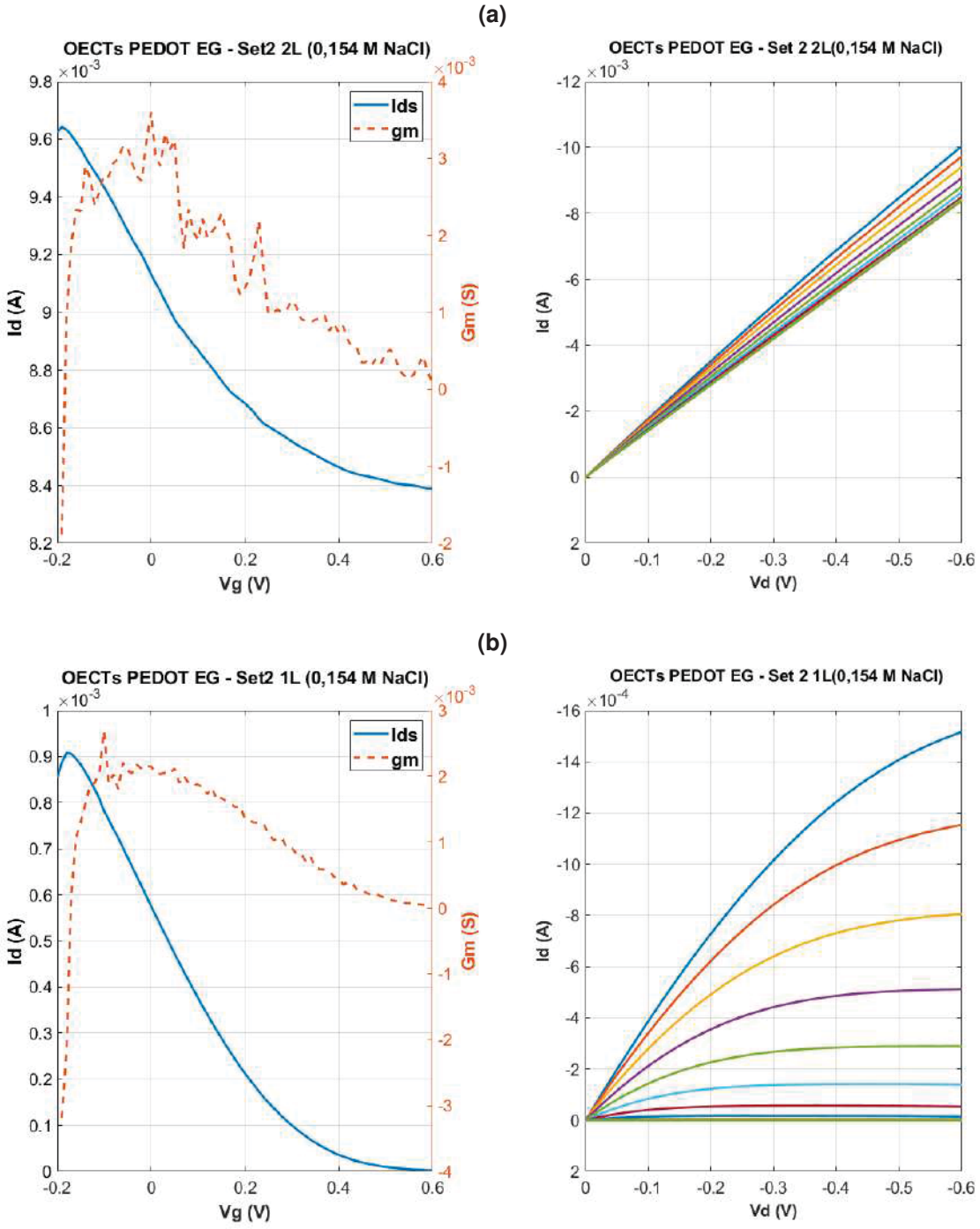

SOURCE: The Author.

Figure 4.13: I_{DS} x V_{GS} (Transfer) and *gm* x V_{GS} (Transconductance) for the OECTs tested with PEDOT:PSS without the EG component. (a) Set 2 1R; (b) Set 2 3R.

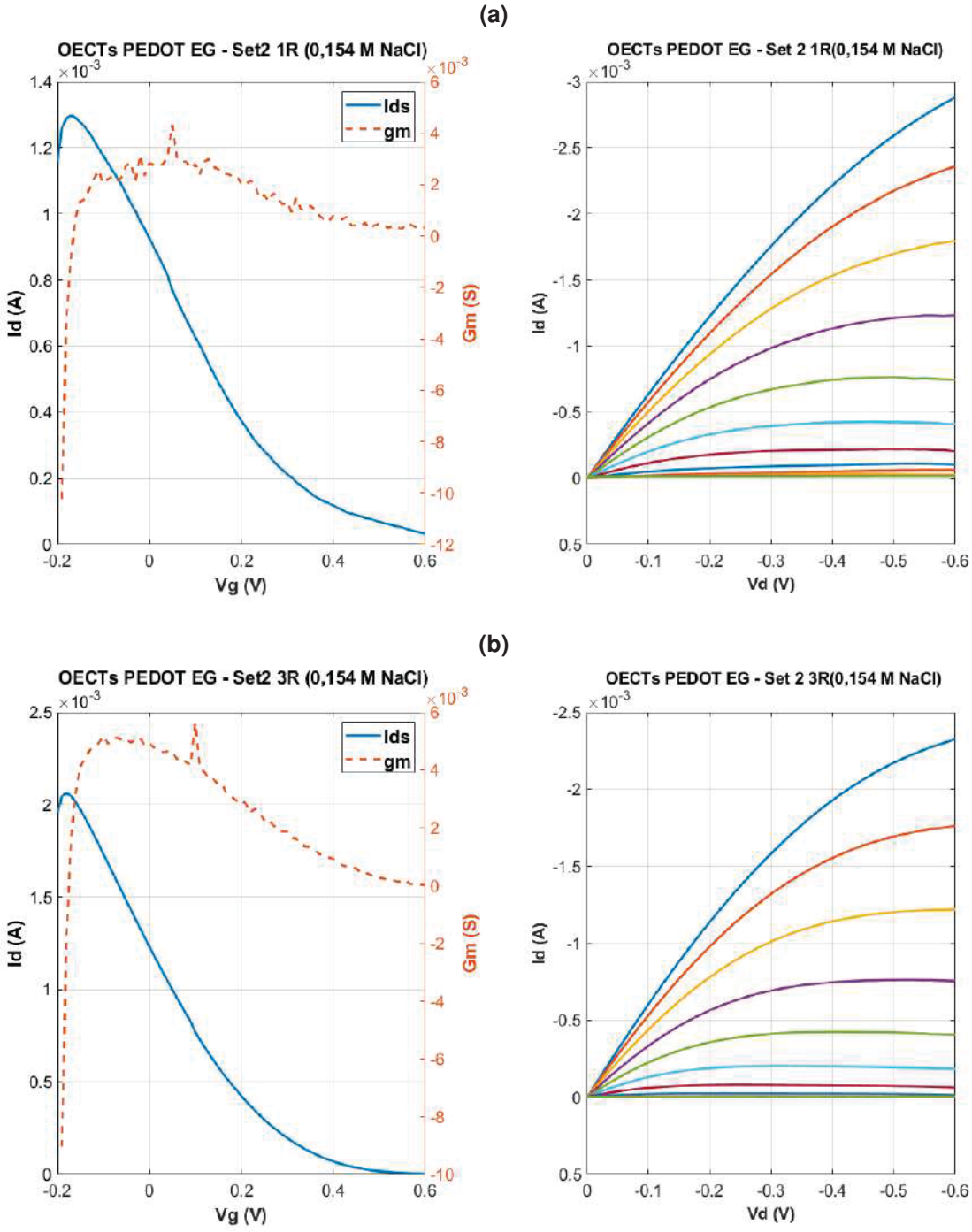

SOURCE: The Author.

On the other hand, Table 4.4 describes the average values for I_{DSon} and gm_{max}, from which is possible to conclude that although the current values are similar to those acquired for transistors made with the EG component, the transconductance is still lower than those seen previously.

4.4.3 PEDOT:PSS + NbO_5 and PEDOT:PSS + YO_3

NbO_5 microparticles (340 μm) and YO_3 nanoparticles (30 nm) were added to the PEDOT:PSS

Table 4.4: Mean, variance and standard deviation values for I_{DSon} and gm_{max} in PEDOT:PSS EG OECTs.

	I_{DSon}	gm_{max}
Mean	5.2 mA	3.8 mS
Variance	1.56 e^{-5}	1.16e^{-6}
Standard Deviation	0.004	0.001

SOURCE: The Author.

solution to explore the potential of these materials as active layers in OECTs since they presented good performance in OSCs. The devices were tested with two electrolytes, 0.1 M KCl and 0.1 M NaCl, chosen due to availability.

As seen in Figure 4.14a and Figure 4.15a, the responses obtained with both types of particles mostly resemble noise other than the typical I_{DS} x V_{GS} and *gm* x V_{GS} curves. Even though there is a tendency for current modulation, it is not significant, which can be proven by the output curves seen in Figure 4.14b and Figure 4.15b.

Figure 4.14: I_{DS} x V_{GS} (Transfer), *gm* x V_{GS} (Transconductance) and output curves for the OECTs tested with PEDOT:PSS + NbO_5 microparticles.

(a)

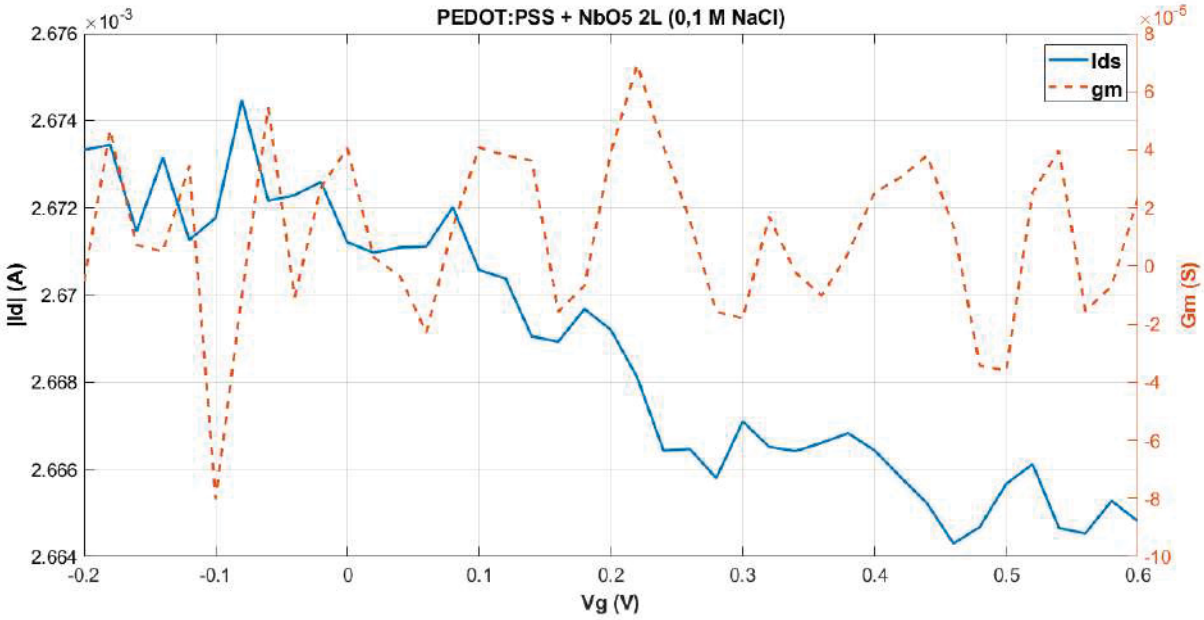

(b)

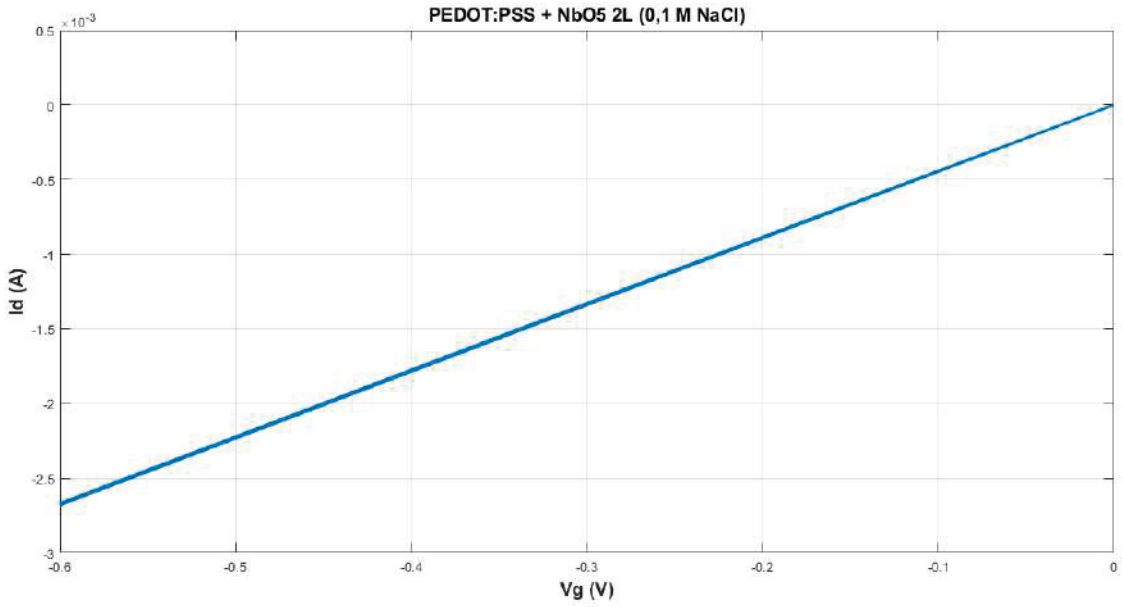

SOURCE: The Author.

Figure 4.15: I_{DS} x V_{GS} (Transfer), *gm* x V_{GS} (Transconductance) and output curves for the OECTs tested with PEDOT:PSS + Y_3 microparticles.

(a)

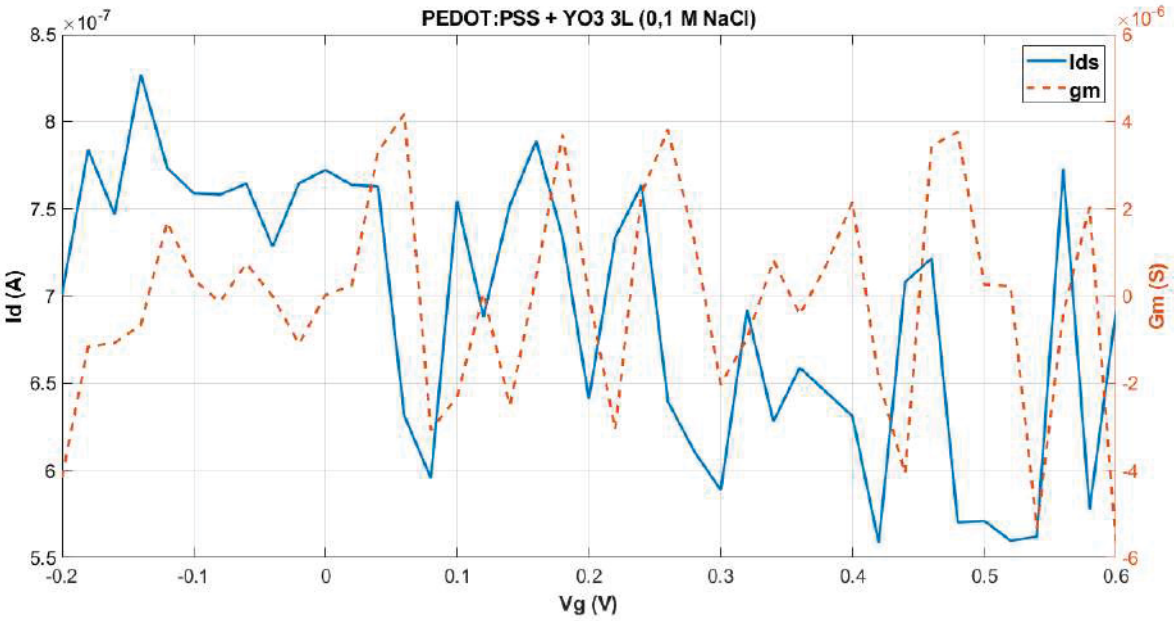

(b)

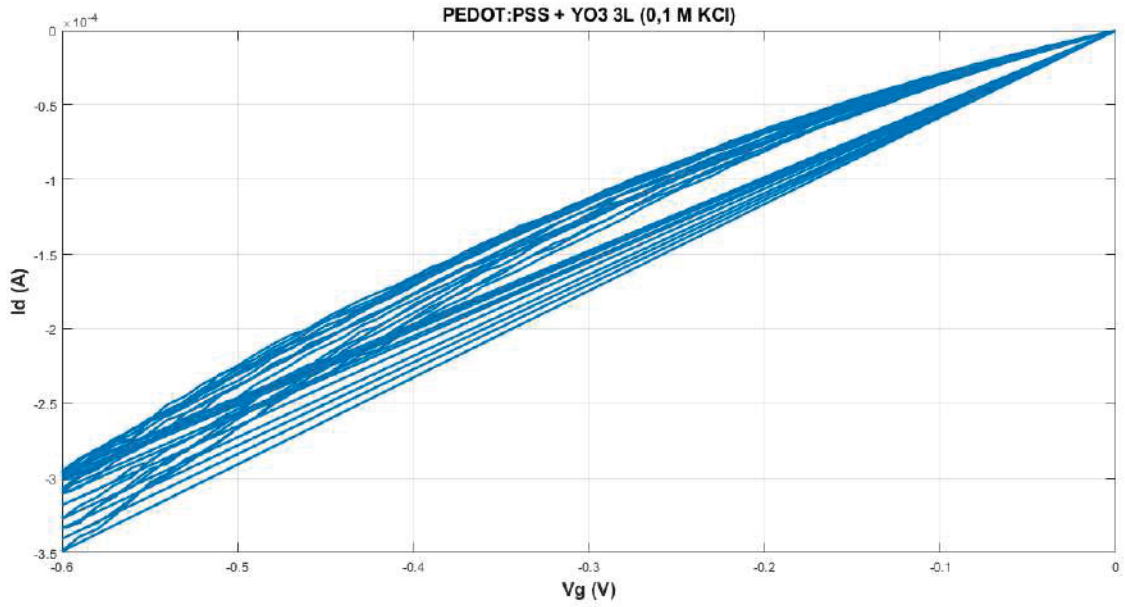

SOURCE: The Author.

4.4.4 Magic Quebec and RGH-14

The Magic Quebec channel consisted of two layers, the Quebec polymer, naturally de-doped, and its dopant, the Magic Blue, used to dope the first layer.

Firstly, the OECTs were tested with the Quebec film by itself and the results are exhibited in the transfer curve and the output curve seen in Figure 4.16a. It is possible to verify that the devices

presented low conductivity and there is no influence of the potential at the gate.

Also, Figure 4.16b shows the transfer and output curves for the Magic Quebec (doped film) and the device's response indicates high conductivity without the influence of the gate potential.

With regards to the RGH-14 response, as seen in Figure 4.17, the curves show I_{DS} responses in the order of 10^{-8} and do not indicate influence of the gate modulation, which can be confirmed by the output curve that presents mostly noise.

Figure 4.16: I_{DS} x V_{GS} (Transfer), *gm* x V_{GS} (Transconductance) and output curves for the OECTs tested with Magic Quebec.

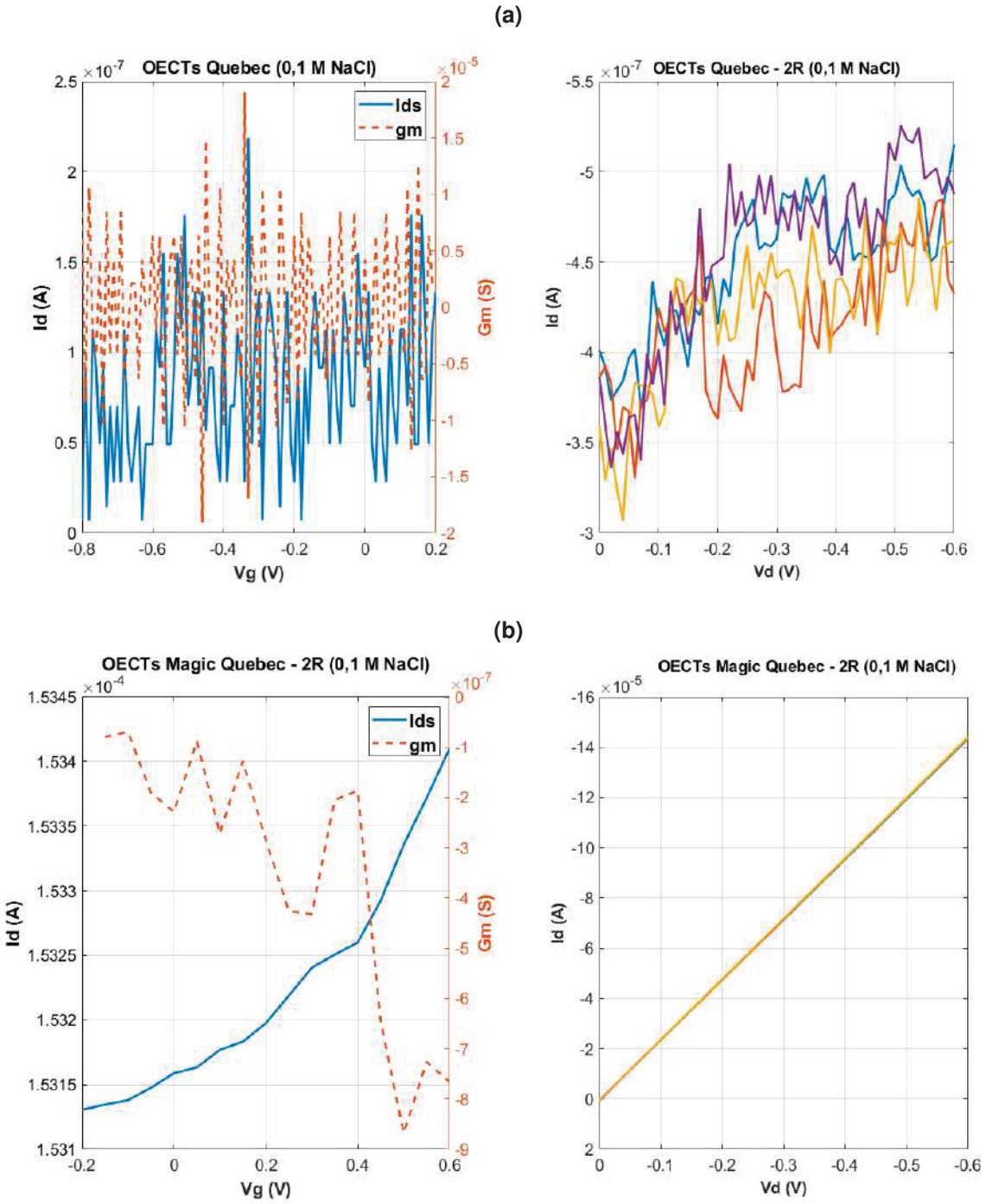

SOURCE: The Author.

Figure 4.17: I_{DS} x V_{GS} (Transfer), *gm* x V_{GS} (Transconductance) and output curves for the OECT tested with RGH-14.

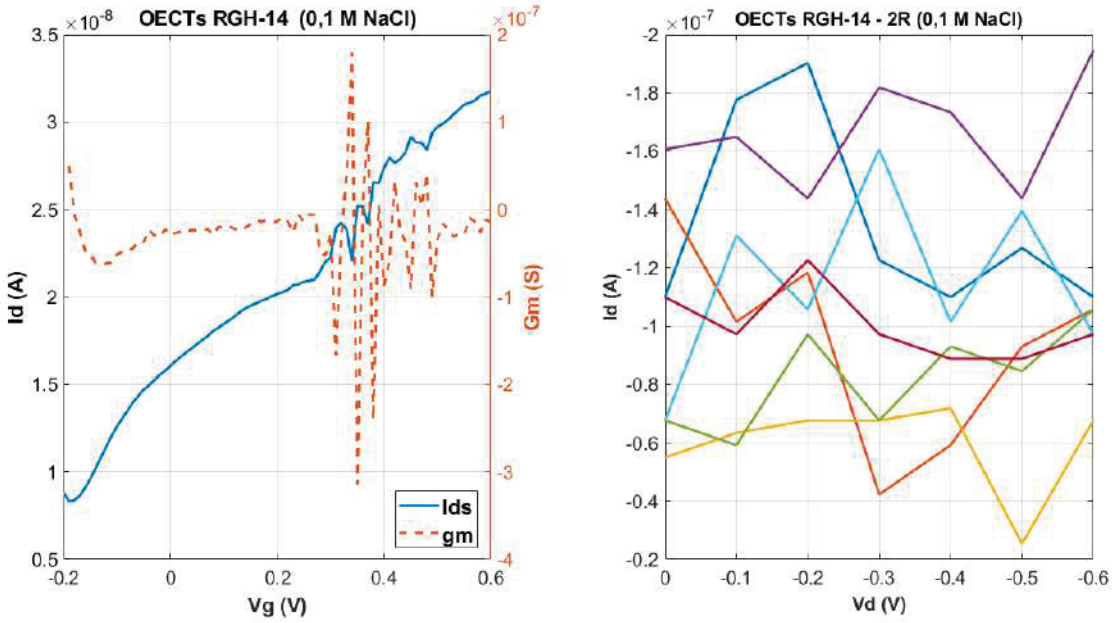

SOURCE: The author.

4.5 CHAPTER CONCLUSIONS

In this chapter, the steady-state characteristics of both PEDOT:PSS and P3HHT were analyzed. The main goal was to validate the experimental methodology and to explore performance parameters, such as ON drain current and maximum transconductance, and how they could be affected by changes in channel thickness (PEDOT:PSS OECTs) and by electrolyte composition/concentration.

As discussed in the literature, the transconductance in PEDOT:PSS OECTs is directly dependent on the channel geometry, including its thickness. In the present project the PEDOT:PSS thickness varied from 140 nm to 390 nm, values accomplished by changing the deposition velocity in the spin coater from 3000 rpm to 800 rpm. The responses acquired for each channel proved that as thick the film, the higher the I_{DSon} and gm_{max}. However, the drawback of tuning the OECT parameters through the channel thickness is that the thicker the layer, the slower the response, which means that the cutoff frequency would be lower. This phenomenon happens due to the volumetric doping/de-doping of the active layer, so if the channel is thicker, the ions would take longer to dope/de-dope the whole volume of the polymer.

In addition, the electrolyte effect on the performance parameters was also investigated for PEDOT:PSS and P3HHT active layers. The impact of the electrolyte composition was proved by testing the transistors in NaCl, KCl, and KPF_6 aqueous solutions. In both polymers, the KPF_6 electrolyte was demonstrated to provide a boost in the device response, with I_{DSon} and gm_{max}

being 8 to 10 times higher than in NaCl and KCl for P3HHT.

Considering the electrolyte concentration, the devices were analyzed in 0.05 M, 0.1 M, 0.15 M, 0.3 M, and 0.5 M NaCl aqueous solutions. In the PEDOT:PSS transistors the relationship between the concentration and the performance parameters is clear, as the values decrease as the concentration increases. In these OECTs, there were drops of 75% and 68% in the I_{DSon} and gm_{max} between 0.05 M and 0.5 M NaCl, respectively. As for the P3HHT active layer, no correlation between the electrolyte concentration and the performance parameters was observed, since the responses appeared to be random.

Also, instead of using PEDOT:PSS and P3HHT as active layers, other possibilities were explored in this chapter, such as PEDOT:PSS with different deposition techniques and compositions, and different polymers that are usually applied to other organic devices.

Through the characterization of the different active layers, it was possible to verify that those which present good performance in other devices might not work well with OECTs. This could be related to mixed conductivity and other specific requirements necessary to buid operational OECTs. Besides, even though the variations of the PEDOT:PSS solution exhibited responses to the applied gate potential, there were concerns related to the stability, reproducibility and the overall performance of the layers.

5 DEVICE STABILITY
PEDOT:PSS VS. P3HHT

As OECTs can be used for diverse applications in organic bioelectronics, including ion and biomarker detection as well as cell and brain signal recording, the long-term stability of the organic films and device operation in aqueous media should be considered if practical applications are targeted (KIM et al., 2018; ZHANG et al., 2016). Therefore, in this chapter, the stability of PEDOT:PSS and P3HHT devices is tested in two main fronts: stability and electrical stress stability.

The measurements for the devices in immersion were conducted in the same characterization setup as the steady-state analysis to record transfer curves at the same applied potentials reported in Chapter 4.

Furthermore, the characterization box was also adopted in the electrical stability assays, however, the applied signals were generated in both a waveform generator (Agilent 33500B) and the semiconductor analyzer (Keithley 4200S), which was used to acquire the OECTs response to the stimuli.

5.1 IMMERSION STABILITY

After an initial evaluation of their electrical characteristics (*t0*), the P3HHT and PEDOT:PSS OECTs were immersed in three different electrolytes (0.1 M NaCl, 0.1 M KCl and 0.1 M KPF_6) at room temperature for a period of forty days.The samples were tested every 10 days (*t10*, *t20*, *t30* and *t40*) with the same conditions.

For the immersion stability tests, besides checking for visual signs of delamination, which were not apparent, three main performance parameters were analyzed, I_{DSon}, gm_{max} and V_{th} for each device.

Figures 5.1.a and 5.1.d present the response to the immersion stability assays for the 0.1 M NaCl (aq.) electrolyte, while Figures 5.1.b and 5.1.e depict the results for OECTs immersed in 0.1 M KCl (aq.) solution, and Figures 5.1.c and 5.1.f show the behavior for OECTs tested with 0.1 M KPF_6 (aq.).

As observed in Chapter 4, the difference between the drain current responses for P3HHT and PEDOT:PSS continues in different orders of magnitude, μA for P3HHT and mA for PEDOT:PSS. This characteristic is seen due to the larger quantity of charge carrier and charge carrier mobility

in PEDOT:PSS. Besides, the behavior of the transistors tested in KPF_6 repeated itself as there are higher values of I_{DSon} for both polymers.

Figure 5.1: Transfer characteristics at stability tests for P3HHT at (a) 0.1 M NaCl, (b) 0.1 M KCl and (c) 0.1 M KPF_6, and PEDOT:PSS at (d) 0.1 M NaCl, (e) 0.1 M KCl and (f) 0.1 M KPF_6. Constant applied V_{DS} of - 0.6 V.

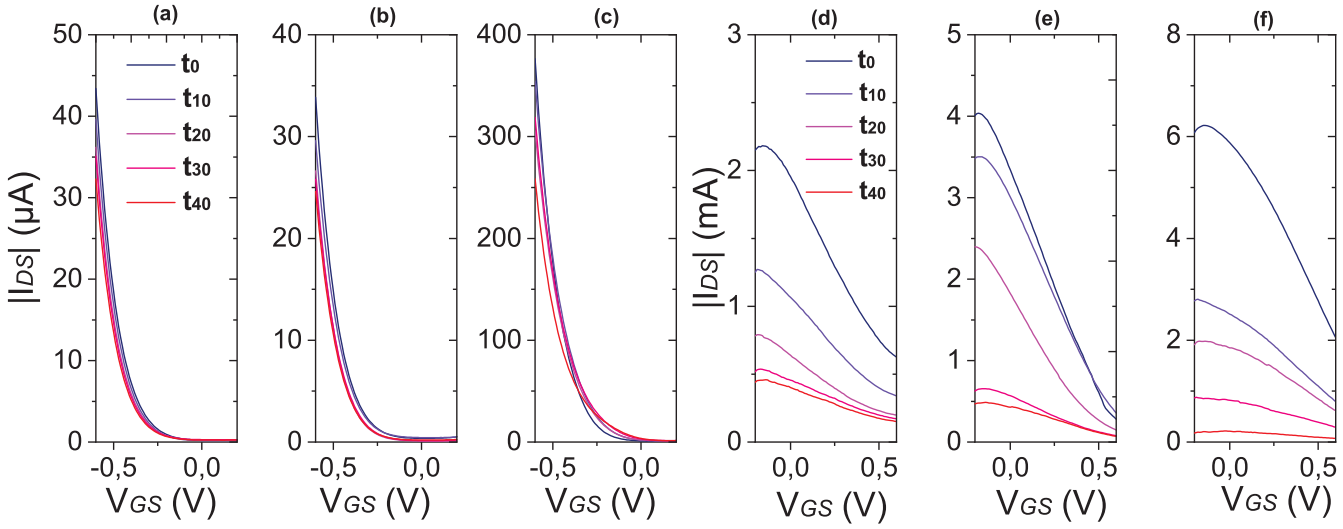

The first possible observation obtained from the curves in Figure 5.1 is that the PEDOT:PSS devices show less reproducibility of the performance parameters over the immersion period than P3HHT.

In thius context, the performance parameters retrieved from the P3HHT devices are displayed in Table 5.1, through which, it is possible to verify that the smallest change in I_{DSon}, even after the 40-day immersion period, is found for the NaCl electrolyte, with a recorded drop of 25.6%.

Table 5.1: Values of I_{DS} ON, G_m max and V_{th} between *t0* and *t40* for each tested electrolyte.

			0.1 M NaCl	0.1 KCl	0.1 KPF_6
t0	I_{DS} ON (mA)	P3HHT	0.043	0.033	0.376
		PEDOT:PSS	2.15	6.08	4.01
	G_m max (mS)	P3HHT	0.341	0.255	2.66
		PEDOT:PSS	3.12	7.35	7.59
	V_{th} (V)	P3HHT	-0.30531	-0,28841	-0.26637
		PEDOT:PSS	1.22867	1.7411	0.92228
t40	I_{DS} ON (mA)	P3HHT	0.032	0.024	0.258
		PEDOT:PSS	0.440	0.177	0.466
	G_m max (mS)	P3HHT	0.257	0.188	1.67
		PEDOT:PSS	1.01	0.981	1.11
	V_{th} (V)	P3HHT	-0.30531	-0.29478	-0.22761
		PEDOT:PSS	1.38884	2.1423	0.96767

SOURCE: The Author.

In addition, the gm_{max} for NaCl is reportedly the lowest drop at 24.6% when compared to KPF_6, the largest one, which presented a 37.2% drop from *t0* to *t40*.

However, it is important to highlight that for both KCl and NaCl, the values of gm_{max} still are around decimals of mS while for KPF_6 the values are greater than 1.5 mS. This effect could be associated to the facilitated injection, into the electrolyte, of larger, more polarizable anions with lower surface density.

It is also noteworthy that the shift in V_{th} seen for KPF_6 is accentuated at the end of the immersion tests, while the OFF state drain current (I_{DSoff}) remained considerably stable for all tested

devices.

As reported for OECTS with crosslinked PEDOT:PSS, after a 21-day immersion period, the devices presented a drop in I_{DSon} of at least 50% and the maximum transconductance dropped 49% from day 0 to day 21 (KIM et al., 2018). This is validated by the results obtained with the studied crosslinked PEDOT:PSS OECTs, which presented a less stable response during the 40-day immersion period, as seen in Figure 5.1, with drops in I_{DSon} and gm_{max} of 79.5% 67.6% for NaCl, 97.1% and 86.6% for KCl, and 88.4% and 85.4 % for KPF_6.

In comparison with state-of-the-art PEDOT:PSS OECTs, the performance of P3HHT devices should be less susceptible to swelling when immersed in aqueous environments, hence the I_{DSon} drops of 25.6%, 27.3% and 31.3% and gm_{max} drops of 24.6%, 26.4% and 37.2% for NaCl, KCl and KPF_6, respectively.

As seen with the P3HHT OECTs, the PEDOT:PSS devices also show an intriguing response to the use of PF_6^- anions in the electrolyte.

5.2 ELECTRICAL STABILITY

The experimental setup used to conduct the electrical stress stability tests is depicted in Figure 5.2a while the equipment used to provide the V_{GS} pulses is seen in Figure 5.2b. Also exhibited in Figure 5.2a is a P3HHT set with a polydimethylsiloxane (PDMS) well to confine the electrolyte on top of the channel and to avoid evaporation of the solution during the experiment.

Figure 5.2: (a) Experimental setup used to conduct the electrical stability tests. In the image, there is a P3HHT set being positioned for characterization; (b) osciloscope and waveform generator used to create the V_{GS} pulses.

(a) **(b)**

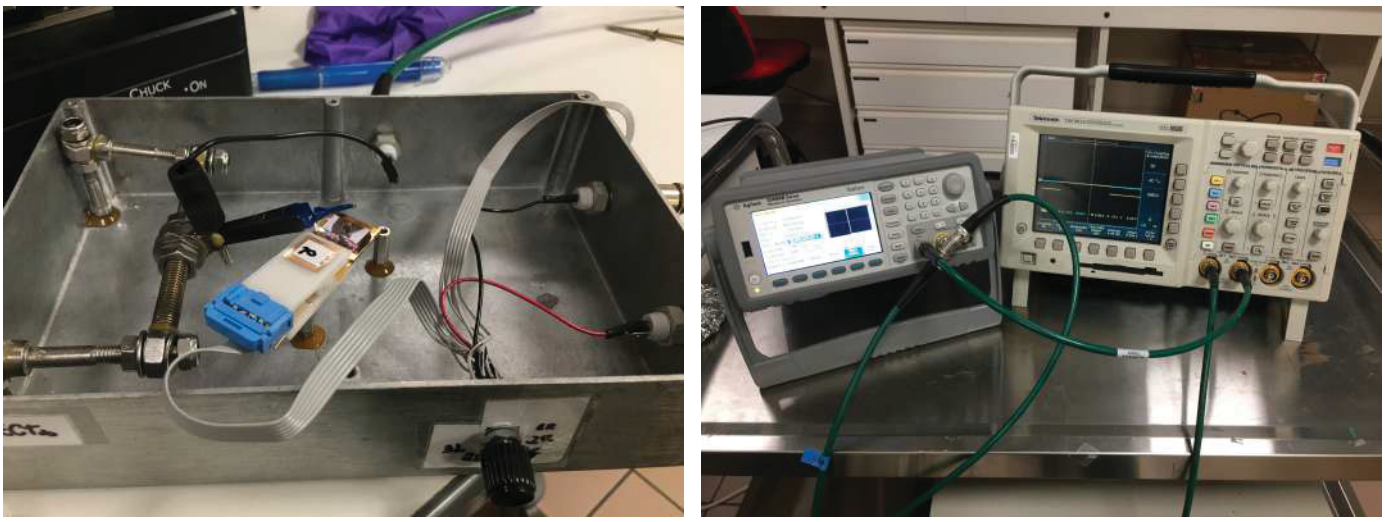

SOURCE: The author.

Figure 5.3 depicts drain current curves in function of time for an accumulation mode P3HHT

OECT and a depletion mode PEDOT:PSS OECT tested in 0.1 M KCl (aq.). The objective of this assay was to evaluate the stability of the device response after a cycling (repetitive ON/ OFF) process, in which the drain current was measured while successive gate pulses (δV_{GS}= 0.4 V, 20 s pulse period) were applied to the transistor at a constant drain potential (V_{DS} = -0.6 V) over a 15 minutes time span (50 pulses).

Figure 5.3: Operational stability of P3HHT and PEDOT:PSS OECTs after 50 electrochemical cycles in 0.1 M KCl. Applied pulses were 10 seconds long with V_{GS} = 400 mV.

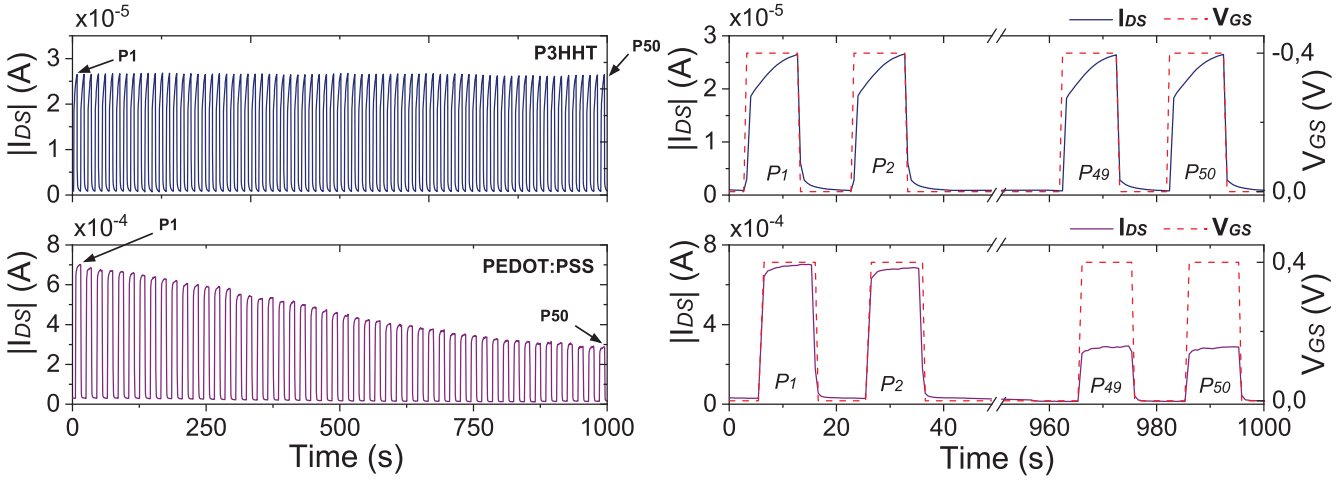

By disregarding the first cycle, in which the devices stabilize, it is possible to visualize that the P3HHT transistor presents a stable response throughout the stress test by retaining almost 100% of its ON-state current ($I_{DSmax,P1}$ = 26.67μA and $I_{DSmax,P50}$ = 26.60 μA).

Besides, it is possible to observe that at first there is a fast increase in the current response to the applied pulses in addition to a ramp at the top followed by a sharp decrease in the current signal. This behavior indicates a non-symmetric I_{DS} response, which could be a consequence of slow or erratic ON/OFF kinetics of the P3HHT OECTs.

Moreover, the measured drain current in the PEDOT:PSS devices decreases drastically throughout the pulse application period, retaining 41% of their initial current values after the cycling process. Although less stable regarding their drain current behavior, the PEDOT:PSS transistors presented more symmetrical responses to the applied pulses than the P3HHT devices.

This indicates that the transduction capabilities of PEDOT:PSS are considerably less stable than its accumulation counterpart, even though it present higher magnitudes on performance parameters and faster switching.

5.3 CHAPTER CONCLUSIONS

The fabricated accumulation and depletion mode OECTs were characterized to evaluate their performance parameters under immersion in aqueous electrolytes and electrical cycling.

Through the immersion tests in NaCl (aq.), KCl (aq.), and KPF_6 (aq.), it was possible to verify

that (a) the KPF_6 electrolyte provides an increase in orders of magnitude in the performance parameters and a shift in the threshold voltage; (b) the use of the KPF_6 electrolyte also resulted in the largest drops in PEDOT:PSS transistors; (c) the PEDOT:PSS devices did not present a stable response, behavior which was also observed regarding their repeatability; (d) P3HHT OECTs appeared much more stable than their depletion counterparts, which could be a consequence of their low swelling properties.

The response of PEDOT:PSS OECTs towards the use of PF_6^- anions could be explaioned by its low surface density, which makes them hydrophobic ions, meaning that these ions are injected into the channels without a large amount of water molecules. This characteristic could result in deswelling when PF_6^- is pushe into the PEDOT:PSS, a hydrophobic material, hence, the negative effect.

Still, the electrical stress assays also proved that the PEDOT:PSS OECTs are less stable than those that use P3HHT as their active layer despite the higher order of magnitude for all of their performance parameters. Although more stable, the P3HHT transistors showed some non-symmetrical response to the applied pulse at the gate, which could indicate slower performance.

6 CONCLUSIONS

The present investigation has culminated in the establishment of a comprehensive methodology for the fabrication of Organic Electrochemical Transistors (OECTs) through microfabrication. This method was underpinned by an exhaustive exploration of device characteristics, involving the application of distinct active layers and electrolytes. A detailed review of the current State-of-the-Art, with particular acknowledgment of the contributions by Jonathan Rivnay, George Malliaras, and their research groups, facilitated a nuanced understanding of OECTs' operational principles, figures of merit, applications, and the malleability of their performance parameters.

The adopted structural and fabrication approach, inspired by the pioneering work utilizing a PaC-2 sacrificial layer, innovatively incorporated a protective layer derived from the SU-8 2002 photoresist. This deviation obviated the necessity for a third patterning step in device structuring. Concurrently, a bespoke characterization setup was devised to enable seamless interfacing between the Keithley 4002 Parameter Analyzer and the Source, Drain, and Gate electrodes, with device selection facilitated by a mechanical switch.

The devices produced through this meticulous fabrication process exhibited behavior akin to State-of-the-Art depletion-mode OECTs, demonstrating a maximal drain current (I_{DS}) of f in positive gate voltage. Furthermore, the bell-shaped transconductance (gm) curves, with values in the order of millisiemens, affirmed the viability and reproducibility of the fabricated Organic Electrochemical Transistors, notwithstanding the absence of channel patterning.

Specifically focusing on PEDOT:PSS devices, the research extended to encompass performance parameter tuning experiments. Variations in electrolyte composition/concentration and channel thickness were scrutinized. The investigation revealed a discernible correlation between the characteristics of PEDOT:PSS and the ion size, transport, and conductivity, particularly exemplified by a decrease in IDS and gmmax intensities with increasing NaCl (aq.) concentration.

In exploring alternative active layers for accumulation mode OECTs, low-swelling P3HHT films emerged as promising candidates. Characterization at diverse electrolyte compositions and concentrations elucidated the influence of the polyatomic anion PF^{6-}, albeit without a clear correlation between electrolyte concentration and steady-state response a phenomenon attributed to the film's low-swelling properties.

However, endeavors to introduce alternative materials, including variations of PEDOT:PSS, RGH14, and Magic Quebec, were met with challenges. Notably, these variations did not exhibit stable or reliable responses, and in some cases, failed to respond at all. Despite their utility

in other organic devices, RGH14 and Magic Quebec did not manifest gate influence or current modulation, essential features for operational OECTs.

The investigation further extended to the evaluation of device stability through immersion and electrical stress assays. P3HHT films exhibited notable resilience under immersion, showcasing minimal IDS ON drops and moderate gmmax reductions over a 40-day period with varied electrolytes. Contrastingly, crosslinked PEDOT:PSS OECTs displayed considerable degradation, with I_{DSon} and gm_{max} drops exceeding 75% and 65%, respectively, and only 41% retention of the initial drain current after 50 electrical stress cycles.

This comprehensive exploration underscores the significance of the electrolyte in influencing OECT performance. As anticipated, P3HHT films emerged as promising candidates for long-term stability, substantiating earlier suggestions. The established methodology and findings culminated in the successful achievement of the proposed objectives, including a thorough investigation of State-of-the-Art OECTs, adaptation of materials and fabrication processes, creation of a dedicated characterization setup, validation of the experimental methodology, exploration of device design influences, and the systematic study of diverse polymer materials as active layers.

The culmination of this research is encapsulated in a collaborative scientific paper authored in partnership with Institut Charles Gerhardt Montpellier and the School of Materials Science Engineering and School of Chemical Biomolecular Engineering at the Georgia Institute of Technology. Published in the prestigious "Journal of Materials Chemistry C," the paper primarily details the outcomes of the stability assays conducted during the course of this study (MENEZES et al., 2023).

This research project, serving as the precursor for the OECT research line at both IMS and our research group, continues to exert a lasting impact. The proposed fabrication process remains integral to ongoing initiatives, with other students at IMS utilizing it for the development of high-density OECTs arrays.

Bibliography

[1] SHAW, J. M., SEIDLER, P. F., *Organic Electronics: Introduction*. IBM Journal of Research and Development, v. 45, n. 1, p. 3-9, January 2001.

[2] MA , H., YIP, H., HUANG, F., JEN, A. K. Y., *Interface Engineering for Organic Electronics*. Advanced Functional Materials, v. 20, n. 9, p. 1371 - 1388, April 2010.

[3] MALLIARAS, G., MCCULLOCH, I., *Introduction: Organic Bioelectronics*. Chemical Reviews, 122, 4, 4323-4324, 2022.

[4] JEN, A. K. Y., *Interface Engineering of Organic Electronics*. J. Mater. Chem. v. 20, p. 2491-2492, March 2010.

[5] PAPPA, A., PARLAK, O., SCHEIBLIN, G., MAILLEY, P., SALLEO, A., OWENS, R. M., *Organic Electronics for Point-of-Care Metabolite Monitoring*. Trends in Briotechnology, v. 36, n. 1, p. 45-59, January 2018.

[6] COBRA, D., COSTA, A. D. T., *Tecnologia para diagnóstico no ponto de atendimento*. Revista Polyteck, n. 14, p. 3-6, October 2015.

[7] ZHANG, S. DING, P., RUOKO, T., WU, R., STOECKEL, M., MASSETTI, M., LIU, T.,VAGIN, M., MELI, D., KROON, R., RIVNAY, J., FABIOANO, S., *Toward Stable p-Type Thiophene-Based Organic Electrochemical Transistors*. Advances Functional Materials, 2023.

[8] Vasudev, A.; Kaushik, A.; Tomizawa, Y.; Norena, N.; Bhansali, S., *An LTCC-based microfluidic system for label-free, electrochemical detection of cortisol*. Sensors and Actuators B, v. 182, p. 139-146, March 2013.

[9] Wang, X.; Liu, Z.; Zhang, T., *Flexible Sensing Electronics for Wearable/Attachable Health Minitoring*, Small, v. 13, March 2017.

[10] Gao, W.; Emaminejad, S.; Nyein, H. Y. Y.; Challa, S.; Chen, K.; Peck, A.; Fahad, H. M.; Ota, H.; Shiraki, H.,, Kiriya, D.; Lien, D.; Brooks, G. A.; Davis, R. W.;, Javey, A., *Fully integrated wearable sensor arrays for multiplexed in situ perspiration analysis*, Nature, v. 529, p. 509-514, January 2016.

[11] Yao, S.; Swetha, P.; Zhu, Y., *Nanomaterial-Enabled Wearable Sensors for Healthcare*, Adv. Healthcare Mater., v. 7, p. 1700889, November 2017.

[12] TAN, S. T. M., GUMYUSENGE, A., QUILL, T. J., LECROY, G. S., BONACCHINI, G. E., DENTI, I., SALLEO, A., *Mixed Ionic–Electronic Conduction, a Multifunctional Property in Organic Conductors*. Advanced Materials, v. 34, 21, 2022.

[13] Peake, J. M.; Kerr, G.; Sullivan, J. P., *A Critical Review of Consumer Wearables, Mobile Appliclations, and Equipment for Providing Biofeedback, Monitoring Stress, and Sleep in Physically Active Populations*, Frontiers in Physiology, v. 9, n. 743, June 2018.

[14] Shavanova, K.; Bakakina, Y.; Shtepliuk, I.; Viter, R.; Ubelis, A.; Beni, V.; Starodub, N.; Yakimova, R.; Khranovskyy, V., *Application of 2D Non-Graphene Materials ans 2D Oxide Nanostructures for Biosensing Technology*, Sensors, v. 16, n. 223, February 2016.

[15] KOCH, M., TSENG, H., WEISSBACH, A., INIGUEZ, B., LEO, K., KLOES, A., KLEEMAN, H., DARBANDY, G., *Device Physics, Modeling and Simulation of Organic Electrochemical Transistors*. IEEE Journal of the Electron Devices Society, 2023.

[16] Corrie, S. R.; Coffey, J. W.; Islam, J.; Markey, K. A.; Kendall, M. A., *Blood, sweat, and tears: developing clinically relevant protein biosensors for integrated body fluid analysis*, Analyst, v. 140, p. 4350 - 4364, April 2015.

[17] Glennon, T.; O'Quigley, C.; McCaul, M.; Matzeu, G.; Beirne, S.; Wallace, G. G.; Stroiescu, F.; O'Mahoney, N.; White, P.; Diamond, D., *'SWEAT': A Wearable Platform for Harvesting and Analysing Sweat Sodium Content*, Electroanalysis, v. 28, p. 1283-1289, April 2016.

[18] MARKS, A. GRIGGS, S., GASPARINI, N., MOSER, M., *Organic Electrochemical Transistors: An Emerging Technology for Biosensing*. Advanced MAterials Interfaces, v. 9, 6, 2022.

[19] YAO, Y., HUANG, W., CHEN, J., LIU, X., BAI, L., CHEN, W., CHENG, Y., PING, J., MARKS, T. J., FACCHETTI, A., *Flexible and Stretchable Organic Electrochemical Transistors for Physiological Sensing Devices*. Advanced Materials, v. 35, 35, 2023.

[20] STRAKOSAS, X., BONGO, M., OWENS, E., *The organic electrochemical transistor for biological applications*. Journal of Applied Polymer Science, v. 132, n. 15, January 2015.

[21] KERGOAT, L., PIRO, B., HOROWITZ, G., PHAM, M., *Advances in organic transistor-based biosensors: From organic electrochemical transistors to electrolyte-gated organic field-effect transistors*. Anal. Bional. Chem., v. 402, n. 5, p. 1813-1826, February, 2012.

[22] BAI, L., ELÓSEGUI, C. G., LI, W., YU, P., FEI, J., MAO, L., *Biological applications of organic electrochemical transistors: Electrochemical biosensors and electrophysiology recording*. Front. Chem., v. 7., May 2019.

[23] FRIEDLEIN, J., RIVNAY, J., DUNLAP, D., MCCULLOCH, I., SHAHEEN, S., MCLEOD, R., MALLIARAS, G. G., *Influence of disorder on transfer characteristics of organic electrochemical transistors*. Applied Physics Letters, v. 111, n. 023301 , July 2018.

[24] RIVNAY, J., INAL, S., SALLEO, A., OWENS, R. M., BERGGREN, M., MALLIARAS, G. G., *Organic Electrochemical Transistors*. Nature Reviews Materials, v. 3, n. 17086, p. 1-14, January 2018.

[25] HUTTER, P., ROTHLANDER, T., HAASE, A., TRIMMEL, G., STADLOBER, B., *Influence of geometry variations on the response of organic electrochemical transistors*. Applied Physics Letters, v. 103, n. 4, July 2013.

[26] POLYRAVAS, A., SCHAEFER, N., CURTO, V., CALIA, A., GUIMERA-BRUNET, A., GARRIDO, J., MALLIARAS, G. G., *Effect of channel thickness on noise in organic electrochemical transistors*. Applied Physics Letters, v. 117, n. 7, August 2020.

[27] Nakata, S.; Arie, T.; Akita, S.; Takei, K., *Wearable, Flexible, and Multifuctional Healthcare Device with an ISFET Cheical Sensor for Simultaneous Sweat pH and Skin Temperatura Monitoring*, ACS Sens., v. 2, p. 443-448, March 2017.

[28] Dunn, J.; Runge, R.; Snyder, M., *Wearables and the medical revolution*, Per. Med., v. 15, n. 5, p. 429-448, Setembro 2018.

[29] BERNARDS, D., MALLIARAS, G., *Steady-state and transient behavior of organic electrochemical transistors*. Advanced Functional Materials, v. 17, n. 17, p. 3538-3544, October 2007.

[30] SESSOLO, M., KHODAGHOLY, D., RIVNAY, J., MADDALENA, F., GLEYZES, M., STEIDI, E., BUISSON, B., MALLIARAS, G. G., *Easy-to-fabricate conducting polymer microelectrode arrays*. Advanced Materials, v. 25, n. 15, p. 2135-2139, February2013.

[31] OHAYON, D., DRUET, V., INAL, S., *A guide for the characterization of organic electrochemical transistors and channel materials*. Chemical Society Reviews. v.3, 2023.

[32] WHITE, H. S., KITTLESEN, G. P., WRIGHTON, M. S., *Chemical derivatization of an array of three gold microelectrodes with polypyrrole: fabrication of a molecule-based transistor*. J. Am. Chem. Soc., v. 106, n. 18, p. 5375-5377, September 1984.

[33] PAUDEL, P. R., KAPHLE, V., DAHAL, D., KRISHNAN, R. K. R., LUSSEM, B., *Tuning the TRansconductance of Organic Electrochemical Transistors*. Adv. Funct. Mater., 31, p. 2004939, 2021.

[34] SAVVA, A., WUSTONI, S., INAL, S., *Ionic-to-electronic coupling efficiency in PEDOT:PSS films operated in aqueous electrolytes*.Journal of Materials Chemistry C, v. 6, n. 44, p. 12023-12030, 2018.

[35] KEENE, D., VAN DER POL, T., ZAKHIDOV, D., WEIJITENS, C., JANSSEN, R., SALLEO, A., VAN DE BURGT, Y., *Enhancement-Mode PEDOT:PSS Organic Electrochemical Transistors Using Molecular De-Doping*. Advanced Materials, v. 32, n. 19, May 2020.

[36] ZEGLIO, E., INGANAS, O., *Active Materials for Organic Electrochemical Transistors*. Advanced Materials, v. 30, n. 44, July 2018.

[37] SAVVA, A., CENDRA, C., GIUGNI, A., TORRE, B., SURGALLIS, J., OHAYON, D., GIOVANNITTI, A., MCCULLOCH, I., DI FABRIZIO, E., SALLEO, A., RIVNAY, J., *Influence of Water on the Performance of Organic Electrochemical Transistors*. Chemistry of Materials, v. 31, n. 3, p. 927-937, February 2019.

[38] PATERSON, A., FABER, H., SAVVA, A., NIKIFORIDIS, G., GEDDA, M., HIFALGO, T., CHEN, X., MCCULLOCH, I., ANTHOPOULOS, T., INAL, S., *On the Role of Contact Resistance and Electrode Modification in Organic Electrochemical Transistors*. Advanced Materials, v. 31, n. 37, july 2019.

[39] KUMAR, P., YI, Z., ZHANG, S., SEKAR, A., SOAVI, F., CICOIRA, F., *Effect of channel thickness, electrolyte ions, and dissolved oxygen on the performance of organic electrochemical transistors*, Applied Physics Letters, v. 107, n. 5, August 2015.

[40] KAPHLE, V.. PAUDEL, P., DAHAL, D., RADHA, K. R., LUSSEM, B., *Finding the equilibrium of organic electrochemical transistors*. Nature Comm., v. 11, n. 1, December 2020.

[41] K. Guo, S. Wustoni, A. Koklu, E. Diaz-Galicia, M. Moser, A. Hama, A. A. Alqahtani, A. N. Ahmad, F. S. Alhamlan, M. Shuaib, A. Pain, I. McCulloch, S. T. Arold, R. Grunberg and S. Inal. Nature Biomedical Engineering, **5**, 666 (2021).

[42] BERGGREN, M., GLOWACKI, E. D., SIMON, D. T., STAVRINIDOU, E., TYBRANDT K., *In Vivo Organic Bioelectronics for Neuromodulation*. Chemical Reviews 2022 122 (4), 4826-4846DOI: 10.1021/acs.chemrev.1c00390

[43] GAO, Y., JUNYAO, Z., DAPENA, L., TONGRIU, S., JUN, W., LI, L., SHILEI, D., JIANHUA, Z., ZHENGLONG, Y., HUANG, JIA., *Artificial synapses based on organic electrochemical transistors with self-healing dielectric layers*. Chinese Chemical Letters, 108582, 2023.

[44] L. Q. Flagg, R. Giridharagopal, J. Gui and D. S. Ginger. Chemistry of Materials, **30**, 5380 (2018).

[45] INAL, S., RIVNAY, J., LELEUX, P., FERRO, M., RAMUZ, M., BRENDEL, J. C., SCHMIDT, M. M., THELAKKAT, M., MALLIARAS, G. G., *A high transconductance accumulation mode electrochemical transistor*. Advanced Materials, v. 26, n. 44, p. 74550-7455, 2014.

[46] A. Giovannitti, C. B. Nielsen, D. Sbircea, S. Inal, M. Donahue, M. R. Niazi, D. A. Hanifi, A. Amassian, G. G. Malliaras, J. Rivnay and I. McCulloch. Nature Communications, **7**, 13066 (2016).

[47] C. Cendra, A. Giovannitti, A. Savva, V. Venkatraman, I. McCulloch, A. Salleo, S. Inal and J. Rivnay. Advanced Functional Materials, **29**, 1 (2019).

[48] L. Q. Flagg, C. G. Bischak, J. W. Onorato, R. B. Rashid, C. K. Luscombe and D. S. Ginger. Journal of the American Chemical Society, **141**, 4345 (2019).

[49] C. B. Nielsen, A. Giovannitti, D. Sbircea, E. Bandiello, M. R. Niazi, D. A. Hanifi, M. Sessolo, A. Amassian, G. G. Malliaras, J. Rivnay and I. McCulloch. J. Am. Chem. Soc., **138**, 10252 (2016).

[50] T. Nicolini, J. Surgaillis, A. Savva, A. D. Scaccabarozzi, R. Nakar, D. Thuau, G. Wantz, L. J. Richter, O. Dautel, G. Hadziioannou and N. Stingelin. Advanced Materials, **33**, 2005723 (2021).

[51] LI, P., LEI, T., J., *Molecular design strategies for high-performance organic electrochemical transistors*. Polym. Sci. 2022, 60(3), 377.

[52] ANGARITA-GOMEZ, S. and BALBUENA, P. B., *Ion mobility and solvation complexes at liquid–solid interfaces in dilute, high concentration, and localized high concentration electrolytes*, v. 15, 2022.

[53] KIM, S., KIM, C., KIM, Y., KIM, N., LEE, W., LEE, E., KIM, D., PARK, S., LEE, K., RIVNAY, J., YOON, M., *Influence of PEDOT:PSS crystallinity and composition on electrochemical transistor performance and long-term stability*. Nature Comm., v. 9, n. 1, December 2018.

[54] YANG, A. LI, Y. YANG, C., FU, Y., WANG, N., LI, L., YAN, F., *Fabric Organic Electrochemical Transistors for Biosensors*. Advanced Materials, v. 30, n. 23, June 2018.

[55] ATHANASIOU, V., PECQUEUR, S., VUILLAUME, D., *On a generic theory of the organic electrochemical transistor dynamics*. Organic Electronics, v. 72, p. 39-49, September 2019.

[56] TARABELLA, G., SANTATO, C., YANG, S., IANNOTTA, S., MALLIARAS, G. G., CICOIRA, F., *Effect of the gate electrode on the response of organic electrochemical transistors.*Applied Physics Letters, v. 97, n. 12, September 2010.

[57] BERNARDS, D., MACAYA, D., NIKOLOU, M., DEFRANCO, J. A., SIICHI, T., MALLIARAS, G. G., textitEnzymatic sensing with organic electrochemical transistors. J. Mater. Chem., v. 18, p. 116-120, 2008.

[58] KHODAGHOLY, D., RIVNAY, J., SESSOLO, M., GURFINKEL, M., LELEUX, P., JIMISON, L., STAVRINIDOU, E., HERVE, T., SANAUR, S., OWENS, R., MALLIARAS, G. G., *High transconductance organic electrochemical transistors*. Nature Comm., v. 4, July 2013.

[59] WU, R., MATTA, M., PAULSEN, B. D., RIVNAY, J., *Operando Characterization of Organic Mixed Ionic/Electronic Conducting Materials*. v. 12, p. 4493-4451, 2022.

[60] RASHID, R. B., EVANS, A. M., Hall, L. A., DASARI, R. R., ROESNER, E. K., MARDER, S. R., D'ALLESANDRO, D. M., DICHTEL, W. R., RIVNAY, J., *A Semiconducting Two-Dimensional Polymer as an Organic Electrochemical Transistor Active Layer*. Adv. Mater. 2022, 34, 2110703.

[61] RIVNAY, J., LELEUX, P., SESSOLO, M., KHODAGHOLY, D., HERVE, T., FIOCCHI, M., MALLIARAS, G. G., *Organic electrochemical transistors with maximum transconductance at zero gate bias*, Advanced Materials, v. 25, n. 48, p. 7010-1014, december 2013.

[62] ZHANG, S., HUBIS, E., GIRARD, C., KUMAR, P., DEFRANCO, J., CICOIRA, F., *Water stability and orthogonal patterning of flexible micro-electrochemical transistors on plastic*. J. Mater. Chem. C, v. 4, n. 7, p. 1382-1385, 2016.

[63] WANG, N., LIU, Y., FU, Y., YAN, F., *AC Measurements Using Organic Electrochemical Transistors for Accurate Sensing*, ACS Appli. Mater. Interfaces, v. 10, n. 31, 2018.

[64] M. Moser, T. C. Hidalgo, J. Surgailis, J. Gladisch, S. Ghosh, R. Sheelamanthula, Q. Thiburce, A. Giovannitti, A. Salleo, N. Gasparini, A. Wadsworth, I. Zozoulenki, M. Berggren, E. Stavrinidou, S. Inall and I. McCulloch. Advanced Materials, **32**, 2002748 (2020).

[65] SPYROPOULOS, G. D., GELINAS, J. N., KHODAGHOLY, D., *Internal ion-gated organic electrochemical transistor: A building block for integrated bioelectronics*. Science Advances, v. 5, n. 2, February 2019.

[66] CICOIRA, F., SESSOLO, M., YAGMAZADEH, O., DEFRANCO, J., YANG, S., MALLIARAS, G. G., *Influence of device geometry on sensor characteristics of planar Organic electrochemical transistors*, Advanced Materials, v. 22, n. 9, 1012-1016, March 2010.

[67] LELEUX, P., RIVNAY, J., LONJARET, T., BADLER, J., BENAR, C., HERVE, T., CHAUVEL, P., MALLIARAS, G G.,*Organic electrochemical transistors for clinical applications*, Advanced Healthcare Materials, v. 4, v. 1, p. 142-147, January 2015.

[68] GKOUPIDENIS, P., SCHAEFER, N., GARLAN, B., MALLIARS, G. G., *Neuromorphic Functions in PEDOT:PSS Organic Electrochemical Transistors*, Advanced Materials, v. 27, n. 44, p. 7176-7180, November 2015.

[69] KHODAGHOLY, D. GURFINKEL, M., STAVRINIDOU, E., LELEUX, P., HERVE, T., SANAUR, S., MALLIARAS, G. G., *High speed and high density organic electrochemical transistor arrays*, Applied Physics Letters, v. 99, n. 16, October 2011.

[70] SESSOLO, M., RIVNAY, J., BANDELLO, E., MALLIARAS, G. G., BOLINK, H., *Ion-selective organic electrochemical transistors*, Advanced Materials, v. 26, n. 28, p. 4803-4807, October 2014.

[71] VENKATRAMAN, V. FRIEDLEIN, J., GIOVANNITTI, A., MARIA, I., MCCULLOCH, I., MCLEOD, R., RIVNAY, J., *Subthreshold Operation of Organic Electrochemical Transistors for Biosignal Amplification*. Advanced Science, v. 5, n. 8, August 2018.

[72] DONAHUE, M., WILLIAMSON, A., STRAKOSAS, X., FRIEDLEIN, J., MCLEOD, R., GIESKOVA, H., MALLIARAS, G. G., *High-Performance Vertical Organic Electrochemical Transistors*. Advanced Materials, v. 30, n. 5, February 2018.

[73] WUSTONI, S., COMBE, C., OHAYON, D., AKHTAR, M., MCCULLOCH, I., INAL, S., *Membrane-Free Detection of Metal Cations with an Organic Electrochemical Transistor*. Advanced Functional Materials, v. 29, n.44, November 2019.

[74] SRIVASTAVA, A., CHAKRABARTI, P., *An organic Schottky diode (OSD) based on a-silicon/polycarbazole contact*. Synthetic Metals, v. 207, p. 96-101, 2015.

[75] KOCH, C., RINKE, T. J., *PHOTOLITHOGRAPHY Basics of Microstructuring*: 2^{nd} ed. Friedrichshafen: Siegl Druck & Medien GmbH & Co. KG, 2020.

[76] MENEZES, N. P., NICOLINI, T., BARKER, M., MARIANO, A. A., DARTORA, C. A., WANTZ, G., STINGELIN, N., ABBAS, M., DAUTEL, O. J., THUAU, D., *Improved stability of organic electrochemical transistor performances with a low swelling mixed conducting polymer: a comparative study with PEDOT:PSS*. Journal of Materials Chemistry C, v. 19, p. 1-6, 2023.